INORGANIC POLYPHOSPHATE IN THE MARINE ENVIRONMENT: FIELD OBSERVATIONS AND NEW ANALYTICAL TECHNIQUES

A Dissertation
Presented to
The Academic Faculty

By

Julia M. Diaz

In Partial Fulfillment
Of the Requirements for the Degree
Doctor of Philosophy in the
School of Earth and Atmospheric Science

Georgia Institute of Technology

May 2011

INORGANIC POLYPHOSPHATE IN THE MARINE ENVIRONMENT: FIELD OBSERVATIONS AND NEW ANALYTICAL TECHNIQUES

Approved by:

Dr. Ellery D. Ingall, Advisor
School of Earth and Atmospheric Sciences
Georgia Institute of Technology

Dr. Martial Taillefert
School of Earth and Atmospheric Sciences
Georgia Institute of Technology

Dr. Thomas DiChristina
School of Biology
Georgia Institute of Technology

Dr. Jay A. Brandes
Skidaway Institute of Oceanography

Dr. Claudia R. Benitez-Nelson
Department of Earth & Ocean Sciences
University of South Carolina

Date Approved: 15 March 2011

ACKNOWLEDGEMENTS

This dissertation represents a collaborative effort between myself and a number of talented scientists I have had the good fortune to work with throughout my time as a Ph.D. student. First and foremost among these individuals is my academic advisor, Ellery Ingall, who has not only been a remarkable mentor, but also a great friend. His academic expertise, unwavering support, and keen sense of humor have been instrumental in my success. I also extend sincere thanks to my other thesis committee members: Jay Brandes and Claudia Benitez-Nelson, who have both been constant sources of support and expertise since my first days as a Ph.D. student; Martial Taillefert, who has provided many constructive comments on my research over the years; and Thomas DiChristina, who has helped me balance my work in environmental science with my enduring interest in biology. Other people whose input has been critical to specific projects are acknowledged elsewhere in this thesis.

I would also like to acknowledge the organizations that have given me financial support during my graduate studies. These include my home department at Georgia Tech, the School of Earth and Atmospheric Science, the National Science Foundation, the Goizuetta Foundation, and the Philanthropic Education Organization International Sisterhood.

Finally, I thank my family for their love and support.

TABLE OF CONTENTS

LIST OF TABLES

LIST OF FIGURES

LIST OF ABBREVIATIONS

ACP	Absolutely Calibrated Photodiode
DAPI	4’,6-diamidino-2-phenylindole
DOP	Dissolved Organic Phosphorus
DPC	Differential Phase Contrast
ED/RO	Combined Electrodialysis and Reverse Osmosis
EELS	Electron Energy Loss Spectroscopy
EM	Electron Microscopy
HEPES	4-(2-hydroxyethyl)-1-piperazineethanesulfonic acid
NEXFS	Near Edge X-ray Fluorescence Spectroscopy
NMR	Nuclear Magnetic Resonance
POC	Particulate Organic Carbon
Poly-P	Polyphosphate
PON	Particulate Organic Nitrogen
POP	Particulate Organic Phosphorus
SRP	Soluble Reactive Phosphorus
SXM	Scanning X-ray Microscope
TEM	Transmission Electron Microscopy
TPP	Total Particulate Phosphorus
XANES	X-ray Absorption Near Edge Spectroscopy

SUMMARY

Phosphorus (P) is a requirement for biological growth, but this vital nutrient is present at low or limiting concentrations across vast areas of the global surface ocean. Inorganic polyphosphate (poly-P), a linear polymer of at least three orthophosphate units, is one component of the marine P cycle that has been relatively overlooked as compared to other P species, owing in part to a lack of routine analytical techniques that cleanly evaluate it within samples. This thesis demonstrates that inorganic poly-P is a quantitatively significant and dynamic component of the global marine P cycle while also establishing two new techniques for its analysis in biological and environmental samples. In Chapter 2, experiments using the freshwater algae *Chlamydomonas* sp. and *Chlorella* sp. illustrate X-ray fluorescence spectromicroscopy as a powerful tool for the sub-micron scale assessment of poly-P composition in organisms. This method enabled the discovery, detailed in Chapter 3, of a mechanism for the long-term sequestration of the vital nutrient P from marine systems via the initial formation of poly-P in surface waters and its eventual transformation into the mineral apatite within sediments. The importance of marine poly-P is furthermore established in Chapter 3 by observations showing that naturally-occurring poly-P represents 7-11% of total P in particles and dissolved matter in Effingham Inlet, a eutrophic fjord located on Vancouver Island, British Columbia. In Chapter 4, a new fluorometric protocol based on the interaction of inorganic poly-P with 4',6-diamidino-2-phenylindole (DAPI) is established as a technique for the direct quantification of poly-P in environmental samples. Chapter 5 presents work from Effingham Inlet utilizing this method that show that inorganic poly-P plays a significant role in the redox-sensitive cycling of P in natural systems.

.

CHAPTER 1

INTRODUCTION

1.1 History of Polyphosphate

Polyphosphate (poly-P) is a linear polymer of at least three orthophosphate molecules joined by high energy P-O-P, or phosphoanhydride bonds (Figure 1.1). Poly-P can be organic (e.g., trinucleotides) or inorganic in form. This thesis focuses primarily on natural inorganic poly-P, which is distinct from organic poly-P in its distribution, chemistry, and function in cells. Hereafter, "poly-P" will refer to inorganic poly-P unless otherwise noted.

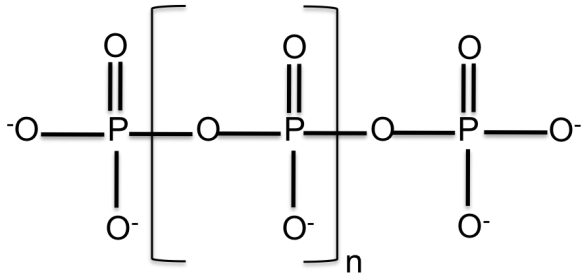

Figure 1.1 Inorganic polyphosphate molecular structure. Poly-P is an unbranched polymer of orthophosphate units (n = 1 to >100) linked by high-energy phosphoanhydride bonds. Owing to the negative charge of orthophosphate units, poly-P granules are ionically complexed with charge-balancing cations in organisms, especially calcium, a major ion in seawater.

Poly-P was first observed in biological systems over a century ago by non-specific staining with basic dyes such as toludine blue [*Lieberman*, 1888; *Meyer*, 1904]. These metachromatic poly-P granules were named "volutin" and were mistaken for

nucleic acid for some years until the advent of electron microscopy, which revealed poly-P to be the main constituent [*Wiame*, 1947].

Early studies on poly-P utilized the biomolecule as a diagnostic feature of medically relevant bacteria, such as *Corynebacterium diphtheriae* [*Kornberg*, 1995]. Due to the lack of an established physiological function for poly-P, however, it became regarded as a "molecular fossil," a reputation that is still in the process of changing today [*Brown and Kornberg*, 2004]. Although modern molecular approaches have demonstrated poly-P to be a widespread biomolecule involved in vital cellular processes and possibly even the origin of life [*Brown and Kornberg*, 2004; *Kornberg*, 1995; *Kornberg et al.*, 1999; *Rao et al.*, 2009; *Yamagata et al.*, 1991], contemporary reviews still refer to poly-P as "forgotten," as it is not even mentioned in textbooks of biology and chemistry [*Brown and Kornberg*, 2004].

If poly-P has been forgotten in the fields of microbiology and biochemistry, then it has certainly been forgotten, perhaps even dismissed, in the environmental sciences. Whereas early microbiological work on poly-P revealed its indubitable presence in ecologically important groups such as diatoms [*Eppley*, 1962; *Keck and Stich*, 1957; *Kuhl*, 1962; *Perry*, 1976], early detection methods for poly-P in seawater and sediments were highly insensitive and failed to detect its presence in the marine environment from the 1950's through the 1970's (e.g., [*Armstrong and Tibbitts*, 1968; *Solorzano and Strickland*, 1968]). These initial approaches utilized UV difference methods for the enumeration of poly-P. UV irradiation leaves polyphosphate intact but breaks down all other phosphorus-containing molecules. Therefore, in these UV-based approaches, polyphosphate content was determined by the difference in total phosphorus content with and without UV irradiation [*Armstrong and Tibbitts*, 1968; *Hansen and Koroleff*, 1999a; *Solorzano and Strickland*, 1968]. This approach is effective only under the

environmentally atypical conditions of very high poly-P content and low background orthophosphate levels. Not surprisingly, initial work on marine poly-P only identified significant concentrations of the molecule in coastal and industrially impacted areas, where natural levels of poly-P were augmented by pollution sources [*Armstrong and Tibbitts*, 1968; *Solorzano and Strickland*, 1968]. This result, coupled with the rapid turnover of synthetic poly-P observed in cultured isolates [*Solorzano and Strickland*, 1968], lead scientists to conclude that the accumulation of poly-P in the environment was unlikely except in organisms and industrially polluted areas [*Armstrong and Tibbitts*, 1968; *Solorzano and Sharp*, 1980].

Subsequent analytical methods for natural poly-P, including sequential extraction (e.g., [*Miyata and Hattori*, 1986]) and photometric analysis with basic dyes (e.g., [*Nikata et al.*, 2001]), also proved fruitless. Not until the application of Phosphorus-31 Nuclear Magnetic Resonance (^{31}P-NMR) Spectroscopy was poly-P identified to any significant extent in the environment [*Diaz et al.*, 2008; *Hupfer and Gachter*, 1995; *Hupfer et al.*, 2004; *Kenney et al.*, 2001; *Sannigrahi and Ingall*, 2005].

NMR is a non-destructive bulk analytical technique for the determination of element-specific speciation [*Clark et al.*, 1999; *Hedges et al.*, 2002; *Sannigrahi et al.*, 2005]. In principle, the method is based on the response of atomic nuclei to perturbations in a magnetic field. The resonance frequency emitted following a perturbation event is indicative of the bonding pattern about the nuclei of interest. Thus, NMR offers compositional information on the basis of the relative abundances of major bond classes. In the case of P, these bond classes are P-esters (P-O-C bonds, abundant in P-lipids and nucleic acid), phosponates (P-C bonds), and poly-P.

The widespread prevalence of environmental poly-P became well established first in the study of lake sediments. NMR studies revealed that poly-P accounted for 1-

10% of total P in sediments, and investigators proposed poly-P as a labile source of P that contributes significantly to the release of P during diagenesis [*Hupfer and Gachter*, 1995; *Hupfer et al.*, 2004; *Kenney et al.*, 2001]. Following these discoveries, accounts of substantial poly-P in marine sedimentary environments were put forth (e.g., [*Sannigrahi and Ingall*, 2005; *Schulz and Schulz*, 2005]). As presented in Chapter 3 of this thesis, a paradigm shift in the study of marine poly-P came with the discovery that this important species is directly involved in the geologic sequestration of P [*Diaz et al.*, 2008]. This process takes place through the ability of poly-P to nucleate the precipitation of authigenic apatite, a common and previously enigmatic calcium phosphate mineral that represents the largest sink of P worldwide [*Benitez-Nelson*, 2000; *Diaz et al.*, 2008].

This mechanistic significance of poly-P, combined with the simultaneous detection of natural poly-P not only in sediments and common marine diatoms, but sinking particles and dissolved matter (Chapter 3) [*Diaz et al.*, 2008], has served to solidify the importance of poly-P as a key component of the global marine P cycle and linked ocean-atmosphere-climate system. For example, because P is considered the ultimate limiting nutrient over geologic timescales [*Redfield*, 1958; *Tyrell*, 1999; *Van Cappellen and Ingall*, 1994; 1996], the formation and storage of biogenic poly-P as apatite in sediments forms a negative feedback on nutrient availability and biological productivity. This mechanism, in turn, exerts an indirect influence on the atmospheric greenhouse through its effect on the marine carbon pump.

1.2 Overview of the Marine Phosphorus Cycle

P is a major component of organic matter (e.g., P-lipids, ATP, and DNA) and an essential nutrient for all life on earth. P availability in the environment is typically low, both in marine and terrestrial systems, and can limit biological growth [*Benitez-Nelson*,

2000; *Paytan and McLaughlin*, 2007]. While it is generally accepted that P is the ultimate limiting factor to primary production in the ocean over geologic timescales [*Redfield*, 1958; *Tyrell*, 1999; *Van Cappellen and Ingall*, 1994; 1996], research over the past few decades has also revealed that P is present at limiting concentrations in the ocean over modern timescales [*Benitez-Nelson*, 2000; *Jackson and Williams*, 1985; *Karl et al.*, 1997; *Karl and Yanagi*, 1997; *Krom et al.*, 1991; *MacRae et al.*, 1994]. Thus, through its control of ocean primary productivity, P cycling in the ocean is linked across a broad range of timescales to marine carbon sequestration and therefore global climate.

Riverine inputs represent the largest source of P to the ocean (3-15 $\times$ 10^{10} mol P yr^{-1}) followed by atmospheric deposition (1 $\times$ 10^{10} mol P yr^{-1}) [*Benitez-Nelson*, 2000]. Formation of authigenic apatite and other calcium phosphate mineral phases in marine sediments constitutes the largest sink of P from the ocean, at > 8 $\times$ 10^{10} mol P yr^{-1}. Other important removal mechanisms of marine P are organic matter burial and precipitation with iron oxyhydroxides, each representing approximately 1-5 $\times$ 10^{10} mol P yr^{-1} [*Benitez-Nelson*, 2000]. Global P removal estimates have been repeatedly revised upward over recent years owing to the discovery of new sedimentary sinks, causing estimates of oceanic P residence time to drop from 80,000 years to less than 10,000 [*Benitez-Nelson*, 2000].

Dissolved P in the surface ocean is typically present at concentrations ranging from ~1nM (e.g., Sargasso Sea) to ~1μM (e.g., coastal systems). Dissolved P in the ocean exists in a variety of chemical forms, including the most biologically available form, which is inorganic (ortho)phosphate (PO_4^{3-}) and its derivatives, phosphoric acid (H_3PO_4), dihydrogen phosphate ($H_2PO_4^-$), and hydrogen phosphate (HPO_4^{2-}), the later being the most abundant in the natural pH range of seawater. In oligotrophic regions,

however, P contained in dissolved molecules becomes the more dominant form of P within the dissolved P pool, accounting for up to 75-80% of total dissolved P [*Benitez-Nelson*, 2000; *Björkman and Karl*, 1994]. Out of convention, the pool of dissolved P contained in molecules is operationally defined as dissolved organic P (DOP). However, inorganic molecules such as poly-P represent a substantial fraction of "DOP" [*Young and Ingall*, 2010], thus the term DOP can be misleading and must be interpreted with this caveat in mind. In keeping with convention, however, this thesis will refer to the pool of dissolved P contained in molecules as DOP.

Because most of the global surface ocean is oligotrophic, the pool of DOP represents a substantial source of P to organisms on the planet. Recognizing this reality, much research has focused on characterizing the composition and cycling of the marine DOP pool. Studies have revealed that the DOP pool consists of a variety of biogenic P compounds, which vary in their reactivity bioavailability, and therefore residence time in seawater.

Most information regarding the composition of marine DOP has come from ^{31}P-NMR. Research has shown that the relative proportions of P-esters, poly-P, and phosphonates are approximately constant across a wide variety of marine environments, from oligotrophic to eutrophic and polar, with P-esters accounting for 80% of DOP, and phosphonates and poly-P each accounting for approximately 10% each [*Clark et al.*, 1998; *Diaz et al.*, 2008; *Young and Ingall*, 2010]. Many questions remain regarding the source of phosphonates to the marine environment and the bioavailability of both phosphonates and poly-P.

1.3 Polyphosphate in Organisms

Poly-P is found in representatives of every major group of life [*Brown and Kornberg*, 2004; *Kornberg et al.*, 1999; *Rao et al.*, 2009]. In mammalian organelles and tissues, poly-P is typically present at low concentrations (ppb) between chain lengths of 50 and 800 [*Kornberg et al.*, 1999]. Microorganisms, by comparison, accumulate relatively large amounts of poly-P. For example, certain fungi and bacteria can form poly-P up to 1000's of phosphate groups in length [*Brown and Kornberg*, 2004; *Nesmeyanova*, 2000], and some yeast can accumulate poly-P as high as 10-20% of dry weight [*Brown and Kornberg*, 2004; *Kornberg et al.*, 1999]. While the major source of poly-P to the environment is biological, poly-P can be formed abiotically at volcanic sites and hydrothermal vent systems and was probably present on the prebiotic Earth [*Brown and Kornberg*, 2004; *Yamagata et al.*, 1991]. It has therefore been hypothesized that poly-P could have been a key component in the origin of life, as its polyanionic structure could have served as an efficient scaffold for the synthesis of organic macromolecules [*Brown and Kornberg*, 2004; *Yamagata et al.*, 1991].

The role of poly-P in modern organisms is highly diverse. The most common functions served by poly-P include energy and P storage, sequestration of toxic metal cations, and regulation of pH, osmotic balance, cell development, and gene expression [*Brown and Kornberg*, 2004; *Kornberg et al.*, 1999; *Kulaev and Kulakovskaya*, 2000]. In mammals, for example, poly-P is thought to participate in the regulation of calcification and osteoblast proliferation [*Yamaoka et al.*, 2008]. In some bacteria, e.g. *Acinetobacter* spp., poly-P can act as a substitute and source of ATP in the absense of oxygen as a terminal electron acceptor [*Kornberg et al.*, 1999; *Seviour et al.*, 2003]. In these organisms poly-P is synthesized under aerobic conditions and degraded under anaerobic conditions, making poly-P a redox-sensitive molecule. This property is utilized in the treatment of wastewater for enhanced biological phosphorus removal (EBPR), as

poly-P accumulating organisms are enriched an anaerobic phase and then harvested along with their rich intracellular poly-P reserves in the aerobic phase, leaving behind a phosphorus-clean effluent [*Seviour et al.*, 2003].

According to the current understanding of poly-P metabolism in microbes, organisms accumulate poly-P through two general mechanisms: poly-P overplus and luxury uptake [*Karl and Björkman*, 2002]. Luxury uptake allows organisms to form poly-P when another nutrient other than P limits growth, thereby permitting the organism to accumulate excess P reserves that would become highly valuable under future potential P starvation. For example, Diaz et al. (*2008*) (Chapter 3) measured poly-P concentrations of ~7% in coastal diatoms (*Skeletonema* spp.) under nutrient replete (~0.5 μM phosphate) conditions and hypothesized a luxury uptake response.

On the other hand, poly-P overplus is the process by which P-starved cells assimilate and store large quantities of P in the form of poly-P when P becomes temporarily available. This process could be significant in more oligotrophic systems, where spatio-temporal variability in the P supply is typical. For example, Orchard et al. (*2010*) found that as much as 25% of the cellular P in the cyanobacteria *Trichodesmium* was in the form of poly-P, despite physiological data that indicated the Sargasso Sea colonies were P deplete (~2 nM phosphate). They hypothesized that *Trichodesmium* had taken advantage of small-scale episodic fluxes in P supply [*Orchard et al.*, 2010].

1.4 Organization of this Thesis

As the field of environmental poly-P research expands, the biggest challenge to the growth of this area of study is the establishment of effective analytical techniques. For example, while ^{31}P-NMR has provided vital insight into the cycling of natural poly-P, including findings presented in this thesis, it too has limitations. For example, ^{31}P-NMR

is not particularly sensitive to poly-P, and it does not distinguish between organic and inorganic poly-P forms. Thus, a large part of this thesis has been not only been devoted to the study of poly-P in the environment but also the development of new methods for the study of natural poly-P.

Chapter 2, published in *Limnology & Oceanography: Methods* [*Diaz et al.*, 2009], presents critical experiments relevant to the establishment of X-ray spectromicroscopy (combined spectroscopy and microscopy) as an important and widely useful biological and biogeochemical tool for the characterization of poly-P and associated elements. X-ray fluorescence microscopy is a powerful yet relatively little known methodological tool in the field of environmental science. In particular, this technique can investigate sub-micron scale chemical processes that have eluded analysis by bulk techniques such as NMR and chemical extraction methods, as demonstrated in Chapter 3.

Chapter 3, published in *Science* [*Diaz et al.*, 2008], presents field evidence supporting a new mechanism for the long-term sequestration of the vital nutrient P from marine systems via the initial formation of poly-P in surface waters and its eventual transformation into apatite within sediments. These findings explain a long-standing, fundamental mystery regarding the biogeochemical cycling of P in marine systems by: 1) defining a major component of the P pool (i.e., poly-P) that has not been identified previously in the dissolved or particulate phase to any significant extent, and 2) identifying a mechanism for the transformation of poly-P into apatite, a commonly dispersed mineral whose origin has, until now, remained enigmatic. Combined, these results have worldwide implications for nutrient geochemistry, paleoproductivity and hence, global climate. A key aspect of these results is the application of novel, high sensitivity X-ray methods discussed in Chapter 2 that allow critical questions in P cycling to be addressed for the first time.

Chapter 4, published in *Environmental Science & Technology* [*Diaz and Ingall*, 2010], presents critical experiments in the development of a method for the direct quantification of poly-P in environmental samples. The method is based on the interaction of poly-P with the standard fluorochrome 4',6-diamidino-2-phenylindole (DAPI), commonly used as a stain for nucleic acid. With this technique, oceanographic questions related to poly-P cycling have become newly tractable, such as the study of redox-sensitive P cycling, discussed in Chapter 5.

Chapter 5 presents field data and a set of reactive transport models addressing the role of natural poly-P in redox-sensitive P cycling. Results show that conventional mechanisms for redox sensitive P cycling are insufficient and that poly-P cycling by microbes may account for as much as 35% of the hypoxic release of P in our study site. Through its role in the enhanced regeneration of P that is observed under hypoxic and anoxic conditions in marine systems worldwide, biological poly-P cycling exerts control on atmospheric O_2 content and the global nutrient cycles of P, N, and associated elements, especially due to the modern anthropogenic expansion of oxygen minimum zones [*Naqvi et al.*, 2000; *Rabalais et al.*, 2001; *Stramma et al.*, 2008]. Critical to these findings is the application of the direct DAPI-based fluorometric quantification of inorganic poly-P discussed in Chapter 4.

CHAPTER 2

CHARACTERIZATION OF PHOSPHORUS, CALCIUM, IRON, AND OTHER ELEMENTS IN ORGANISMS AT SUB-MICRON RESOLUTION USING X-RAY FLUORESCENCE SPECTROMICROSCOPY

2.1 Abstract

X-ray spectromicroscopy (combined X-ray spectroscopy and microscopy) is uniquely capable of determining sub-micron scale elemental content and chemical speciation in minimally-prepared particulate samples. The high spatial resolutions achievable with this technique have enabled the close examination of important micro-scale processes relevant to the cycling of biogeochemically important elements. Here, we demonstrate the value of X-ray microscopy to environmental and biological research by examining the phosphorus and metal chemistry of complete individual cells from the algal genera *Chlamydomonas* sp. and *Chlorella* sp. X-ray analysis revealed that both genera store substantial intracellular phosphorus as distinct, heterogeneously distributed granules whose X-ray fluorescence spectra are consistent with that of polyphosphate. Polyphosphate inclusions ranged in size from 0.3-1.4μm in diameter and exhibited a non species-specific average phosphorus concentration of 6.87±1.86μg cm^{-2}, which was significantly higher than the average concentration of phosphorus measured in the total cell, at 3.14±0.98 μg cm^{-2} (95% confidence). Polyphosphate was consistently associated with calcium and iron, exhibiting average P:cation molar ratios of 8.31±2.00 and 108±34, respectively (95%confidence). In some cells, polyphosphate was also associated with potassium, zinc, manganese, and titanium. Based on our results, X-ray spectromicroscopy can provide high-resolution elemental data on minimally-prepared,

Diaz, J., E. Ingall, S. Vogt, M. D. de Jonge, D. Paterson, C. Rau, and J. A. Brandes. 2009. *Limnology & Oceanography: Methods* 7: 42-51.

unsectioned cells that are unattainable through alternative microscopic methods and conventional bulk chemical techniques currently available in many fields of marine chemistry.

2.2 Introduction

The sub-micron scale cycling of metals and nutrient elements by microorganisms are important processes in aquatic systems (e.g., [*Ingall and Jahnke*, 1994; *Van Cappellen and Berner*, 1991]), including transformations involving lower-abundance biogenic compounds (e.g., [*Clark et al.*, 1998; *Diaz et al.*, 2008]). Yet these spatially heterogeneous, cellular-level processes provide a significant analytical challenge, as they typically elude the bulk chemical techniques prevalent in many fields of marine and freshwater research.

For example, over the past fifteen years, bulk methods such as Nuclear Magnetic Resonance (NMR) spectroscopy and sequential extraction techniques have yielded key insights into the chemistry and cycling of particulate phosphorus in aquatic systems. Sediment extraction has enabled examination of the burial pathways that ultimately result in the removal of phosphorus from marine systems. In particular, this technique has revealed that sedimentary phosphorus exists in many dynamic pools, including mineral, organic, and inorganic forms [*Ruttenberg*, 1992; *Ruttenberg and Berner*, 1993; *Slomp et al.*, 2004; *Sutula et al.*, 2004; *Tamburini et al.*, 2003]. Similarly, ^{31}P-NMR has also provided important insights into the composition of phosphorus in marine and freshwater systems. For example, NMR has identified several classes of phosphorus compounds in aquatic environments, including polyphosphates, phosphonates, and phosphorus monoesters and diesters [*Benitez-Nelson et al.*, 2004; *Diaz et al.*, 2008; *Kolowith et al.*, 2001; *Paytan et al.*, 2003; *Sannigrahi and Ingall*, 2005].

High resolution examination of phosphorus content and speciation within minimally prepared particulate samples has become feasible with the recent advent of synchrotron based X-ray technologies [*Brandes et al.*, 2007; *Myneni*, 2002; *Twining et al.*, 2003; *Twining et al.*, 2004a; *Twining et al.*, 2004b]. X-ray spectromicroscopy (combined X-ray spectroscopy and microscopy) is used to map elemental distributions at high spatial resolution and to determine submicron-scale chemical speciation in minimally treated particulate specimens, including complete individual cells. This analytical ability makes X-ray spectromicroscopy a unique tool for examining the storage and cycling of phosphorus and various other elements within cells and detrital material [*Brandes et al.*, 2007; *Diaz et al.*, 2008; *Myneni*, 2002].

In comparison to Electron Microscopy (EM) techniques that offer compositional information at similar or higher spatial resolution, X-ray spectromicroscopy has less restrictive sample requirements and typically results in far less radiation damage to soft specimens [*Cazaux*, 1985; *Glaeser*, 1971; *London et al.*, 1992; *Talmon*, 1987]. For example, Electron Energy Loss Spectroscopy (EELS) can reveal atomic composition, chemical bonding, and the redox state of individual atoms in a specimen, but this technique is limited to ultrathin sample sections (5-50nm) [*Leapman and Ornberg*, 1988] or the surface layers of thicker specimens. Because X-ray spectromicroscopy can analyze thick samples (~10μm) and requires micrograms or less of minimally treated material, it is capable of analyzing complete cells and preserves sample integrity very well.

X-ray spectroscopy and microscopy techniques have been available for general scientific use for more than ten years. These techniques have been applied in marine carbon, iron, and phosphorus studies, and several studies in the materials, atmospheric, biological, and earth sciences [*Bertsch and Hunter*, 2001; *Boese et al.*, 1997; *Brandes et*

al., 2004; *Diaz et al.*, 2008; *Hitchcock and Ishii*, 1987; *Lam et al.*, 2006; *Peak et al.*, 2002; *Twining et al.*, 2003; *Twining et al.*, 2004a; *Twining et al.*, 2004b]. Here, we present X-ray spectromicroscopic data from the examination of two algal species, *Chlamydomonas* sp. and *Chlorella* sp., to demonstrate the potential value of X-ray spectromicroscopy in the environmental and biological sciences, especially nutrient and metal research.

2.3 Materials and Procedures

Many aspects of the X-ray spectromicroscopy experimental procedure depend on the unique technical specifications and set-up of the beamline(s) being used. Every instrument is different. As such, we endeavor to provide enough methodological detail in the following sections to portray the capabilities of the X-ray spectromicroscopy technique in general. Beamline staff are present at synchrotron facilities to provide expert information on the individual instruments that a potential user may operate, and this should be the primary source of information for specific issues related to instrument specifications and use.

X-ray spectromicroscopy relies on the quantized interaction of X-rays with an element's electrons, often the innermost k-shell electrons. In principle, an incident X-ray beam of sufficient energy will eject a bound electron to a higher energy level, and an outer shell electron may relax into the vacated orbital position, emitting a fluorescent X-ray in the process. The sudden increase in X-ray absorption/fluorescence that occurs just above the binding energy of the k-shell electrons corresponds to the k-edge energy of a given element. K-edge energies increase as a function of atomic number, thus the range of elements detectable through X-ray spectromicroscopy is constrained by the energy of the incident X-ray beam [*Kirz et al.*, 1995]. Bulk X-ray spectromicroscopy

studies may be performed using a broad beam, but small structures such as individual cells can be examined at high spatial resolution (~60nm) and high sensitivity (~10^{-18} g cm^{-2}) by employing a focused beam.

X-ray spectromicroscopy involves two independent methods: X-ray spectroscopy and X-ray microscopy. In high sensitivity imaging or microscopy mode, a finely focused, monochromatic X-ray beam is used to probe a defined sample area at a given step size, and energy-specific element signals (principally k-edge intensities) are collected per pixel in order to generate sub-micron resolution elemental distribution maps. The illuminating wavelength should be chosen to be slightly higher than the primary k-edge peak of the heaviest element of interest. Since full fluorescence/absorbance spectra containing all the elemental peaks of interest are acquired at each scan position, co-registration of different elements is ascertained. Thus, a set of elemental maps are constructed simultaneously during a single scan of a specimen. Spectra may be integrated over spatial regions of interest in order to improve the precision in quantifying elemental abundances. Further, elemental maps can be overlain to reveal chemical associations.

X-ray spectroscopy techniques can be used to interrogate sub-micron sized particles identified in elemental maps and thereby determine chemical speciation in a sample. For example, Near Edge X-ray Fluorescence Spectroscopy (NEXFS) and X-ray Absorption Near Edge Spectroscopy (XANES) are common techniques used for this purpose. Whereas XANES detects the initial absorption event that occurs upon bombarding a sample with the X-ray beam, NEXFS is used to measure the X-ray emission event. With soft X-rays (<10keV) and samples containing a substantial fraction of the element of interest, one typically works in absorption contrast, e.g., XANES [*Kirz et al.*, 1995]. With intermediate and hard X-rays, probing elements present only in minor

or trace levels, one often works in fluorescence contrast (e.g., NEXFS). Micro-NEXFS was used in this study because sample thickness variations, such as those inherent in the organisms examined here, create undesirable shifts in absorption spectra baselines.

In micro-NEXFS, the X-ray beam is focused on a particular sample region, and the beam energy is varied across the k-edge of the element of interest in order generate a spectroscopic energy scan of fluorescence intensity. Fine spectral features in NEXFS scans reflect the local bonding environment of an element and thereby reveal compound identity. A compilation of standard phosphorus NEXFS spectra is available in Brandes et al. (*2007)* and Ingall et al. (*2011*).

For X-ray microscopy and X-ray spectroscopy, sample preparations are examined on a Scanning X-ray Microscope (SXM), which uses a series of optical devices to manipulate the energy and size of the X-ray beam (Figure 2.1). A monochromator is used to select a narrow range of incident X-ray energies, and the X-ray beam is focused onto the sample with a Fresnel zone plate. Multiple detectors may be set up to simultaneously measure X-ray absorbance and fluorescence. All components of the SXM are controlled remotely. Samples are bathed in a continuous helium stream during analysis in order to reduce radiation-induced oxidation and minimize interference from atmospheric gases.

To obtain adequate signal from small samples and to filter the X-ray beam to a sufficiently narrow width and energy range, high sensitivity X-ray spectromicroscopy requires a source of bright, high flux light. Sources of such light are presently limited to synchrotron facilities, which produce broad-spectrum electromagnetic radiation by magnetically manipulating electrons cycling at near-relativistic speeds. Synchrotrons typically make instruments available for user experiments through a competitive

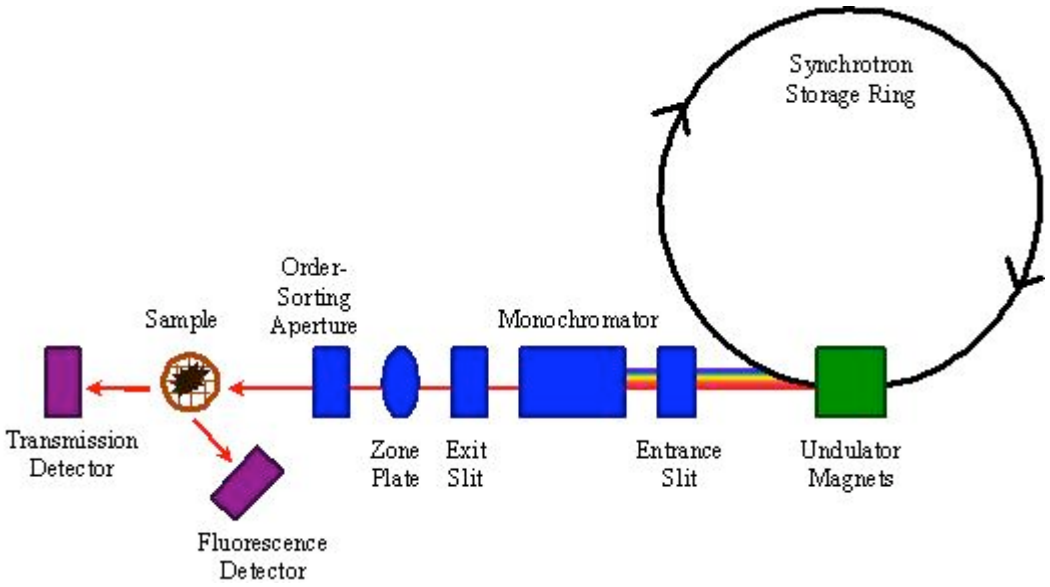

Figure 2.1 Scanning X-ray microscope. Broad-spectrum synchrotron radiation is produced by using magnets to alter the path of an electron beam cycling within the storage ring vacuum chamber. This broad-spectrum light is channeled into a beamline that employs a series of optical devices to produce a monochromatic, highly focused X-ray beam suitable for sample analysis. Specimens are mounted on a motorized stage and analyzed by moving the sample relative to the fixed X-ray beam. Multiple detectors can be set up to collect X-ray fluorescence and transmission/absorbance data. Note: figure is not to scale. Further technical details on the specific instruments used in this study are available in [*McNulty et al.*, 2003].

application process, and many synchrotrons are currently in operation worldwide [*Lehmann et al.*, 2009].

Samples for X-ray spectromicroscopic analysis can be mounted using silicon nitride windows or Transmission Electron Microscopy (TEM) grids that are backed with a supporting film, typically carbon/formvar. Cell mounts are prepared by gently centrifuging preserved cell suspensions (~2800 rpm) directly onto TEM grids [*Twining et al.*, 2003], or cells can be directly deposited onto sample mounts by pipetting several microliters of solution onto the mounting surface. Sediments can also be prepared by pipetting several microliters of a sediment slurry onto the sample mount to produce a thin distribution of particles. Care must be taken to minimize the thickness of samples prepared in this way, as excessive thickness will complicate the spectroscopic signature of the sample. Covered samples should be allowed to dry for several minutes in order to avoid dust and airborne contamination.

Samples are often examined under dehydrated conditions, but some instruments also allow probing of wet and cryo-preserved samples. Sample targets can be relocated on a benchtop light microscope or the SXM using an in-line visual light microscope, if available. TEM finder grids with numeric or alphanumeric grid cell identifications are especially useful for this purpose.

2.4 Assessment

Individual cells of the freshwater algal genera *Chlamydomonas* sp. and *Chlorella* sp. were analyzed at the Advanced Photon Source of Argonne National Laboratory in Argonne, Illinois. Specimens were obtained from Carolina Biological Supply and cultivated in a vitamin-enriched growth medium based on the freshwater medium of [*Chu*, 1942]. Cells were collected and analyzed in early stationary phase.

Experiments were conducted using the X-ray microprobes at beamlines 2-ID-B and 2-ID-E. Fluorescence mapping was performed primarily at the hard X-ray microprobe of station 2-ID-E. While this beamline can access a wide range of X-ray energies (7-17keV), it is optimized to use 10 keV incident X-rays to map most relevant elements (e.g, Al-Zn) at a spatial resolution of 0.25 to 0.5μm. It is a side branch station with a single bounce silicon monochromator and thus cannot vary incident X-ray energies without inducing significant spatial deflection of the X-ray beam. Samples would need to be moved over large distances in response to variations in beam energy, making 2-ID-E incapable of carrying out micro-NEXFS experiments at the spatial resolution of mapping mode.

Micro-NEXFS spectra were generated at station 2-ID-B, which is optimized to conduct X-ray microscopy and spectroscopy using 1-4 keV X-rays at down to 60nm spatial resolution [*McNulty et al.*, 2003]. The use of two separate beamlines for our analysis requires the exact location of sample targets to be known, so as to allow the full examination of the same specimen by both beamlines. Exact coordinates of target cells were initially determined by using a visual light microscope equipped with a motorized x/y stage. Sample coordinates were then translated to the SXM and verified at the beamline using an in-line microscope. Because of the large size of the sample cells used in this study, cells could also be relocated on the X-ray microscope by comparing the X-ray image to photographs of the sample taken on a visual light microscope. Sample alteration between analysis on each beamline may be a concern but was minimal in our experiments, as little X-ray damage was evident on the carbon/formvar backing of the sample mount. The set-up of every X-ray spectromicroscopy beamline is unique, so depending on the experiments being performed, it may not be necessary for every user to employ separate beamlines.

Sample mounts were prepared weeks before X-ray analysis. Algal cultures were preserved with a final concentration of 3% formaldehyde, and fixed cell suspensions were then centrifuged onto carbon/formvar-backed copper TEM grids (150-mesh, Ted Pella). During the drying process and between analysis on each beamline, cell mounts were covered in order to prevent airborne contamination.

A total of thirty-one cells were imaged using X-ray fluorescence microscopy. Regions covering ten to several hundred square microns were interrogated with the X-ray beam in order to simultaneously generate a set of elemental distribution maps (see Figure 2.2 for instrument set-up). In the phosphorus distribution maps of *Chlamydomonas* sp. and *Chlorella* sp. phosphorus localized predominantly as one to several round hotspots. Figure 2.3 presents X-ray fluorescence maps generated from four representative cells, in which this heterogeneous intracellular phosphorus distribution is evident.

For each specimen, elemental content (Si-Zn) was quantified in the phosphorus hotspots, as well as the total cell and background regions. Each of these three regions of interest (ROIs) were manually drawn for every scan using MAPS, a custom X-ray microscopy data processing program [*Vogt*, 2003]. The boundary between the cell and background was ascertained via differential phase contrast, whereas phosphorus hotpots were revealed in phosphorus elemental maps in which the fluorescence intensity was scaled across the entire image. To quantify elemental content for each ROI, per-pixel elemental fluorescence peaks were summed and then corrected for background fluorescence from the carbon/formvar backing (typically <10% of specimen fluorescence). The summed, background-corrected peak of each element was then fit to a summed exponentially modified Gaussian (EMG) peak model using a Marquardt-Levenberg iterative search algorithm in Matlab (version 5.3, MathWorks Corp).

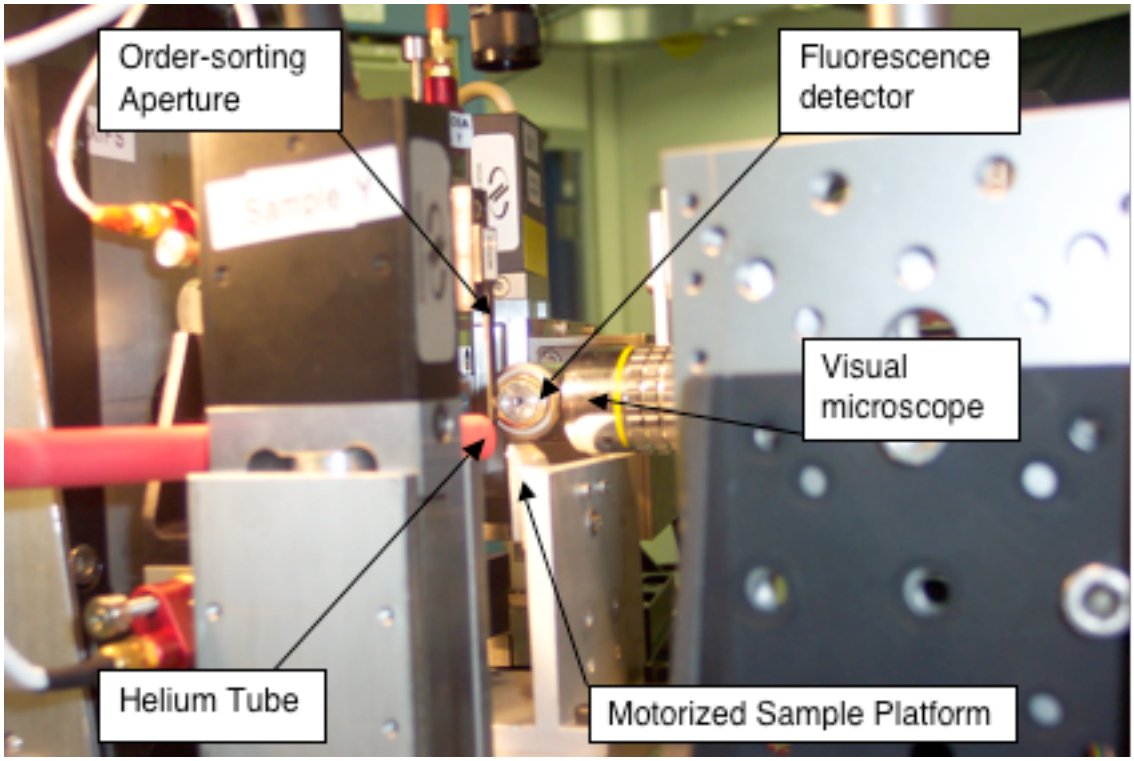

Figure 2.2 Instrument set-up at beamline 2-ID-B. Analyses are performed with multiple X-ray detectors and optical components positioned at millimeter to centimeter distances away from the sample. Instruments are moved using high spatial resolution piezomotors. Specimens (not shown) are mounted onto a mototorized sample platform. A visual microscope is used to locate sample targets prior to analysis. During analysis, the visual microscope is replaced with an Absolutely Calibrated Photodiode (ACP) (not shown) that measures bulk X-ray transmission through the sample. The order-sorting aperture, which helps to focus the X-ray beam onto the sample, is positioned just downstream of the zone plate (not shown), another optical device used for focusing. X-ray fluorescence from the specimen is collected by an energy dispersive fluorescence detector positioned ~17 degrees in front of the sample. Samples are bathed in a continuous stream of helium gas during analysis in order to reduce radiation-induced oxidation and minimize interference from atmospheric gases.

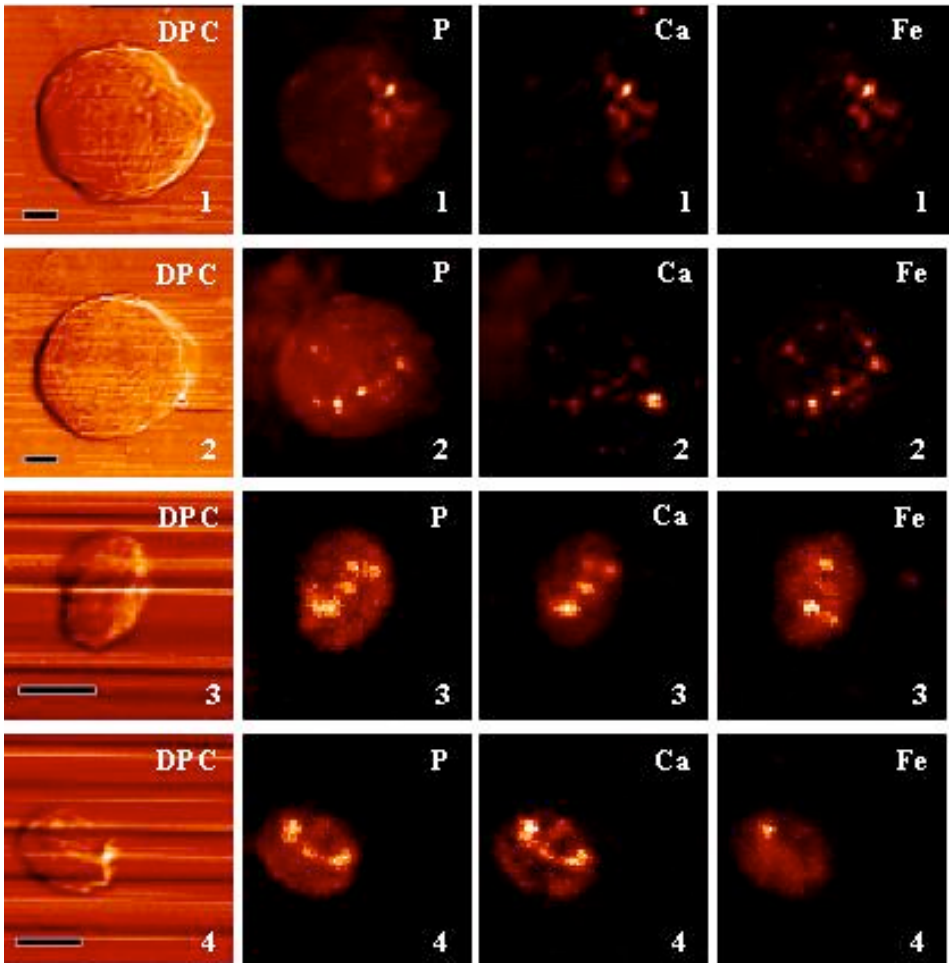

Figure 2.3 Elemental distributions in individual cells of *Chlorella* sp. and *Chlamydomonas* sp. Each row of images depicts data collected from the same single cell. Cells (*1*) and (*2*) are *Chlamydomonas* sp., while cells (*3*) and (*4*) are *Chlorella* sp. X-ray differential phase contrast images (DPC) depict cell boundaries, while X-ray fluorescence maps show the distribution of phosphorus (P), calcium (Ca), and iron (Fe). As evident in these images, intracellular high-concentration phosphorus regions co-localize with calcium and iron. The color bar depicting elemental content in each image is scaled to the maximum concentration in that image. High concentration regions may obscure lower concentration regions. The elemental content of each cell in this figure is given in Table 2.1. Scale bars are 2μm.

Peak areas were used to calculate elemental concentrations (μg cm^{-2}) using the standard peak area:concentration ratios determined from NIST thin-film standards (SRM 1832 and 1833). Additional standard reference materials may be used to independently confirm the accuracy of micro-fluorescence measurements, including standards that better approximate the physical state of the samples being examined (e.g. crystalline v. amorphous structure).

Phosphorus hotspots were similarly sized in each genus (0.3-1.4μm diameter) and exhibited a non species-specific average phosphorus concentration of 6.87±1.86 μg cm^{-2} (95% confidence). This average phosphorus concentration and all other average element concentrations were derived from the ROI elemental content of each specimen and thus represents compositional variation between cells. By comparison to the phosphorus content of hotspots, the non species-specific average phosphorus concentration of the total cell was a significantly lower 3.14±0.98 μg cm^{-2} (95% confidence). Analytical error associated with elemental concentration measurements obtained from the 2-ID-E X-ray fluorescence microprobe was typically less than 10% of the reported value for each element examined. For example, the analytical error associated with phosphorus was 3.2%, while associated error with calcium and iron measurements were 3.1% and 3.9%, respectively. Table 2.1 presents the corresponding elemental concentration data for the images in Figure 2.3.

Micro-NEXFS spectra, normalized for variations in incident beam intensity using a transmission scan on an adjacent clear region of the carbon/formvar grid backing, were collected from the phosphorus-rich regions identified in phosphorus elemental maps. These NEXFS spectra consistently exhibited a single broad peak located at 17-21eV above the phosphorus primary peak (Figure 2.4), which is characteristic of

Table 2.1 Elemental concentrations within individual cells of *Chlamydomonas* sp. and *Chlorella* sp. Data are given for the numbered cells presented in Figure 2.3. Cells (*1*) and (*2*) are *Chlamydomonas* sp., while cells (*3*) and (*4*) are *Chlorella* sp. Elemental concentrations are reported in $\mu g\ cm^{-2}$. Analytical errors associated with the measurement of P, Ca, and Fe are 3.2%, 3.1%, and 3.9% of the reported values, respectively.

	Phosphorus Hotspots within Cell			**Total Cell**			**Background**		
Cell Number in Figure 2.3	P	Ca	Fe	P	Ca	Fe	P	Ca	Fe
1	8.07	5.04	4.29×10^{-1}	2.35	5.73×10^{-1}	5.76×10^{-2}	1.68×10^{-1}	4.67×10^{-2}	2.28×10^{-3}
2	11.16	4.10	5.19×10^{-1}	4.69	6.76×10^{-1}	6.98×10^{-2}	7.89×10^{-1}	6.13×10^{-2}	3.84×10^{-3}
3	2.99	5.54×10^{-1}	4.73×10^{-2}	1.35	1.84×10^{-1}	2.58×10^{-2}	3.40×10^{-2}	2.75×10^{-3}	7.70×10^{-4}
4	4.22	3.63×10^{-1}	6.97×10^{-2}	1.86	1.30×10^{-1}	3.72×10^{-2}	2.85×10^{-2}	3.64×10^{-3}	8.56×10^{-4}

polyphosphate [*Brandes et al.*, 2007]. The presence of polyphosphate in these organisms was confirmed by staining with the standard fluorochrome 4',6-diamidino-2-phenylindole (DAPI), which fluoresces yellow under UV illumination when bound to polyphosphate. Several independent studies have also demonstrated the presence of polyphosphate in cells of *Chlamydomonas* sp. and *Chlorella* sp. [*Eixler et al.*, 2005; *Ruiz et al.*, 2001].

In both *Chlamydomonas* sp. and *Chlorella* sp. the high concentration polyphosphate regions invariably co-localized with calcium and iron (Figure 2.3; Table 2.1). These findings are consistent with observations from independent chemical extraction results, which have shown that algae store substantial intracellular phosphorus as iron and calcium-associated polyphosphate [*Brown and Kornberg*, 2004; *Eixler et al.*, 2005; *Kornberg*, 1995; *Ruiz et al.*, 2001]. Molar P:Ca and P:Fe ratios in polyphosphate were 8.31±2.00 and 108±34, respectively (95% confidence). These values are significantly different than the surrounding cellular P:Ca (average=22.3; $p<<0.01$) and P:Fe (average=160; $p<0.01$). NEXFS spectra lacked any pre-edge features indicative of oxidized Fe association, suggesting that the Fe associated with high phosphorus regions was Fe (II) or only weakly associated with phosphorus. Several NEXFS spectra exhibited weak shoulders above the primary fluorescence peak, which is indicative of association with calcium (Figure 2.4) [*Brandes et al.*, 2007].

Other metals are known to complex with polyphosphate, including zinc, magnesium, manganese, cadmium, and mercury [*Brown and Kornberg*, 2004]. Consistent with the demonstrated metal sequestering capacity of polyphosphate, we found that polyphosphate was variably associated with potassium (75% of scans), zinc (60%), manganese (40%), and titanium (30%). Associations with potassium and manganese were observed in both algae. Zinc associations, in contrast, occurred

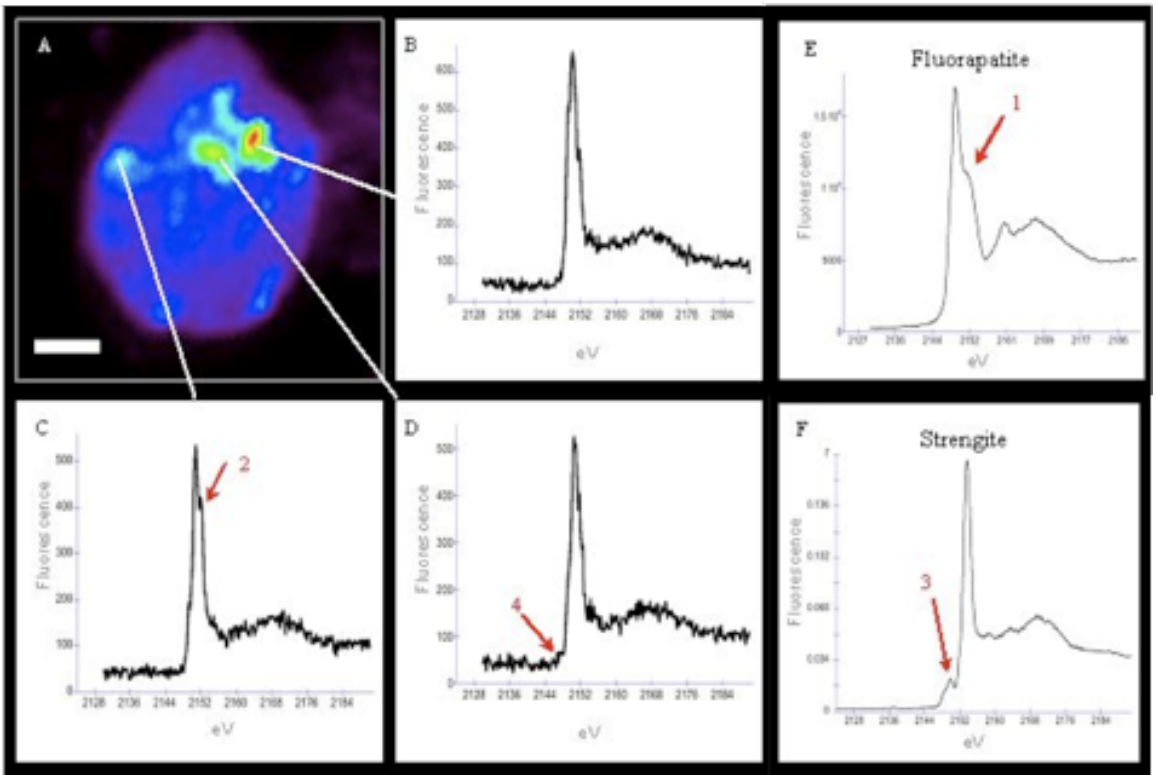

Figure 2.4 Phosphorus speciation in *Chlamydomonas* sp. As shown in the phosphorus distribution map of a typical *Chlamydomonas* sp. specimen examined in this study (A), phosphorus occurs as several round hotspots. These hotspots exhibit phosphorus fluorescence spectra characteristic of polyphosphate (B-D), which exhibits a single broad peak located at 17-21eV above the phosphorus primary peak (2150eV) [*Brandes et al.*, 2007; *Diaz et al.*, 2008]. The appearance of a primary peak shoulder in and only in the phosphorus fluorescence spectra of many calcium phosphate minerals such as igneous fluorapatite (E) is indicative of a calcium-phosphorus association (1) [*Brandes et al.*, 2007]. Some intracellular polyphosphate spectra collected in this study exhibited a small shoulder just above the primary peak (2), indicating association with calcium. As seen in the phosphorus fluorescence spectrum of the oxidized iron-phosphate mineral Strengite (F), a pre-edge peak at ~2146eV reflects association with oxidized iron (3) [*Brandes et al.*, 2007]. However, the spectra collected in this study did not exhibit this feature (4), indicating that intracellular polyphosphate was not associated with oxidized iron in our samples. The scale bar is 2μm.

preferentially in *Chlorella* sp., while titanium associations were observed exclusively in *Chlamydomonas* sp. Several cells of *Chlorella* sp. exhibited potential copper associations, but interfering fluorescence from the copper TEM grid bars overwhelmed the true cellular copper signal. Table 2.2 presents species-specific data regarding the elemental content of cells examined in this study.

Other phosphorus-rich structures present in the cells examined, including nuclei and phospholipids, were not visualized in X-ray fluorescence maps. This result likely occurred because the phosphorus concentrations in these structures may have not been sufficiently higher than the background cellular phosphorus concentration. The phosphorus atoms in these structures are likely not as numerous or closely packed as in a structure like polyphosphate, for instance, which could lead to a much weaker phosphorus fluorescence signal by comparison.

2.5 Discussion

Based on our analyses, X-ray spectromicroscopy generates elemental data at resolutions sufficient for elucidating the concentration and speciation of elements in complete, minimally-prepared cells. This unique methodological capability fills a growing need in environmental and biological research for a technique capable of examining sub-micron scale chemical processes in natural samples without introducing invasive pre-treatment steps. In particular, this method is well suited to the study of organisms that are difficult to culture or otherwise obtain in large quantities as well as fragile organisms that are not easily examined with microscopy methods that require destructive sample manipulation. The richness of data attainable with X-ray spectromicroscopy and the relative ease with which it is applied hold great promise for the study of micro-scale

Table 2.2 Average species-specific elemental content in cells of *Chlamydomonas* sp. and *Chlorella* sp. A large number of elements are detectable with X-ray fluorescence microscopy. Further, elements can be quantified within specific spatial regions of interest identified in X-ray fluorescence maps. In this study, elemental concentrations were determined over 20 X-ray fluorescence microscopy scans, which together comprised 31 total cells. Here, elemental concentrations are given as 95% confidence intervals constructed from the elemental content of individual ROIs. Units are $\mu g\ cm^{-2}$. See text for a discussion regarding the chemistry of phosphorus, calcium, iron and other metals in the organisms investigated.

	***Chlamydomonas* sp.**			***Chlorella* sp.**		
	Phosphorus Hotspots within Cell	Total Cell	Background	Phosphorus Hotspots within Cell	Total Cell	Background
Si	$1.14\pm1.94\times10^{-1}$	$9.10\times10^{-1}\pm1.70\times10^{-1}$	$6.70\times10^{-1}\pm3.55\times10^{-1}$	$3.67\times10^{-1}\pm1.58\times10^{-1}$	$1.76\times10^{-1}\pm9.32\times10^{-2}$	$1.67\times10^{-2}\pm1.11\times10^{-2}$
P	9.57 ± 2.56	4.51 ± 1.46	$6.19\times10^{-1}\pm2.40\times10^{-1}$	4.16 ± 1.5	$1.77\pm6.66\times10^{-1}$	$5.90\times10^{-2}\pm3.65\times10^{-2}$
S	$1.18\pm2.33\times10^{-1}$	$8.29\times10^{-1}\pm1.7\times10^{-1}$	$8.42\times10^{-2}\pm2.48\times10^{-2}$	$3.71\times10^{-1}\pm8.96\times10^{-2}$	$2.67\times10^{-1}\pm6.75\times10^{-2}$	$1.23\times10^{-2}\pm6.36\times10^{-3}$
Cl	$3.00\times10^{-1}\pm2.32\times10^{-1}$	$2.53\times10^{-1}\pm1.60\times10^{-1}$	$9.54\times10^{-2}\pm5.58\times10^{-2}$	$3.28\times10^{-1}\pm1.63\times10^{-1}$	$2.39\times10^{-1}\pm1.07\times10^{-1}$	$1.61\times10^{-2}\pm4.02\times10^{-3}$
Ar	$1.82\times10^{-2}\pm7.37\times10^{-3}$	$1.10\times10^{-2}\pm4.28\times10^{-3}$	$2.12\times10^{-2}\pm1.69\times10^{-3}$	$1.14\times10^{-2}\pm7.07\times10^{-3}$	$1.22\times10^{-2}\pm3.73\times10^{-3}$	$2.41\times10^{-2}\pm9.30\times10^{-4}$
K	$4.30\times10^{-1}\pm2.51\times10^{-1}$	$2.29\times10^{-1}\pm1.67\times10^{-1}$	$2.03\times10^{-2}\pm1.81\times10^{-2}$	$6.53\times10^{-1}\pm2.83\times10^{-1}$	$3.69\times10^{-1}\pm1.57\times10^{-1}$	$1.37\times10^{-2}\pm7.33\times10^{-3}$
Ca	2.86 ± 1.24	$4.39\times10^{-1}\pm1.39\times10^{-1}$	$1.89\times10^{-1}\pm1.55\times10^{-1}$	$5.06\times10^{-1}\pm1.52\times10^{-1}$	$1.19\times10^{-1}\pm4.14\times10^{-2}$	$4.65\times10^{-3}\pm2.08\times10^{-3}$
Ti	$1.55\times10^{-2}\pm6.07\times10^{-3}$	$5.63\times10^{-3}\pm4.67\times10^{-3}$	$2.45\times10^{-3}\pm1.63\times10^{-3}$	$1.09\times10^{-3}\pm3.79\times10^{-4}$	$7.06\times10^{-4}\pm2.19\times10^{-4}$	$1.83\times10^{-4}\pm1.03\times10^{-4}$
Cr	$7.52\times10^{-4}\pm2.1\times10^{-4}$	$2.89\times10^{-4}\pm8.93\times10^{-5}$	$3.57\times10^{-4}\pm3.25\times10^{-4}$	$4.42\times10^{-4}\pm1.63\times10^{-4}$	$1.61\times10^{-4}\pm5.05\times10^{-5}$	$1.02\times10^{-4}\pm1.98\times10^{-5}$
Mn	$7.96\times10^{-3}\pm4.44\times10^{-3}$	$2.41\times10^{-3}\pm7.09\times10^{-4}$	$5.40\times10^{-4}\pm2.06\times10^{-4}$	$1.10\times10^{-2}\pm1.31\times10^{-2}$	$6.12\times10^{-3}\pm7.21\times10^{-3}$	$3.07\times10^{-4}\pm2.14\times10^{-4}$
Fe	$2.78\times10^{-1}\pm9.03\times10^{-2}$	$5.54\times10^{-2}\pm8.00\times10^{-3}$	$6.69\times10^{-3}\pm4.01\times10^{-3}$	$6.24\times10^{-2}\pm2.88\times10^{-2}$	$2.28\times10^{-2}\pm6.52\times10^{-3}$	$1.04\times10^{-3}\pm2.03\times10^{-4}$
Co	$1.87\times10^{-3}\pm5.62\times10^{-4}$	$1.45\times10^{-3}\pm4.63\times10^{-4}$	$4.79\times10^{-4}\pm3.74\times10^{-4}$	$5.50\times10^{-4}\pm3.20\times10^{-4}$	$4.91\times10^{-4}\pm1.48\times10^{-4}$	$1.41\times10^{-4}\pm8.18\times10^{-5}$
Ni	$1.47\times10^{-3}\pm1.33\times10^{-3}$	$1.36\times10^{-3}\pm1.09\times10^{-3}$	$1.08\times10^{-3}\pm1.29\times10^{-3}$	$7.30\times10^{-4}\pm5.04\times10^{-4}$	$5.69\times10^{-4}\pm4.02\times10^{-4}$	$4.22\times10^{-4}\pm3.20\times10^{-4}$
Cu	$5.32\times10^{-1}\pm5.42\times10^{-1}$	$5.74\times10^{-1}\pm6.53\times10^{-1}$	$6.76\times10^{-1}\pm9.36\times10^{-1}$	$3.86\times10^{-1}\pm2.72\times10^{-1}$	$3.34\times10^{-1}\pm2.49\times10^{-1}$	$3.10\times10^{-1}\pm2.40\times10^{-1}$
Zn	$2.20\times10^{-1}\pm1.98\times10^{-1}$	$1.36\times10^{-1}\pm1.18\times10^{-1}$	$3.39\times10^{-1}\pm3.93\times10^{-1}$	$6.63\times10^{-2}\pm6.32\times10^{-2}$	$1.58\times10^{-2}\pm5.46\times10^{-3}$	$1.40\times10^{-3}\pm4.68\times10^{-4}$

biogeochemical processes that have until now eluded close examination by conventional bulk techniques. These processes may include cellular-level storage and conversion of biogeochemically important elements as well as diagenetic processes in sediments. For example, *Diaz et al.* (2008) used X-ray spectromicroscopy to show that polyphosphate chemically converts into calcium phosphate minerals in marine sediments, thereby explaining a long-standing mystery regarding phosphorus sequestration in the ocean.

Several issues may slow the widespread use of X-ray spectromicroscopy in future research. The largest obstacle facing the expansion of X-ray spectromicroscopy as a prevalent technique is the limited availability of suitable X-ray sources. Instruments may become more readily accessible over the next decade as tunable free-electron laser sources are developed to create lower resolution laboratory X-ray microprobes capable of reaching a broad range of X-ray energies [*Jacobsen*, 2000]. In addition, more standard materials must be analyzed before X-ray spectromicroscopy can become more widely used. These standard libraries are growing as we and other groups compile sets of NEXFS and XANES spectra from chemically well-known organic, inorganic, and mineral compounds, e.g [*Ingall et al.*, 2011].

Ideally, features in micro-NEXFS spectra should be defined in absolute terms. Unfortunately, drifts in monochromator position during sample analysis can cause entire spectra to shift by ±2eV [*Brandes et al.*, 2007]. Monochromator drift poses a significant problem with respect to organic phosphorus compounds, whose X-ray spectra can differ by as little as a single eV shift in primary peak position [*Myneni*, 2002]. In many cases, monochromator drift can be compensated for by characterizing spectral features relative to the primary fluorescence peak. Alternatively, incorporation of an in-line standard would maintain instrument calibration. For example, a calibration stick consisting of

standard mineral apatite powder has recently been included on the beamline 2-ID-B at the Advanced Photon Source [*de Jonge et al.*, 2010b].

The maximum spatial resolutions achievable in this study (60-200nm) make X-ray spectromicroscopy ideal for mapping cells as small as 3μm. While smaller organisms may not be sufficiently resolved in X-ray micrographs at the moment, cellular elemental contents may nevertheless be measured in imaging mode. Small, flat cells are still challenging to locate on the SXM using strictly visible light and/or X-ray differential phase contrast, however.

The use of standard microscopy techniques as a complement to X-ray spectromicroscopy may improve the ability to distinguish among intracellular structures with similar compositions. In some cases for example, nuclei and polyphosphate may be difficult to distinguish in X-ray fluorescence maps because they both contain significant amounts of polymeric orthophosphate. By using a nucleoid stain such as DAPI as a complement to X-ray micrcographs, nuclei and polyphosphate can be easily distinguished. Another illustration of this principle is the ability to distinguish autofluorescing chloroplasts from other potential Fe-rich cellular regions.

X-ray spectromicroscopy can provide elemental concentrations based on the integration of fluorescence spectra defined within a two-dimensional region of interest. Until high spatial resolution spectromicroscopy is combined with three dimensional techniques such as X-ray tomography [*de Jonge et al.*, 2010a], per volume estimates of elemental concentration must be determined using simplifying geometrical assumptions. Alternatively, elemental content can be expressed relative to an entire cell. Because absolute elemental contents are determined using three-dimensional fluorescence signals, however, molar ratios in a defined region of interest represent a per volume estimate.

As achieved through the X-ray imaging and spectroscopic methods demonstrated in this study, the sub-micron scale elemental analysis of particles in complete cells complements existing data and can illuminate enigmatic microbial and other sub-micron scale processes involved in the biogeochemical cycling of nutrients and trace metals.

2.6 Comments and Recommendations

Important aspects of the X-ray spectromicroscopic procedure to mention here include precautions regarding sample mounting and X-ray damage. Salts must be removed from marine samples prior to analysis, by washing fixed cells either before or after mounting. Otherwise, fluorescence from salts that precipitate during the drying process will obscure lower-intensity intracellular element signals. Mounting devices must be composed of a material other than the element of interest. Sample damage resulting from overexposure to the X-ray beam is also an issue. Precautions must be taken to protect the sample while data is not being acquired, and it is important to note that sample damage makes any post X-ray analyses difficult. Overall, the relatively non-invasive sample preparation required for this method requires few adaptations for examining organisms and sediments in a variety of fresh water and marine environments.

2.7 Acknowledgements

This work was funded by the National Science Foundation under Grant No. 0526178. Use of the Advanced Photon Source was supported by the US Department of Energy, Office of Science, Office of Basic Energy Sciences, under Contract No. DE-AC02-06CH11357. The authors thank Dr. Marshall Darley of the University of Georgia,

Department of Plant Biology, for providing the specimens examined in this study. Thanks also go to Ian McNulty at the Advanced Photon Source for technical assistance.

CHAPTER 3

MARINE POLYPHOSPHATE: A KEY PLAYER IN GEOLOGIC PHOSPHORUS SEQUESTRATION

3.1 Abstract

The *in situ* or authigenic formation of calcium phosphate minerals in marine sediments is a major sink for the vital nutrient phosphorus. However, because typical sediment chemistry is not kinetically conducive to precipitation of these minerals, the mechanism behind their formation has remained a fundamental mystery. Here, we present evidence from high-sensitivity X-ray and electrodialysis techniques to describe a mechanism by which abundant diatom-derived polyphosphates play a critical role in the formation of calcium phosphate minerals in marine sediments. This mechanism can explain the puzzlingly dispersed distribution of calcium phosphate minerals observed in marine sediments worldwide.

3.2 Results and Discussion

Phosphorus is a vital macronutrient that profoundly influences global oceanic primary production on both modern and geologic timescales [*Benitez-Nelson*, 2000; *Van Cappellen and Ingall*, 1996]. Over the past several decades, the residence time of phosphorus in the ocean has been repeatedly revised down-wards as new sedimentary sinks have been discovered [*Benitez-Nelson*, 2000; *Paytan et al.*, 2003]. Among these new sinks are ubiquitous fine-grained authigenic apatite minerals [*Ruttenberg and Berner*, 1993], whose origin is enigmatic [*Van Cappellen and Berner*, 1991]. Given the

---

Diaz, J., E. Ingall, C. Benitez-Nelson, D. Paterson, M. D. de Jonge, I. McNulty, J. A. Brandes. 2008. *Science* 320: 652-655.

strong influence of this mineral sink on the global cycling of phosphorus and its potential impact on long-term nutrient availability and biological production, understanding the underlying mechanisms that lead to the formation and burial of apatite in modern and ancient sediments is critically important. Here, we show that polyphosphate is a key component in the formation of apatite in marine sediments.

Polyphosphate is a relatively understudied component of the marine phosphorus cycle. A linear polymer of orthophosphate units linked by phosphoanhydride bonds (Figure 1.1), polyphosphate is present in cells as dense, calcium-associated cytoplasmic inclusions [*Brown and Kornberg*, 2004]. Under phosphate-enriched conditions, cultured marine algae synthesize polyphosphate as a luxury nutrient reserve [*Lawerence et al.*, 1998; *Mateo et al.*, 2006; *Miyata et al.*, 1986; *Perry*, 1976; *Romans et al.*, 1994; *Solorzano and Strickland*, 1968]. The biological synthesis of significant amounts of polyphosphate in natural marine systems, in contrast, has been hypothesized to be inconsequential [*Perry*, 1976], as phosphorus is present at biologically limiting concentrations in much of the global ocean [*Benitez-Nelson*, 2000; *Paytan and McLaughlin*, 2007]. Correspondingly, investigations into the composition of marine biogenic phosphorus compounds have typically focused on organic forms [*Benitez-Nelson*, 2000; *Karl and Björkman*, 2002]. The lack of commonly used analytical techniques that cleanly evaluate polyphosphate within samples has further resulted in a paucity of research on the importance of this phase. With the recent development of high-resolution X-ray spectromicroscopy methods, various particulate organic, mineral, and polymeric phosphorus-containing phases like polyphosphate can now be identified and mapped at sub-micron scales. In addition, a new combined electrodialysis/reverse osmosis technique allows for a more comprehensive examination of phosphorus composition in the dissolved phase. We have developed insights into the origin and

transformation of marine polyphosphate through the application of these high-resolution X-ray [*Brandes et al.*, 2007] and high-recovery electrodialysis [*Vetter et al.*, 2007] techniques.

Organisms, sediments, and dissolved and particulate matter were collected during April and July 2007 from Effingham Inlet, a Pacific fjord located on Vancouver Island, British Columbia (Figure 3.1). During the spring bloom of April 2007, intracellular polyphosphate inclusions were observed in individual diatoms, including the globally ubiquitous and abundant *Skeletonema* spp. (Figure 3.2). Based on bulk ^{31}P-NMR characterization of the spring bloom plankton community, inorganic polyphosphate represented a substantial 7% of total phosphorus in surface water biomass. Surface water dissolved phosphate concentrations were 0.5μM, which reflects a level of

Figure 3.1 Effingham Inlet. The study site is circled in red.

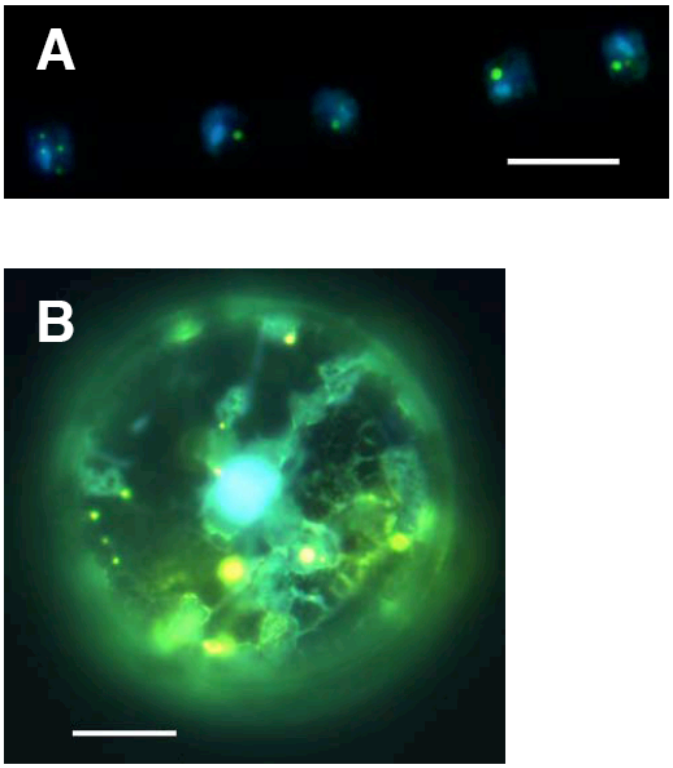

Figure 3.2 Polyphosphate in diatoms collected from Effingham Inlet. Cells collected from the coastal waters of Effingham Inlet, British Columbia, were fixed and stained with the standard fluorochrome 4',6-diamidino-2-phenylindole (DAPI). In our samples, DAPI not only revealed cell nuclei (blue) but also many large intracellular polyphosphate inclusions (yellow to green), as seen in (A) *Skeletonema* sp. and (B) a solitary centric diatom. This image shows that plankton collected from natural marine waters synthesize polyphosphate at non-enriched, sub-micromolar dissolved phosphate concentrations that are typical of many regions in the global ocean. Scale bars are 10μm.

phosphorus availability typical of coastal marine systems. Nutrient ratios were also consistent with phosphorus limitation in our field site (N/P=~40). By comparison, in laboratory cultures with enriched ~1-10μM phosphate concentrations, *Skeletonema* spp. and *Thalassiosira* spp. can accumulate polyphosphate to correspondingly high levels of 30% and 19-43% of total cellular phosphorus, respectively [*Perry*, 1976; *Solorzano and Strickland*, 1968]. Notably, the population of diatom-dominated plankton in Effingham Inlet exhibited near-Redfield elemental stoichiometry, with a molar C:N:P composition of 188:16:1. The presence of substantial polyphosphate in these organisms thus appears not to alter their elemental content relative to the classic composition of marine phytoplankton. This finding suggests that inorganic polyphosphate, rather than being a novel intracellular phosphorus pool inconsistent with Redfield stoichiometry, has conventionally been quantified as a component of organic biomass.

Polyphosphate can exist within a range of sizes and molecular weights inside cells, depending on the length of the polyphosphate polymer. Destruction of polyphosphate-containing diatoms by zooplankton grazing, viral infection, and senescence may liberate the intracellular contents of these cells, including variably sized polyphosphate inclusions. Consistent with these processes, we observed significant polyphosphate in the <0.45μm fraction of dissolved matter. In sub-surface seawater samples processed by the high-recovery electrodialysis/reverse osmosis technique [*Vetter et al.*, 2007], polyphosphate accounted for ~11% of the total dissolved phosphorus pool. Previous dissolved matter characterizations do not report polyphosphate [*Clark et al.*, 1999; *Kolowith et al.*, 2001; *Sannigrahi et al.*, 2006], likely due to the lower-recovery methods used in these studies. By adding the critical step of deionizing seawater samples prior to concentrating dissolved molecules, the combined

electrodialysis/reverse osmosis technique can isolate up to 90% of marine dissolved matter, the highest recovery yet possible [*Vetter et al.*, 2007].

In addition to dissolved matter, polyphosphate was also present in sinking particles, representing 7% of total phosphorus in sinking material. Individual diatoms containing intracellular polyphosphates were observed throughout the water column, which suggests that sinking polyphosphate reaches the sediment protectively encased within intact cells. Indeed, diatoms have been shown to play major roles in the mineral-ballasted transport of material to depth [*Armstrong et al.*, 2001; *Buesseler et al.*, 2007]. Table 3.1 summarizes our results on the polyphosphate, total phosphorus, and biogenic silica composition of major phosphorus pools investigated in this study. Mass balance estimates based on these data demonstrate that plankton-derived polyphosphate can account for the entire polyphosphate content of sinking particles.

Table 3.1 Key chemical parameters of major phosphorus pools. Polyphosphate content for each pool was measured by ^{31}P-NMR. Total phosphorus and percent by weight biogenic silica content were determined using standard chemical techniques. Where available, error estimates represent measurement reproducibility based on replicate analyses. Analytical errors associated with the polyphosphate measurement are ±10% of the reported value. For example, a polyphosphate measurement of 7% would have an associated error of ±0.7%. Replicate total phosphorus measurements agreed to within <5%.

	Polyphosphate (% total P)	Total P (μmol g^{-1})	Biogenic Silica (% w/w)
Plankton	7	123.0 ± 1.7	40.4 ± 1.4
Dissolved Matter	11	17.4	--
Sinking Particles	7	59.76 ± 0.42	43.7 ± 2.3
Surface sediment	8*	44.71	12.08 ± 0.65

*Data from [*Sannigrahi and Ingall*, 2005]

To make this calculation, the concentration of polyphosphate in plankton and sinking material can be expressed relative to biogenic silica content, which is roughly conserved between these two pools. Using the total phosphorus concentrations of plankton and sinking particles, the silica-normalized polyphosphate content of sinking material is ~ 45% of that in organisms. This estimate, although based on a single particle flux measurement, shows that plankton are a plausible and sufficient source for the polyphosphate found in sinking material.

Bacterial decomposition of the organic diatom frustule matrix results in rapid dissolution of the mineral shell [*Bidle and Azam*, 1999] and the consequent release of polyphosphate and other cellular contents to the sediment environment. This scenario is consistent with the relatively low biogenic silica content of Effingham Inlet surface sediments (Table 3.1) and with microscopy results showing damaged and vacant diatom frustules in sediments. In addition, high resolution X-ray spectromicroscopy methods [*Brandes et al.*, 2007] revealed an abundance of free 0.5-3μm polyphosphate granules in surface sediments. This size range is similar to that observed within diatoms, again suggesting a diatom source.

X-ray fluorescence data indicated that among the hundreds of phosphorus rich particles identified in our sediment samples, ~ 50% were polyphosphate, with the remaining fraction comprised of apatite, a common calcium phosphate mineral (Figure 3.3). Previous ^{31}P-NMR analysis of Effingham Inlet surface sediments has shown that polyphosphate accounts for 8% of total phosphorus in surface sediment samples [*Sannigrahi and Ingall*, 2005]. In other studies, polyphosphate has eluded detection by bulk techniques such as ^{31}P-NMR because such methods are relatively insensitive to the presence of less prevalent phases. Because synchrotron-based X-ray spectromicroscopy is unique in its capacity to simultaneously image and chemically

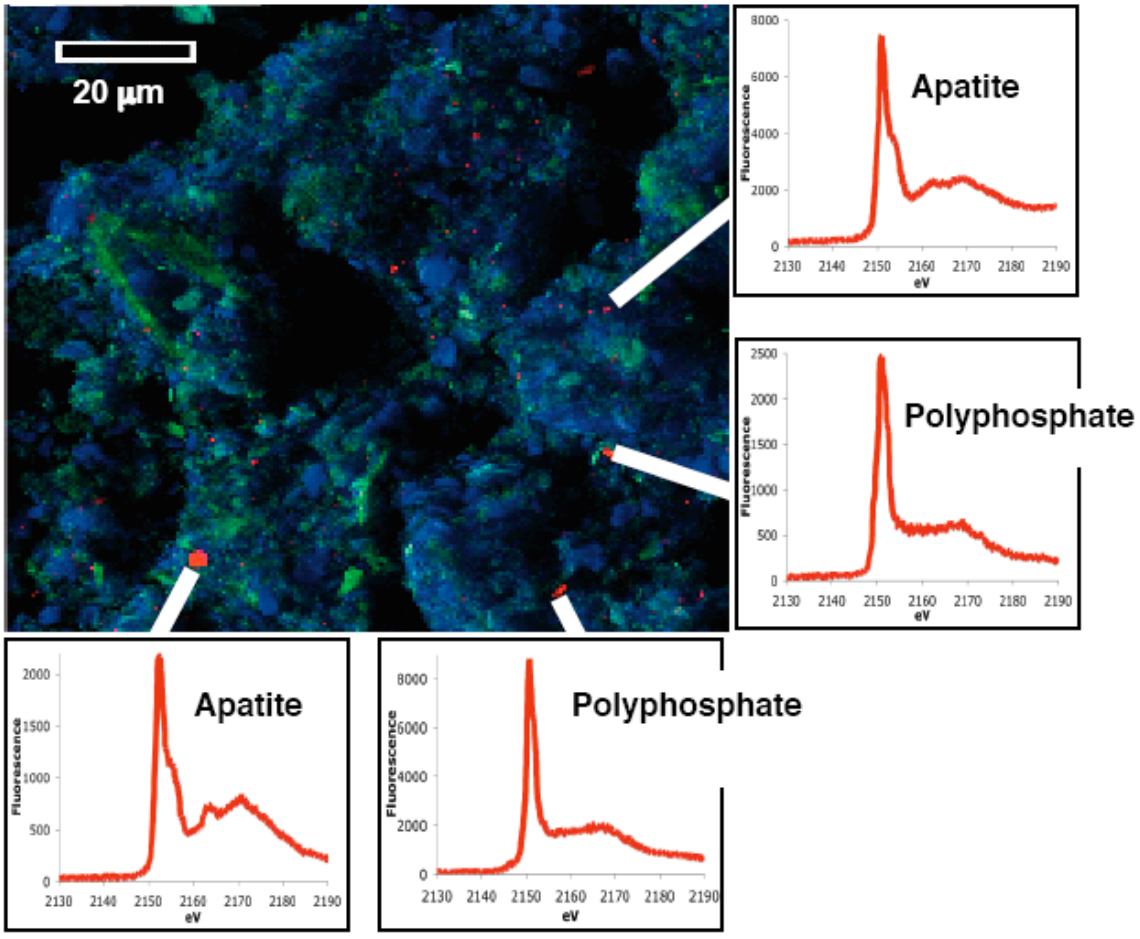

Figure 3.3 X-ray fluorescence micrograph and fluorescence spectra of phosphorus-rich regions in Effingham Inlet sediment. Sedimentary phosphorus (red) appears as distinct, heterogeneously distributed sub-micron sized particles against a comparatively uniform background of sedimentary aluminum (blue) and magnesium (green). Based on high resolution X-ray spectroscopic characterization, about half of the 147 phosphorus rich regions examined in our samples were found to be polyphosphate, while the other half were classified as apatite, a common calcium phosphate mineral.

characterize minimally-prepared particulate samples at sub-micron resolution, this highly sensitive method is key to the direct identification of less prevalent phases in a wide variety of environments [*Brandes et al.*, 2007].

Our findings demonstrate that marine polyphosphate accounts for 7-11% of the phosphorus in dissolved and particulate pools (Table 3.1). This level of abundance is comparable to that of more commonly identified organic phosphorus forms. For example, phosphonates typically represent ~ 3% of total phosphorus in fresh organic matter [*Clark et al.*, 1998]. The relative polyphosphate contents of plankton, sinking particulates, and sediments are nearly identical in our samples (Table 3.1). The consistency of the polyphosphate signal throughout the water column and surface sediment suggests that extracellular polyphosphate may not be readily bioavailable. Rapid enzymatic hydrolysis of polyphosphate by benthic microbes has been observed to occur, but only intracellularly [*Schulz and Schulz*, 2005]. Because the phosphoanhydride bonds linking orthophosphate units of polyphosphate are relatively stable in the absence of hydrolytic enzymes [*Brown and Kornberg*, 2004], free sedimentary polyphosphate may be an efficient storage form of phosphorus over long periods. Indeed, using X-ray analysis, we observed the presence of extracellular polyphosphate in Effingham Inlet sediments up to 60 years old, which suggests that a portion of the free sedimentary polyphosphate pool is not remobilized over decadal timescales.

Though a portion of the sedimentary polyphosphate pool may be relatively stable, mass balance calculations reveal that some polyphosphate is removed from surface sediments over relatively short timescales. Using the bulk sediment trap flux from our field site (136 g m^{-2} y^{-1}), the sedimentary flux of polyphosphate is estimated to be 48 μg P m^{-2} d^{-1}. The accumulation rate of polyphosphate in recent (< 3 year-old) sediments

from Effingham Inlet is 86% of this flux, based on the polyphosphate and total phosphorus content of surface sediments (Table 3.1). This disparity reflects a 14% loss of polyphosphate in surface sediments, a loss that may increase as sediments age.

The loss of sedimentary polyphosphate in sediments does not necessarily indicate that phosphorus is remobilized from polyphosphate particles. Rather, as evidence from X-ray spectromicroscopy reveals, the relative stability of free sedimentary polyphosphate permits diagenetic transformations that result in the long-term sequestration of phosphorus. In addition to demonstrating that polyphosphate and apatite are prevalent in sediments from Effingham Inlet, results from X-ray spectromicroscopy also showed an abundance of fine, dispersed particles that exhibit spectral features transitional between pure polyphosphate and apatite (Figure 3.4). Polyphosphate thus appears to nucleate authigenic apatite growth, thereby converting surface water derived polyphosphate to stable phosphorus containing mineral phases that reside in sediments over geologic timescales.

Authigenic apatite formation in marine sediments has been recognized in numerous studies as an important phosphorus sink [*Ruttenberg and Berner*, 1993]. However, the processes leading to the precipitation and growth of these authigenic apatites are not well understood. Massive apatitic phosphorite deposits that account for as much as 25% of total phosphorus in the sediments underlying major coastal upwelling zones may be related to the activity of polyphosphate accumulating sulfur bacteria [*Schulz and Schulz*, 2005]. Enzymatic hydrolysis of intracellular polyphosphate by these bacteria releases considerable amounts of dissolved phosphate to sediment porewaters. As a result, porewaters achieve the high degree of supersaturation required to overcome

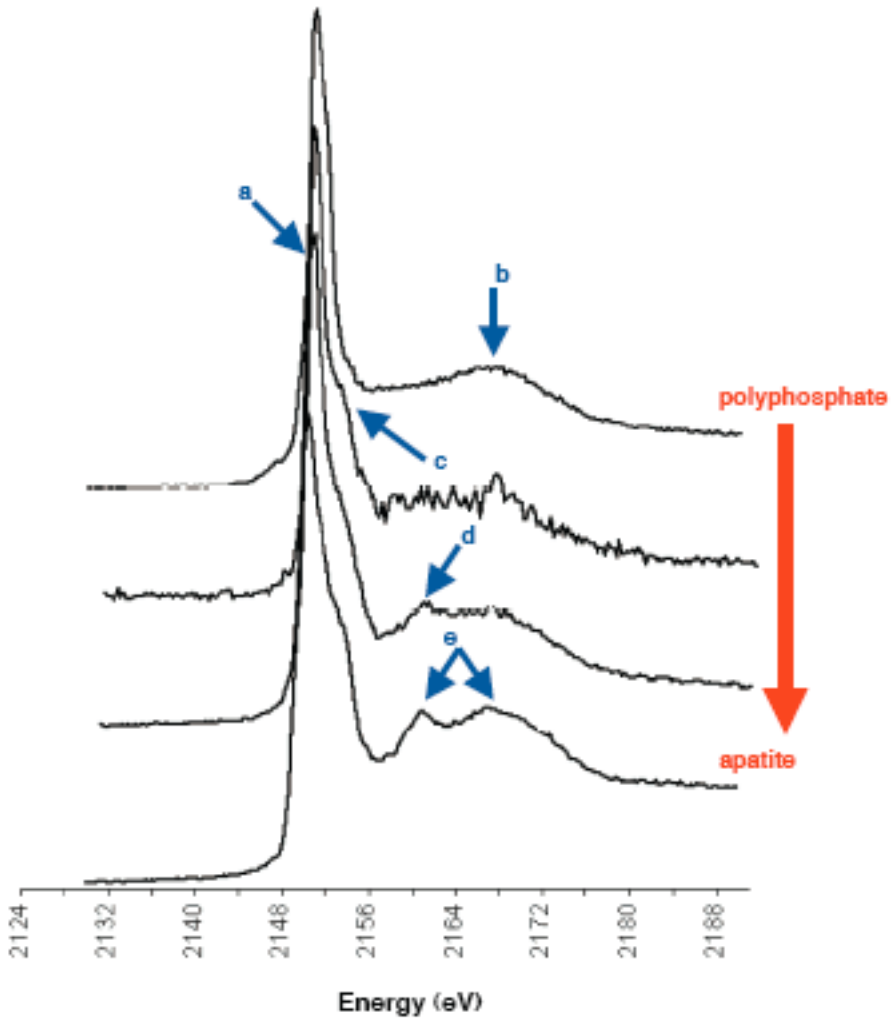

Figure 3.4 Diagenetic transformation of polyphosphate to apatite. An overlay of phosphorus X-ray fluorescence spectra collected from micron-sized phosphorus-rich regions in Effingham Inlet sediment illustrates the diagenetic transition from polyphosphate (top) to apatite (bottom). The primary phosphorus fluorescence peak occurs at 2150eV (a). Spectral features above the primary peak reflect the local bonding environment of phosphorus. Polyphosphate, a simple linear polymer associated with calcium in cells, is characterized by a single peak 18eV above the primary peak (b). In the diagenetic transition from polyphosphate to apatite, the association between phosphorus and calcium becomes more crystalline, which may account for the appearance of a primary peak "shoulder" (c). As the crystalline mineral matrix develops further, a peak 11eV above of the primary peak appears (d), and secondary peaks become more defined (e). The spectra presented in this figure were collected from a single Effingham Inlet sediment sample less than three years in age. Thus, the relative ages of the particles that yielded these spectra are not known.

the kinetic nucleation barrier to apatite precipitation, and substantial apatite formation consequently occurs [*Schulz and Schulz*, 2005].

In contrast to the massive apatite-rich phosphorite formations characteristic of coastal upwelling zones, however, most marine sediments worldwide possess dispersed, fine-grained authigenic apatites that comprise a comparatively small 9-13% of total sedimentary phosphorus [*Ruttenberg and Berner*, 1993]. The relatively modest accumulation of authigenic apatite that is typical of sediments in non-upwelling zones nevertheless represents a substantial phosphorus sink, due to the much larger areal extent of these environments [*Ruttenberg and Berner*, 1993]. Authigenic apatite formation in these non-upwelling areas may not involve an episodic mechanism to produce high concentrations of dissolved phosphate, however. Rather, our results show that dispersed grains of sedimentary polyphosphate may nucleate apatite growth directly and non-episodically, reducing or removing the nucleation barrier by acting as a mineral template. As noted previously, calcium is associated with polyphosphate in cells [*Brown and Kornberg*, 2004]. The presence of highly concentrated sedimentary phosphorus regions with this calcium association may result in eventual apatite formation without extensive interaction with the free sedimentary phosphate pool. We observed the transition from polyphosphate to apatite within surficial sediments less than three years in age, suggesting that apatite formation from a polyphosphate template may occur over relatively short timescales.

The transport of polyphosphate from its planktonic origin in surface waters to underlying sediments, followed by subsequent diagenetic transformation into stable calcium phosphate minerals provides a “biological pump” mechanism for the geologic sequestration of water column-derived marine phosphorus (Figure 3.5). The polyphosphate accumulating diatoms observed in this study are common in the global

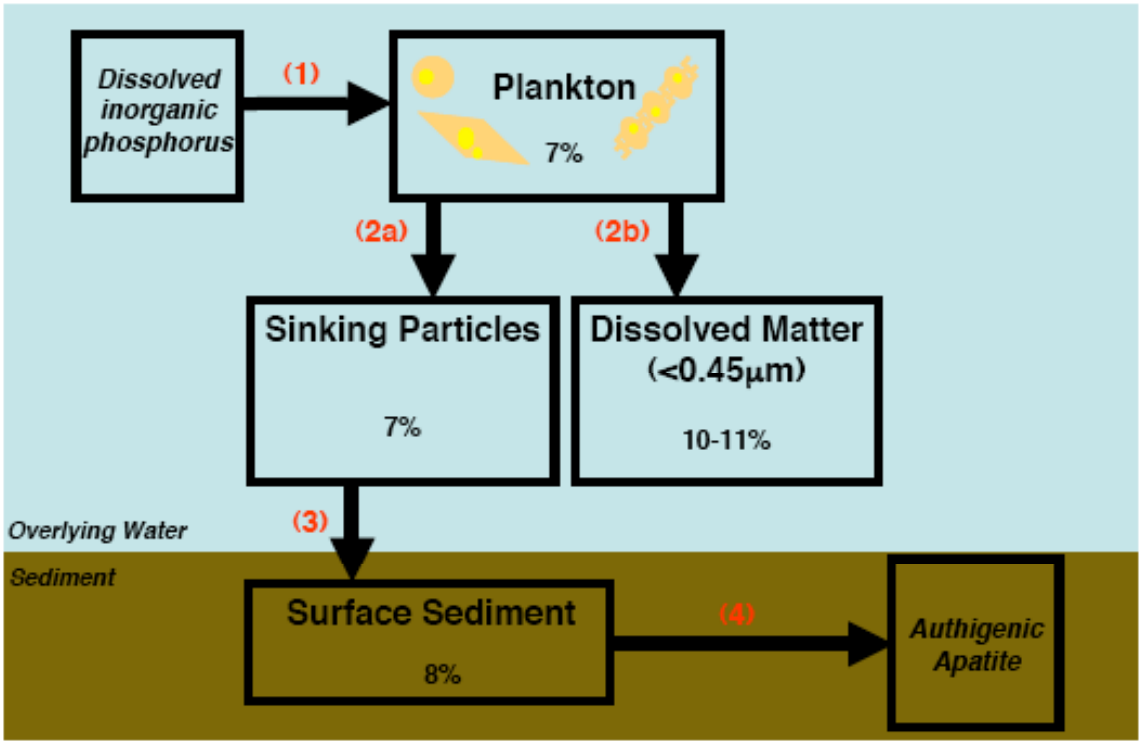

Figure 3.5 "Biological pump" mechanism for geologic sequestration of phosphorus. (1) Plankton in surface waters assimilate dissolved inorganic phosphorus into intracellular calcium-associated polyphosphate granules. In the bulk plankton community, polyphosphate accounts for 7% of total phosphorus. (2a) Intact polyphosphate-rich cells or extracellular polyphosphate particles from the water column sink (polyphosphate represents 7% of the total phosphorus in sinking particles). (2b) Alternatively, biogenic polyphosphate derived from plankton growth in the euphotic zone can enter the dissolved phase, in which polyphosphate accounts for 11% of total phosphorus. (3) Polyphosphate derived from the water column sinks to surface sediments, where polyphosphate is 8% of total phosphorus. (4) In surface sediments, calcium-associated polyphosphate can reduce the kinetic nucleation barrier to the precipitation of calcium phosphate minerals, and diagenetic transformation into fine-grained, geologically stable authigenic apatite particles can thereby occur. Thus, steps 1, 2a, 3, and 4 together constitute a "biological pump" mechanism by which dissolved, water column-derived phosphorus is delivered to underlying sediments and sequestered over geologic timescales as stable mineral phases via an inorganic polyphosphate intermediate.

ocean, including vast regions of coastal and polar seas that exhibit similar phosphate availability to our sampling site [*Louanchi et al.*, 2001]. Therefore, the sequestration of phosphorus through mechanisms involving diatom-derived polyphosphate is likely to be quantitatively significant on a global scale.

We note that another documented source of polyphosphate in natural marine systems involves synthesis by benthic sulfur-oxidizing bacteria [*Schulz and Schulz*, 2005], yet these organisms thrive in specialized environments and are not as globally prevalent as diatoms. Polyphosphate has been identified in *Trichodesmium* spp. and other common marine cyanobacteria [*Lawerence et al.*, 1998; *Mateo et al.*, 2006; *Romans et al.*, 1994], suggesting that these organisms may be a significant source of polyphosphate in the tropical and subtropical oceans where they are abundant. An abiological origin for polyphosphate is unlikely in most marine environments because abiotic polyphosphate synthesis can only occur at the elevated temperatures characteristic of such extreme environments as hydrothermal vent systems [*Brown and Kornberg*, 2004]. There is no evidence that the transformation of polyphosphate to apatite in marine sediments is dependent on the specific source of polyphosphate, however.

Enhanced phosphorus sequestration in marine sediments resulting from the conversion of diatom-derived polyphosphates to apatite may be manifested in the geologic record. The mid-Mesozoic rise of marine diatoms [*Katz et al.*, 2004] coincides with a trend toward lower organic carbon to total phosphorus ratios in marine sediments [*Algeo and Ingall*, 2007]. Because oceanic phosphorus influences atmospheric carbon dioxide levels over geologic time through regulation of marine primary productivity [*Van Cappellen and Ingall*, 1996], geologic fluctuations in phosphorus burial efficiency brought

on by changes in diatom abundance may have also exerted significant paleoclimatic influences.

3.3 Supporting Information

3.3.1 Materials and Methods

3.3.1.1 Field Site and Sampling

Samples were obtained from the upper basin (49° 04.4N, 125° 09.5W) of Effingham Inlet, a Pacific fjord located on the southwestern coast of Vancouver Island, British Columbia, Canada during two cruises conducted in April and July 2007 (Figure 3.1). Sample collection included plankton, dissolved material, particles, and underlying sediments.

Plankton were collected using a plankton net (30μm mesh) in surface (<3m) waters. Two large volume (50 and 120 L) seawater samples were collected over several casts of a Niskin bottle rossette for processing by electrodialysis/reverse osmosis. Sinking particles were collected in a sediment trap positioned at a depth of 45m (120m station depth). A multi-corer was used to collect underlying sediments.

3.3.1.2 X-ray Spectromicroscopy

X-ray spectromicroscopy is a unique methodological tool among techniques currently available in the field of earth science. Specifically, X-ray spectromicroscopy is capable of imaging elemental distributions and determining chemical speciation within minimally-prepared particulate samples. The high spatial resolution achieved with this technique (<1μm) makes the method particularly relevant to the study of micro-scale transformations involved in microbially-mediated processes. X-ray spectroscopy has also been recently applied in several marine carbon and iron cycle studies (e.g., [*Brandes et al.*, 2004; *Lam et al.*, 2006; *Twining et al.*, 2003; *Twining et al.*, 2004b]).

Sub-micron scale X-ray spectromicroscopy techniques are currently only available at synchrotron radiation facilities, which are uniquely capable of producing sufficiently bright X-ray beams for micro-scale X-ray spectromicroscopic work. A wide variety of instrument capabilities are possible among synchrotron X-ray spectromicroscopy beamlines worldwide; thus, analytical protocols are highly beamline-specific, and the prospective user has many different instrumentation options. Most synchrotron facilities make instrument time available to users through a competitive application process.

In principle, the X-ray spectromicroscopy technique relies on the quantized interaction of monochromatic X-rays with an element's electrons, typically the inner k-shell electrons. Each element absorbs/fluoresces X-rays at a specific k-edge corresponding to the energy at which the k-shell electrons are bound. Elemental distribution maps are generated by probing a defined sample area with a highly focused, monochromatic X-ray beam of sufficient energy and then detecting element-specific fluorescent X-rays with a multi-element fluorescence detector. Many elements can be mapped and quantified simultaneously.

Chemical speciation is determined by further analyzing particles identified in elemental maps using spectroscopic mode (X-ray Absorption Near Edge Spectroscopy, XANES; or Near Edge X-ray Fluorescence Spectroscopy, NEXFS). In spectroscopic mode, the X-ray beam is focused on a specific region, and the incident energy is varied within a fixed range about the k-edge energy of interest. In the resulting spectra, intensity is expressed as a function of energy; higher energy features depict the local bonding environment around the element of interest and are therefore species-specific. Other species-specific spectroscopic features also exist. For example, with respect to phosphorus, diagnostic shifts in k-edge position occur between organic phases.

[*Myneni*, 2002] and [*Brandes et al.*, 2007] demonstrated that a wide range of different phosphorus-containing phases (including mineral, organic, and polymeric forms) can be identified by using the spectroscopic "fingerprints" generated with this technique. Although spectroscopic differences between various phosphorus phases may be subtle, the patterns are consistent and can be easily used to distinguish between different particulate phosphorus phases. Further details on the principles of X-ray spectromicroscopy are available in [*Myneni*, 2002].

Material for X-ray analysis was obtained from preserved sediment cores (freeze dried and ground) taken from our field site in Effingham Inlet, British Columbia. To prepare samples for analysis, a few milligrams of crude dry sediment were suspended in approximately 100μL of deionized water. Aliquots of this mixture were then mounted onto formvar/carbon-supported copper Transmission Electron Microscopy (TEM) grids that had been adhered to aluminum mounting supports. Sample mounts were photographed on a light microscope and allowed to dry prior to X-ray analysis.

X-ray surveys of sedimentary phosphorus content were performed with the scanning X-ray microscope (SXM) at beamline 2-ID-B, Advanced Photon Source, Argonne National Laboratory. This microscope was used to obtain elemental maps at ~60nm spatial resolution, in addition to spectroscopic data from particulate specimens. The beamline operates within the 1-4keV energy range, and can map Na, Mg, Al, Si, P, S, and Cl. Details on the specifications of 2-ID-B are available in [*McNulty et al.*, 2003].

Specimens were mounted in the SXM using a magnetic stage. Prior to analysis, regions of interest were identified by obtaining coordinates using an in-line visible-light microscope. The visible-light microscope was replaced with an absolutely calibrated photodiode (ACP) for X-ray analysis in order to monitor bulk X-ray transmission through the specimen. A Fresnel zone plate and order-sorting aperture were used to focus a

bright X-ray beam into a 60nm spot. Fluorescence from the specimen was measured using a silicon drift diode detector oriented approximately 15 degrees relative to the sample plane. In order to prevent atmospheric backscatter, specimens were bathed in a continuous helium stream. Figure 3.6 depicts the instrument set-up.

Elemental distribution maps spanning several hundred square microns were acquired using 2190eV X-rays and a per-pixel dwell time of 0.5 seconds. Elemental maps revealed sub-micron sized phosphorus-rich domains that were then analyzed spectroscopically. To generate phosphorus NEXFS spectra, high concentration phosphorus regions were interrogated over the 2130-2190eV range at 0.25eV energy intervals using a dwell time of 1.0 second. The dwell times used in our experiments were sufficiently low to avoid significant irradiative damage. Raw X-ray spectroscopy data were normalized relative to the fluorescence signal of the carbon/formvar backing. Spectra were characterized based on the standard library of mineral, organic, and inorganic phosphorus species presented [*Brandes et al.*, 2007]. Additional standard phosphorus NEXFS data are accessible in [*Ingall et al.*, 2011] and via the online version of [*Brandes et al.*, 2007] maintained by the journal *Marine Chemistry*. Figures 3.7 and 3.8 provide standard mineral and polyphosphate spectra relevant to this study.

Important to note is the currently non-quantitative nature of the X-ray spectromicroscopy method. As evident in the current work, the methodological strength of X-ray spectromicroscopy currently lies within its ability to determine speciation and the spatial organization of species within a sample, rather than in any quantitative

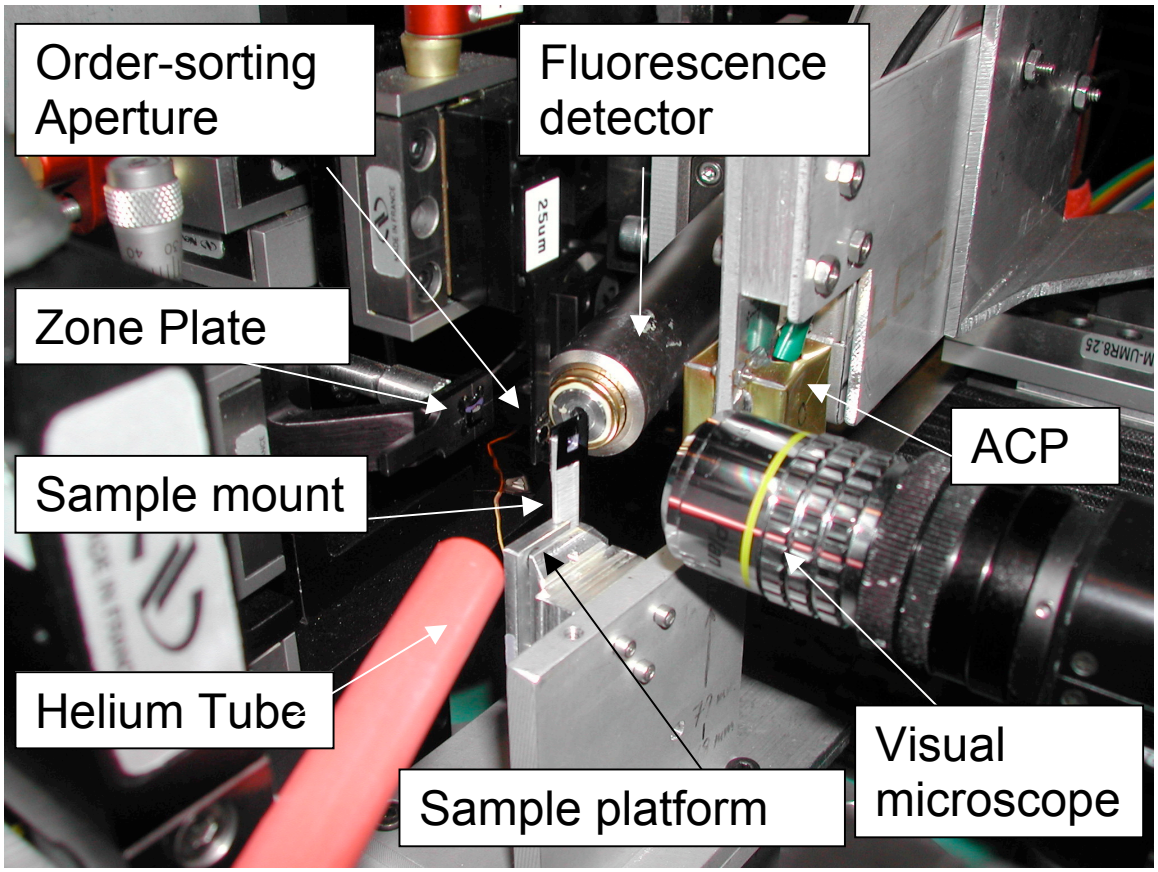

Figure 3.6 Instrument set-up at beamline 2-ID-B for X-ray fluorescence spectromicroscopy. Analyses are performed with multiple X-ray detectors and optical components positioned at millimeter to centimeter distances away from the sample. Instruments are moved using high spatial resolution motors. See text for a description of instrument components. Photo courtesy of Juergen Thieme.

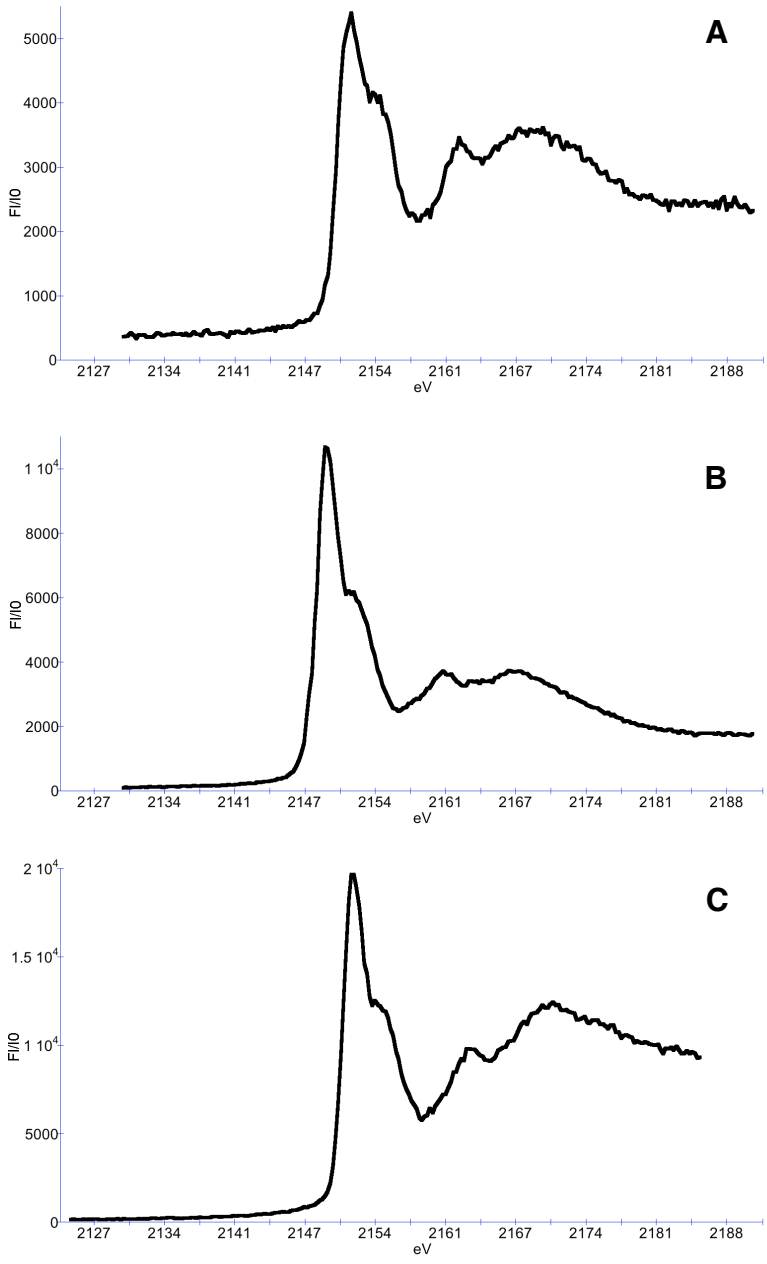

Figure 3.7 X-ray fluorescence spectra of standard calcium phosphate mineral phases. Normalized phosphorus X-ray fluorescence spectra of (A) carbonate fluorapatite, (B) hydroxyapatite, and (C) phosphorite are all characterized by a primary peak "shoulder" and two high-energy peaks located at 11eV and 18eV above the primary peak position. Based on our analyses, other calcium phosphate minerals yield subtly different yet distinct phosphorus X-ray fluorescence spectra.

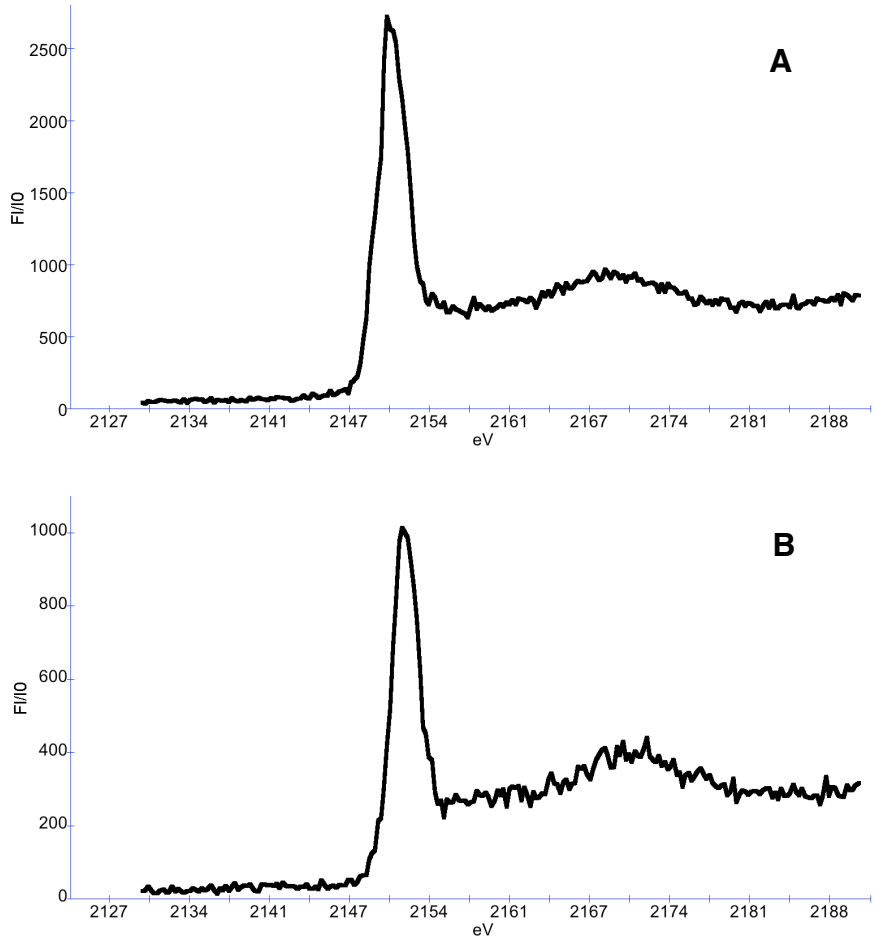

Figure 3.8 X-ray fluorescence spectra of standard biogenic polyphosphate. These phosphorus X-ray fluorescence spectra were collected from intracellular polyphosphate granules of the freshwater algae: (A) Chlamydomonas sp. and (B) Chlorella sp. As shown in these spectra, biogenic polyphosphate yields phosphorus fluorescence spectra characterized by a featureless primary peak and a single high-energy peak located 18eV above the primary peak position.

measurements that the method may be forced to produce. For example, in contrast to more conventional bulk and broad beam spectroscopic studies, spectral modeling of our micro-NEXFS spectra is limited. The position of peaks in NEXFS spectra collected from sub-micron sized particles are highly consistent between identical samples; however, the intensity/amplitude of those peaks varies somewhat between identical samples because the photon flux varies throughout the duration of the NEXFS scan, for reasons related to the optical behavior of an X-ray beam using zone plate optics: The position of the X-ray focus changes as a function of incident X-ray energy/wavelength. A micron-sized sample located at a fixed position in space will therefore receive a variable cross-sectional area of light (and therefore photon flux) from a micro X-ray beam throughout an energy scan. The variable photon flux issue is not an obstacle in bulk samples for which spectral modeling is a conventional mode of analysis, and the simple optics employed at such instruments are typically of a type that do not alter focus with energy shifts. In focused operation using zone-plate optics, the Z position of the sample has to be actively varied over the course of a spectral scan in order to maintain a constant X-ray spot size on the sample. Moving the sample in Z introduces errors in X and Y as there is unavoidable wobble on the order of up to several microns. The two ways in which this problem has been tackled are as follows: first, taking many images at different incident energies (impractical for fluorescence studies) with subsequent software alignment, and second, laser interferometer correction for sample position (expensive and not available at 2-ID-B). Thus, due to time and resource constraints, the microscope at 2-ID-B is operated with fixed Z position during spectral scans. Because of the methodological effect of variable photon flux, any modeling results of micro-NEXFS spectra collected under the above conditions would produce significant experimental artifacts.

3.3.1.3 Electrodialysis/Reverse Osmosis

The combined process of electrodialysis and reverse osmosis (ED/RO) isolates molecules dissolved in seawater by first desalinating and then concentrating high volume (>50 L) samples. Samples for ED/RO were taken at depths of 61 and 78 m from our sampling site in Effingham Inlet during both cruises in April and July 2007.

As the first step in ED/RO, electrodialysis is used to remove ions from the seawater sample (Figure 3.9). In electrodialysis, the seawater sample (to be deionized) is contacted with a concentrate flow (to receive ions) across many pairs of cation and anion exchange membranes. A DC electrical current is directed through the membrane stack. Only ionized dissolved components are targeted by ED.

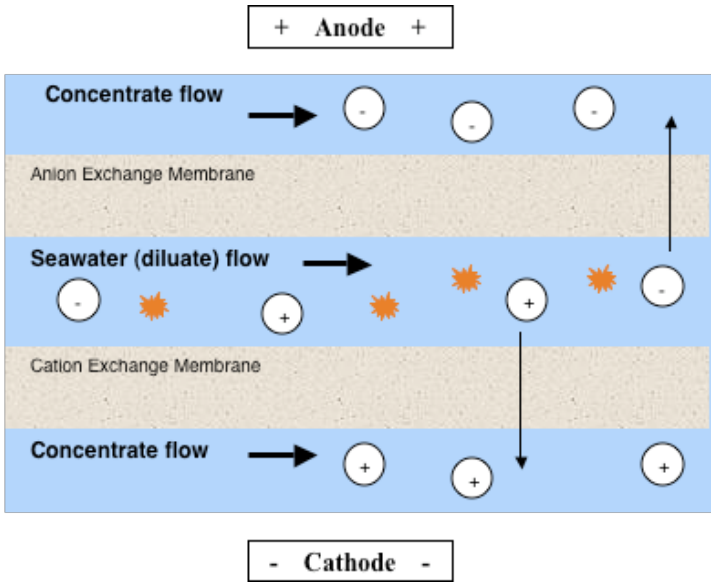

Figure 3.9 Electrodialysis. Seawater contacts a concentrate flow across many pairs of anion/cation exchange membranes through which a DC current is directed. In this process, ions move from the seawater flow (diluate) into the concentrate flow, while dissolved molecules (orange globules) are retained in the diluate flow. Dissolved molecules in the salt-free diluate flow are subsequently concentrated using reverse osmosis.

The ion exchange membranes are non-porous above the size of the interstitial spaces between the polymer chains in the cross-linked hydrated ion exchange resin. The process results in a concentrate solution, which is discarded, and a deionized solution (diluate). The diluate solution is subsequently concentrated via RO in order to isolate dissolved molecules for analysis.

In RO, a feed solution consisting of water and aqueous solutes is placed under pressure and pumped from a sample reservoir across a semi-permeable RO membrane, where the feed solution is separated into a permeate solution (relatively lower concentrations of solutes) and a retentate solution (relatively higher concentrations of solutes). When RO is being used to concentrate solutes from the feed solution, the retentate solution is recycled back to the sample reservoir and the permeate solution is discarded. As more feed solution is added either continuously or discontinuously to the sample reservoir, the concentrations of all solutes, including dissolved organic molecules that are rejected by the membrane, gradually increase in the sample reservoir.

Conventional ultrafiltration methods that do not desalinate seawater samples can only isolate the high molecular weight fraction (>1kDa) of dissolved matter, which comprises only ~30% of total dissolved matter. By comparison, ED/RO is capable of yielding salt-free samples consisting of both high and low molecular weight dissolved matter, resulting in up to 90% recoveries. The high recoveries capable through ED/RO enable the characterization of the chemically distinct low molecular weight species and are therefore key to the comprehensive examination of marine dissolved matter. We recovered ~70% of dissolved matter from our Effingham Inlet samples. See [*Vetter et al.*, 2007] for further technical details on ED/RO.

3.3.1.4 Polyphosphate Content—^{31}P-NMR

Plankton samples, sediment trap material, and dissolved matter isolated from ED/RO were freeze-dried and ground. These samples were then analyzed using solid-state ^{31}P-Nuclear Magnetic Resonance (NMR). Solid-state ^{31}P-NMR analyses were carried out at the NMR center in the School of Chemistry and Biochemistry at the Georgia Institute of Technology. The NMR spectra were acquired on a Bruker DSX 400 spectrometer using Cross Polarization-Magic Angle Spinning techniques at a ^{31}P frequency of 161 MHz. Approximately 90 mg of powdered sample was packed into a 4 mm diameter cylindrical zirconia rotor fitted with a Kel-F cap and spun at 10 000±10 Hz in a Bruker magic-angle spinning probe. For all samples, a cross-polarization sequence, optimized to obtain semi-quantitative data, was used with a 1.0 ms contact time and a pulse delay of 4 s. A total of 8192 to 32768 transients were collected for each sample. The data processing and calculation of integrated peak areas were carried out off-line using the Spinworks software package. The errors associated with determination of the abundance of different chemical forms through integration of solid-state NMR peak areas are on the order of ±10% of the reported value [*Hedges et al.*, 2002; *Sannigrahi and Ingall*, 2005; *Sannigrahi et al.*, 2005]. For example, a polyphosphate measurement of 7% would have an associated error of ±0.7%.

3.3.1.5 Epifluorescence Microscopy

Seawater samples from above and below the photic zone were fixed with a final concentration of 4% formaldehyde. Cells were vacuum-filtered (pressure <10cm Hg) onto 25mm polycarbonate membranes having a nominal pore size of 0.2μm. Filtered samples were stained in the dark for five minutes with ~1mL of 40μgmL^{-1} DAPI (4',6'-Diamidino-2-phenylindole) and subsequently examined and photographed under UV

illumination with an Olympus epifluorescence microscope. The fluorescence of nucleus-bound DAPI (emission at 456nm) was sufficiently distinct from the fluorescence signal of polyphosphate-bound DAPI (emission at 525nm) to distinguish between these two DAPI-sensitive inclusions. Numerous independent studies report the use of DAPI as a stain for polyphosphate in eukaryotic algae, e.g., [*Eixler et al.*, 2005] and [*Ruiz et al.*, 2001].

3.3.1.6 Biogenic Silica

Plankton, sediment trap, and underlying sediment samples were treated by the method of [*Mortlock and Froelich*, 1989] in order to dissolve any opal present (error associated with this measurement is <3%). Dissolved Si content was then determined by the method of [*Hansen and Koroleff*, 1999b], which has a typical analytical error of ±7%.

3.3.1.7 Elemental content

Freeze-dried and ground plankton samples were analyzed for C and N content using an elemental combustion system (Costech instruments, model no. ECS4010). The error for this method is typically ±1% [*Hedges and Stern*, 1984]. In order to determine total and inorganic phosphorus content, plankton, dissolved matter, sediment trap, and underlying sediment samples were acidified, combusted, and analyzed according to the Aspila method [*Aspila et al.*, 1976]. Duplicate samples agreed to within <5%, and the measured value of NIST Standard Reference Material 1573a (tomato leaves) was within ±5% of the certified value.

3.3.1.8 Soluble Reactive Phosphate

In surface seawater samples, soluble reactive phosphorus was determined spectrophotometrically by using the molybdate method of [*Hansen and Koroleff*, 1999c]. Typically errors for this method are <3%.

3.3.1.9 Sediment Traps

Sinking particles were collected in a sediment trap positioned at a depth of 45m in our ~120m depth field site. The sediment trap (1.5m diameter net) was deployed for 44 hours, from which 1.21g of dried material was collected. We note that our single sediment trap measurement cannot account for long-term variations in particle flux. In addition, as is typical for any oceanographic research, replicate trap deployments were unrealistic given our equipment and sampling time for this study. Thus, any calculations based on our trap measurement are meant to provide broad insights into the dynamics of the natural system, rather than rigorous quantitative assessments.

3.3.2 Supporting Results and Discussion

A provisional rate for the process of polyphosphate nucleated apatite precipitation in marine sediments may be calculated. Polyphosphate represents 8% of the total phosphorus in 0-3 year-old surface sediments from Effingham Inlet [*Sannigrahi and Ingall*, 2005]. The polyphosphate concentration in deeper, 18-20 year-old sediments is below the ^{31}P-NMR detection limit [*Ingall et al.*, 2005; *Sannigrahi and Ingall*, 2005] and for the purposes of the current calculation is approximated as zero. Using these two end points, the rate of polyphosphate nucleated apatite growth in sediments is conservatively estimated to be ~0.5% of sedimentary polyphosphate per year.

The ability of X-ray spectromicroscopy to identify polyphosphate in deep Effingham Inlet sediments up to 60 years old highlights the considerable sensitivity and analytical strength of X-ray spectromicroscopy in its ability to identify the presence of low-concentration phases. The X-ray detectable pool of polyphosphate that is present in deeper sediments may be unreactive as a consequence of protective mechanisms involving cation complexation and silica mineral coatings. Regardless of the reactivity

differences between mineral-transformed and recalcitrant polyphosphate, however, sedimentary polyphosphate represents a phosphorus sink.

Until now, the accumulation of substantial authigenic apatite in marine sediments has been a fundamental mystery. For example, apatite precipitation is a kinetically-controlled process in most marine sediments, as calcium phosphate minerals are highly insoluble under typical sedimentary conditions and pore waters are therefore commonly supersaturated with respect to apatite [*Van Cappellen and Berner*, 1991]. Yet most marine sediments contain significantly more authigenic apatite than predicted by kinetic porewater precipitation models [*Van Cappellen and Berner*, 1991].

The polyphosphate template mechanism for apatite formation proposed in this study would produce a dispersed distribution of authigenic apatite in marine sediments based on the observation that polyphosphates appear to be similarly dispersed within the sediments of our field site. This apatite distribution matches the puzzlingly disperse distribution of apatite minerals typically observed in sediments from non-upwelling zones and is thereby the first mechanism to potentially explain the formation of fine-grained apatites in such environments. The potential for polyphosphate as a template for apatite mineral growth in natural systems also gains support from bioengineering research. For example, bone cements enriched with calcium polyphosphate have recently been shown to enhance apatitic bone growth and repair [*Grynpas et al.*, 2002].

3.4 Acknowledgements

This material is based upon work supported by the National Science Foundation under Grant No. 0526178. Use of the Advanced Photon Source is supported by the U.S. Department of Energy, Office of Basic Energy Sciences (DE-AC02-06CH11357). The authors would like to thank the crew of the R/V Barnes, Rick Keil and

John Nuwer for assistance with field sampling, Susan Herron and Gabrielle Lyons for help during field sampling and sample analysis, and Renée Styles and Cindy Jackson for assistance with sample analysis. The authors also thank George Patterson and John Platenius of the Clayoquot Field Station in Tofino, British Columbia, for providing lab space and a welcoming base for our field studies. Thanks also go to Dr. Patricia Sobecky and members of her lab at Georgia Tech for the use of the epifluorescence microscope. The authors declare no competing financial interests.

CHAPTER 4

FLUOROMETRIC QUANTIFICATION OF NATURAL INORGANIC POLYPHOSPHATE

4.1 Abstract

Polyphosphate, a linear polymer of orthophosphate, is abundant in the environment and a key component in wastewater treatment and many bioremediation processes. Despite the broad relevance of polyphosphate, current methods to quantify it possess significant disadvantages. Here, we describe a new approach for the direct quantification of inorganic polyphosphate in complex natural samples. The proposed protocol relies on the interaction between the fluorochrome 4',6-diamidino-2-phenylindole (DAPI) and dissolved polyphosphate. With the DAPI-based approach we describe, polyphosphate can be quantified at concentrations ranging from 0.5-3μM P in a neutral-buffered freshwater matrix with an accuracy of ±0.03μM P. Moreover, the patterns of polyphosphate concentration versus fluorescence yielded by standards exhibit no chain length dependence across polyphosphates ranging from 15-130 phosphorus units in size. Shorter length polyphosphate molecules (e.g., polyphosphate of three and five phosphorus units in length) contribute little to no signal in this approach, as these molecules react only slightly or not at all with chain lengths (e.g., 45-130 phosphorus units), this salt interference is not evident at conductivities up to ~10mS/cm. Our results indicate that standard polyphosphates should be stored frozen for no longer than ten to fifteen days to avoid inconsistent results associated with standard degradation. We have applied the fluorometric protocol to the analysis of five well-characterized natural samples to demonstrate the use of this method.

Diaz, J. M., and E. D. Ingall. 2010. *Environmental Science & Technology* 44: 4665-4671.

4.2 Introduction

Polyphosphate, a linear polymer of orthophosphate, is an important chemical constituent in a wide range of systems, both natural and man-made. For example, polyphosphate forming microbes are a critical component in the removal of excess phosphorus (P) from wastewater [*Seviour et al.*, 2003]. In the ocean, polyphosphate can lead to the long-term burial of nutrient phosphorus in sediments [*Diaz et al.*, 2008]. Despite the relevance of polyphosphate to a variety of fields, ranging from the environmental and biological sciences [e.g., [*Brandes et al.*, 2007; *Brown and Kornberg*, 2004; *Diaz et al.*, 2008; *Diaz et al.*, 2009; *Hupfer et al.*, 2004; *Kulaev and Kulakovskaya*, 2000; *Sannigrahi and Ingall*, 2005; *Schulz and Schulz*, 2005]] to engineering, bioremediation, and medicine [e.g., [*Boswell et al.*, 2001; *Nagata et al.*, 2006; *Oh et al.*, 2005; *Renninger et al.*, 2004; *Seviour et al.*, 2003; *Shiba et al.*, 2003; *Yamaoka et al.*, 2008]], researchers have been lacking an adequate method to quantify polyphosphate in natural samples, which are inherently heterogeneous and chemically complex.

One of the most commonly employed methods to quantify polyphosphate has been ^{31}P-NMR [*Ahlgren et al.*, 2005; *Diaz et al.*, 2008; *Dyhrman et al.*, 2007; *Dyhrman et al.*, 2009; *Hupfer et al.*, 2004; *Hupfer et al.*, 2008; *Lawerence et al.*, 1998; *Sannigrahi and Ingall*, 2005; *Young and Ingall*, 2010]. While this technique has produced a foundational knowledge in the field of polyphosphate research, it possesses significant drawbacks. For instance, ^{31}P-NMR can only detect phosphorus-containing molecules on the basis of bond class. Especially in natural samples that are chemically complex, the method is not ideally suited to distinguish between inorganic polyphosphate and other molecules that also contain phosphoanhydride bonds, such as nucleotides. In addition, for environmental samples, ^{31}P-NMR is typically able to indicate the relative abundance of polyphosphate in comparison to other P bond classes such as P esters and

phosphonates, rather than provide a direct measurement of concentration. Yet even this information on relative abundance is difficult to determine precisely for environmental and biological samples, as the ubiquitous and abundant presence of P-ester compounds can obscure the comparatively smaller polyphosphate signal [*Young and Ingall*, 2010].

Other methods of polyphosphate quantification have been less widely used than ^{31}P-NMR. Some protocols enumerate polyphosphate concentration by difference [*Hansen and Koroleff*, 1999a; *Miyata and Hattori*, 1986; *Solorzano and Strickland*, 1968]. In these methods, polyphosphate is extracted from a sample and then quantified as orthophosphate equivalents after destruction by boiling in an acidic matrix. Unfortunately, these methods offer very low specificity for polyphosphate. And as is often the case for natural samples, high background concentrations of orthophosphate overshadow the relatively low polyphosphate content. Enzymatic methods involving exopolyphosphatase and polyphosphate kinase have been used to quantify polyphosphate with high specificity in bacterial culture samples [*Ault-Riche et al.*, 1998; *Clark et al.*, 1986; *Rao et al.*, 1998; *Vangroenestijn et al.*, 1987]. However, application of these approaches to chemically heterogenous environmental samples is impractical, because they require a highly pure polyphosphate analyte that is difficult to extract. Moreover, the chain length specificity of these enzymes can exclude various size classes of polyphosphate, making these techniques a poor choice for natural samples in which polyphosphates are present in an unknown mixture of chain lengths [*Hupfer et al.*, 2008].

Photometry offers an appealing alternative to the polyphosphate methods discussed above [*Aschar-Sobbi et al.*, 2008; *Hupfer et al.*, 2008; *Nikata et al.*, 2001]. Among the photometric approaches, the most promising rely on the interaction between polyphosphate and the fluorochrome 4',6-diamidino-2-phenylindole (DAPI). The binding

of polyphosphate to DAPI shifts the peak DAPI emission wavelength from 475nm to 525nm (360nm excitation), and the fluorescence intensity at this shifted wavelength is proportional to the concentration of polyphosphate [*Tijssen et al.*, 1982]. This principle has been instrumental in the visual identification of polyphosphate granules within microorganisms [*Diaz et al.*, 2008; *Eixler et al.*, 2005; *Ruiz et al.*, 2001; *Serafim et al.*, 2002], but until recently, DAPI-based methods have been sensitive only to very high concentrations of polyphosphate (~10 mM P) [*Aschar-Sobbi et al.*, 2008]. A recent study by Aschar-Sobbi et al. (2008) optimized wavelength selection to reduce fluorescence interferences from DAPI-bound DNA and to improve the polyphosphate detection limit [*Aschar-Sobbi et al.*, 2008]. Here, we build upon this approach significantly by characterizing the effect of polyphosphate chain length and matrix composition on the fluorescence yielded at different levels of polyphosphate concentration. In addition, we provide critical estimates of accuracy for the method as well as practical guidelines necessary for the implementation of the protocol, including a robust analysis of potential reaction interferences and an analysis of standard polyphosphate stability in solution. These findings provide essential recommendations for the proper collection, storage, and analysis of natural samples. To demonstrate the protocol, we have determined the polyphosphate content of five well-characterized natural samples.

4.3 Experimental Section

4.3.1 Standards and Reagents

Polyphosphate standards with average chain lengths of 15, 60, and 130 orthophosphate units were generously provided by Dr. Toshikazu Shiba and Dr. Yumi Kawazoe of Regenetiss Co., Tokyo, Japan. Polyphosphate standards with average chain lengths of 45 and 5 phosphorus units were purchased from Sigma (products

#S4379 and #S5878, respectively). Sodium tripolyphosphate was also purchased from Sigma (product #T5883), and DAPI was purchased from AnaSpec, Inc (cat #83210). The majority of our standard polyphosphate salts have known molecular weights except for the 45 and 5 chain length standards. When working with these standards, we utilized an assumed molecular weight that was calculated based on an ideal molecular formula:

$$P_nO_{(3n+1)}Na_{(n+2)}$$

where n is the phosphorus chain length. This calculation allowed us to prepare the 45 and 5 chain length standards at concentrations comparable to the better-characterized standard polyphosphates. Alternatively, we recognize that the polyphosphate content of the 5 and 45 chain length standards could be assessed via hot acid hydrolysis followed by enumeration as orthophosphate equivalents [*Hansen and Koroleff*, 1999a; *Miyata and Hattori*, 1986; *Solorzano and Strickland*, 1968]. However, relatively high background levels of orthophosphate that can be present in the standard salts would produce a degree of error in the estimate of polyphosphate content that is very difficult to ascertain. Therefore, owing to the uncertainty in the molecular weights of the 45 and 5 chain length standards, neither was used in the construction of the standard curve.

Standard stock polyphosphate solutions (2.5-3 mM P) were prepared for each polymer in two types of solution matrices: a “salty” matrix of 150mM KCl buffered (pH=7) with 20mM HEPES (4-(2-hydroxyethyl)-1-piperazineethanesulfonic acid), as in Aschar-Sobbi et al. (2008), and a “fresh” matrix of deionized water also buffered with 20mM HEPES [*Aschar-Sobbi et al.*, 2008]. Solution conductivities for all experiments were measured using an Accumet® conductivity meter from Fisher Scientific. Standard stock solutions were stored under a variety of conditions, including benchtop storage (~22°C), refrigeration (5°C), and frozen storage (-20°C), in order to investigate impacts on the stability of the polyphosphate standards over time. DAPI was prepared in

deionized water at a concentration of 1mM and stored frozen in 1mL aliquots until needed, at which time the reagent was diluted to 100µM. DAPI solutions were shielded from light as much as possible to minimize photodegradation of the reagent.

4.3.2 Collection of Standard Data

For the construction of standard curves, a dilution series of each polyphosphate standard was prepared. Special care was taken to keep standards well-mixed during this process with the use of magnetic stirbars. Standard dilution series were prepared in either the 150mM KCl, 20mM HEPES matrix or the plain 20mM HEPES matrix at polyphosphate concentrations ranging from 0.5-3 µM P. For every 1mL of standard solution, 0.1mL of 100µM DAPI reagent was added, resulting in a final DAPI concentration of ~10µM [*Aschar-Sobbi et al.*, 2008]. Reacting solutions were allowed to incubate under ambient light conditions for 7 or 10 minutes to ensure attainment of steady-state fluorescence [*Aschar-Sobbi et al.*, 2008]. Standards were homogenized with a vortex mixer upon addition of DAPI, at the reaction half-point, and just before measurement.

Fluorescence measurements were conducted using a Perkin-Elmer LS-50B luminescence spectrometer. Reacted samples were placed in a 1 cm square quartz cuvette, and relative fluorescence intensity was measured at 550nm upon illumination with 415nm monochromatic light [*Aschar-Sobbi et al.*, 2008]. Triplicate fluorescence measurements were performed sequentially on each sample. Blank values were obtained from aliquots of buffer solution incubated with the DAPI reagent. Rather than subtracting background fluorescence from the data, raw fluorescence values were used for the analysis of standard observations.

4.3.3 Statistical Analysis of Standard Data

Multi-variate linear regression analyses of the standard polyphosphate data were conducted to examine the influence of various factors on DAPI-polyphosphate fluorescence in solution. Statistical analysis of standard data was also used to generate a single-variable linear regression curve for fluorescence as a function of polyphosphate concentration. In all statistical analyses, data were examined using the PASW 18.0 software package.

4.3.4 Sample Analysis

We analyzed five natural samples with the current protocol. These included three marine phytoplankton samples and one marine sediment trap sample, all of which were collected during April or July 2007 from Effingham Inlet, a Pacific fjord along the coast of Vancouver Island [*Diaz et al.*, 2008]. In addition, we also analyzed a bacterial enrichment culture originally described in [*Kolowith et al.*, 2001]. Samples were collected and analyzed previously for total phosphorus and ^{31}P-NMR composition as described in [*Diaz et al.*, 2008] and [*Kolowith et al.*, 2001].

Before analysis, each sample was treated in order to extract polyphosphate into the dissolved phase. The samples were extracted at room temperature into 0.25N NaOH [*Eixler et al.*, 2005] using two successive treatments of 20 minutes each. Samples were syringe-filtered (0.45µm), neutralized with 1N HCl, and then diluted in a 1:10 volume ratio with a neutral-buffered HEPES solution in order to obtain a pH at which the DAPI-polyphosphate reaction is permissible (pH=6.5-7). Alternatively, pH within this range can be achieved by diluting basic extracts in a 1:100 volume ratio with the HEPES buffer. Samples were analyzed by the same protocol described above for the

polyphosphate standards. Measurements of polyphosphate for each sample are based on several replicates.

4.4 Results and Discussion

4.4.1 Fluorescence Measurements Collected from Polyphosphate Standards

All standard data combined, a total of 681 fluorescence measurements were taken. Our entire database is available in Appendix A. As seen in Figure 4.1, fluorescence results fell into two groups based on chain length: 1) the shortest standards, tripolyphosphate (3PP) and the polyphosphate of five phosphorus units (5PP), reacted slightly or not at all with DAPI regardless of matrix composition (fluorescence on average 12-14% higher than the average blank value across all levels of concentration); and 2) the intermediate to long chain polyphosphate standards of 15, 45, 60, and 130 phosphorus units (15PP, 45PP, 60PP, and 130PP, respectively) exhibited highly similar linear patterns of concentration versus fluorescence.

The addition of salt (150mM KCl) to the 20mM HEPES solution matrix (final conductivity ~10mS/cm) had no obvious effect on the 45PP, 60PP, and 130PP fluorescence patterns (Figure 4.1). However, 15PP was strongly influenced by the presence of salt (Figure 4.1). In the case of 15PP, the salt effect suppressed fluorescence at all levels of concentration, but especially at lower levels, thereby compromising the linear relationship with concentration. This result suggests that, under similar salinity conditions, the fluorescence signal from natural polyphosphates of comparable chain lengths may also be suppressed. The result is also consistent with the prevailing idea that the mechanisms of DAPI-substrate interactions are electrostatic in nature [*Barcellona et al.*, 1990].

Taken together, our standard results show that the proposed DAPI-polyphosphate assay is well suited for the quantification of intermediate to long chain polyphosphates

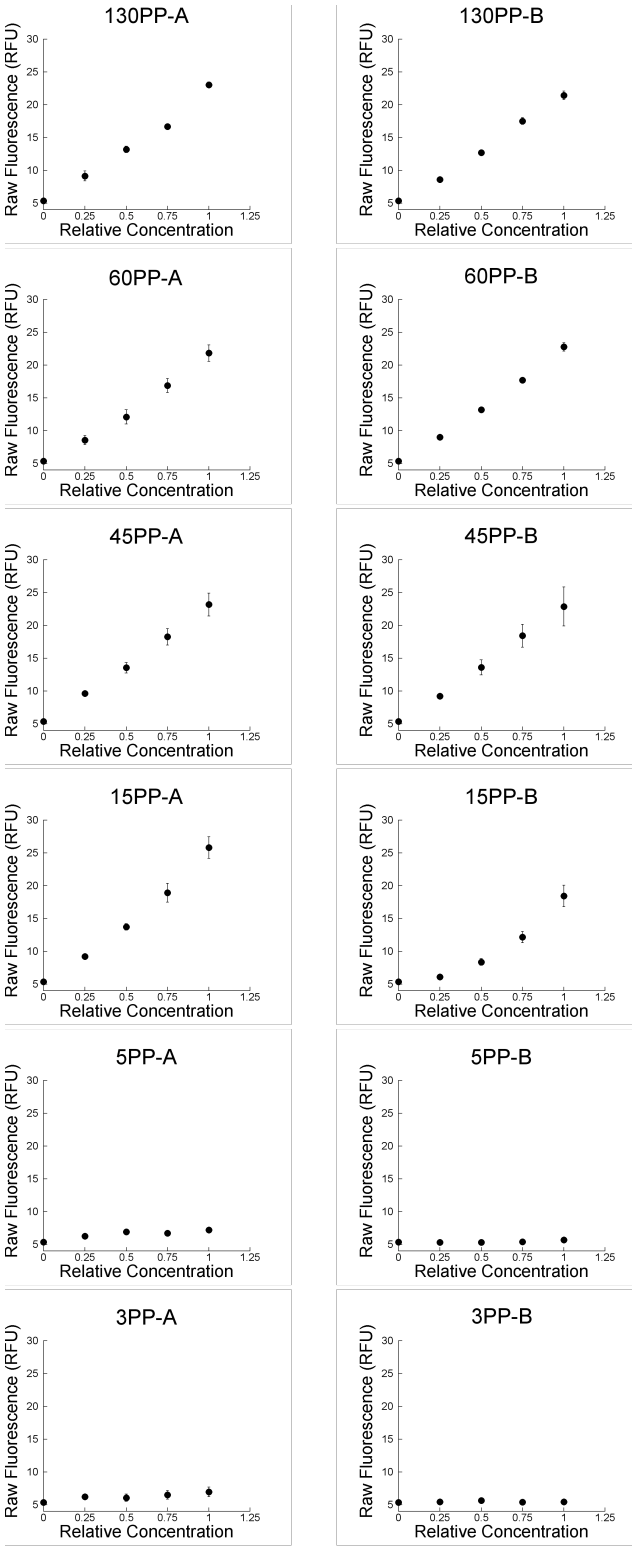

Figure 4.1 Relative polyphosphate concentration v. raw fluorescence for all standards tested.

Figure 4.1 (Continued). In column A, data are presented from polyphosphate standards prepared in 20mM HEPES with no salt addition. Column B depicts data collected from standards prepared in 150mM KCl buffered with 20mM HEPES. Standards are arranged by row according to polyphosphate (PP) chain length (number of phosphorus atoms). The shortest polyphosphates (3PP and 5PP) reacted only slightly or not at all with DAPI, regardless of matrix composition. The longer chain standards (15PP, 45PP, 60PP, and 130PP) showed strong and similar concentration-dependent fluorescence results. 15PP is the only standard exhibiting an obvious salt effect, suggesting that salt may suppress fluorescence from natural polyphosphates of a similar chain length. As detailed in the main text, the molecular weights of the 5PP and 45PP standards have not been characterized, hindering the calculation of polyphosphate concentration for these polymers. For ease of comparison, the concentration scales in these plots are the same and are given in relative units, where the value of one concentration unit is approximately 3µM P for all standards. Error bars represent 95% confidence limits. Fluorescence is given in relative fluorescence units (rfu).

(e.g., 15-130PP) and not suitable for quantification of short chain length polyphosphate (e.g., 3-5PP) over the concentration range tested (0.5-3µM P). Furthermore, our results show that the salinity of the matrix solution must be minimized in order not to interfere with the fluorescence signal of intermediate polyphosphates (e.g., 15PP).

We note that replicable fluorescence results were only obtained when standards were well-mixed during preparation from the standard stock and during incubation with DAPI. Owing to the high molecular weight of polyphosphate (10^3-10^4 g/mol), unmixed standard solutions likely became highly heterogeneous as the polyphosphate molecules gravitationally settled over time, resulting in inconsistent fluorescence results. Using a spectrofluorometer equipped with a cuvette stirbar to continuously mix the solution during measurement would simplify the steps required to maintain solution homogeneity.

4.4.2 Statistical Analysis of Standard Data

The polyphosphate concentration versus fluorescence data were statistically evaluated using multivariate linear regression analysis to investigate the additional factors (besides concentration) that exert a strong influence on the fluorescence yielded from the DAPI-polyphosphate reaction in solution. This statistical analysis is based on standard data collected from polyphosphates of intermediate to long chain lengths (15PP, 60PP, and 130PP). The 45PP data was omitted from the statistical analysis owing to the uncertainty in the calculation of its concentration (see Methods section).

For the multi-variate linear regression analysis of our combined 15PP, 60PP, and 130PP dataset, the response or dependent variable was defined as raw fluorescence. Sixteen independent variables were specified (Table 4.1), including seven main effect terms: concentration (µM P), age (days), reaction time (minutes), one binary variable for matrix composition (plain 20mM HEPES or 20mM HEPES-150mM KCl), and three

binary variables for chain length (15PP, 60PP, or 130PP). The remaining nine variables consisted of interaction terms constructed from the multiplication of two main effect variables. The first set of interaction terms accounted for age-chain length interaction, and the second and final set accounted for matrix-chain length interaction. A more detailed explanation of the independent variables included in this analysis is provided in Table 4.1, along with our statistical outputs provided in Appendix B.

Our multivariate linear regression analysis confirmed some intuitive observations about our data. At the 99% confidence level, only three of our original sixteen independent variables were significant. These independent variables of significance included concentration, the interaction term "salty15PP," and age ($p \ll 0.01$ for all variables). Based on these results, we conclude that the DAPI-polyphosphate assay

Table 4.1 Variables used in our multivariate linear regression model to examine factors governing DAPI-polyphosphate fluorescence in solution. The response variable was defined as raw fluorescence, expressed in relative fluorescence units (rfu). Data were analyzed using the PASW 18.0 software package.

	X_n	Variable Description	Units
Main Effects Terms	X_1	Concentration	μM P
	X_2	Polymer130 (p130)	Binary (1=Y, 0=N)
	X_3	p60	Binary (1=Y, 0=N)
	X_4	p15	Binary (1=Y, 0=N)
	X_5	Reaction time	Minutes
	X_6	Age	Days
	X_7	Matrix	Binary (1="fresh", 0="salty")
	X_{7A}◊	Matrix	Binary (1="salty", 0="fresh")
Interaction Terms	X_8	Agep130 (X_6* X_2)	Days
	X_9	Agep60 (X_6* X_3)	Days
	X_{10}	Agep15 (X_6* X_4)	Days
	X_{11}	Saltyp130 (X_{7A}* X_2)	Binary (1=Y, 0=N)
	X_{12}	Saltyp60 (X_{7A}* X_3)	Binary (1=Y, 0=N)
	X_{13}	Saltyp15 (X_{7A}* X_4)	Binary (1=Y, 0=N)
	X_{14}	Freshp130 (X_7* X_2)	Binary (1=Y, 0=N)
	X_{15}	Freshp60 (X_7* X_3)	Binary (1=Y, 0=N)
	X_{16}	Freshp15 (X_7* X_4)	Binary (1=Y, 0=N)

exhibits no chain length dependence between 15-130PP in a neutral-buffered freshwater matrix for polyphosphate concentrations in the range of 0.5-3μM P. The statistical results also revealed that a reaction time of 7 minutes yields equivalent results to a reaction time of 10 minutes for all chain lengths. Therefore we recommend seven-minute incubation time with DAPI. Based on the statistical analysis, the age (i.e., the number of days between solution preparation and fluorometric analysis) is also a critical parameter to consider.

To get a better understanding of the influence of age on the DAPI-polyphosphate assay, we monitored the degradation of the standard polyphosphates over time (Figure 4.2). As seen in Figure 4.2, storage of standard stock solutions at 5ºC tends to suppress polyphosphate degradation slightly, as compared to storage at room temperature. Yet frozen storage was most efficient at suppressing standard degradation for all chain lengths. Based on these data, we recommend that polyphosphate standard stock solutions be stored in frozen aliquots (-20ºC) and analyzed within ten to fifteen days of solution preparation in order to reduce effects of polyphosphate degradation. Our results also indicate that aqueous samples to be analyzed for polyphosphate should be stored frozen and that long-term storage (i.e., >10-15 days) should be avoided.

4.4.3 Standard Calibration Curve for Polyphosphate Concentration

Data that were free of the known storage and salinity effects detailed above were used to generate the single-variable standard curve for polyphosphate concentration versus fluorescence. In other words, the resulting standard curve is a true and representative numerical relationship for polyphosphate concentration versus

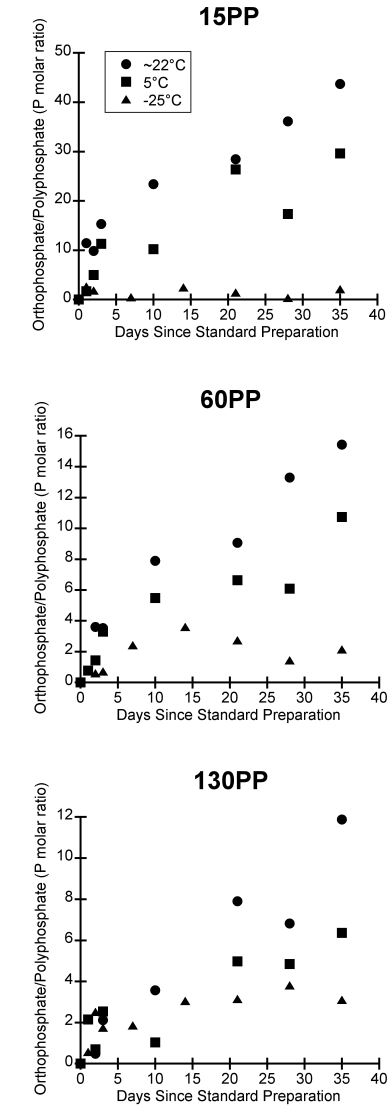

Figure 4.2 Stability of polyphosphate standard stock solutions over time. Stability of polyphosphate standard stocks was examined over time for various chain lengths (15PP, 60PP, and 130PP) and under different storage conditions (~22, 5, and -20 degrees Celsius). The phorphorus (P) molar ratio of accumulated orthophosphate to initial polyphosphate concentration increased over time for all solutions and all conditions examined, reflecting the progressive degradation of polyphosphate to its component orthophosphate units. The freezing of standard stock solutions was most effective at suppressing this degradation for all chain lengths, although this relative efficiency seems to decrease with increasing polymer length. Note that plots are presented on different vertical scales to clearly illustrate the pattern of degradation for each polymer, reflecting variable rates of degradation as a function of polymer length. Orthophosphate was determined as soluble reactive phosphorus by the standard molybdate method of [*Hansen and Koroleff*, 1999c].

fluorescence as long as excessive storage time and salinity effects we have described are avoided.

The standard curve is based on 328 observations of fluorescence versus concentration. Our statistical output is available in Appendix B. The linear regression analysis was constructed by defining the dependent variable (Y) as raw fluorescence and the independent variable (X) as polyphosphate concentration (μM P):

$$Y=\beta_0+\beta_1 X$$

The statistically-determined intercept (β_0) and slope (β_1) are 4.944 and 6.694, respectively (Table 4.2). As expected, the standard curve intercept value is very similar to the average blank value measured, which is 5.35±0.37 (SD; n=136). As expected, the standard curve defined above also lies well within the pattern of standard data on which it is based (Figure 4.3). The high R^2 value of the regression line indicates that the standard curve accounts for about 95.5% of the fluorescence data variation (Table 4.2). The accuracy of the standard curve in predicting polyphosphate concentration as a function of fluorescence was determined based on the standard curve's 95% confidence limits of fluorescence, which were fed into the standard curve to provide the 95% confidence limits of predicted concentration. On average, these upper and lower limits of concentration were 0.030 μM P (SD=0.007) higher or lower than the actual concentration value. For ease of use, the key parameters of the statistical analysis and other information are summarized in Table 4.2. We emphasize that a linear standard curve for the concentration of polyphosphate 15-130 phosphorus units in length is replicable in any system under the assumptions given. However, exact slope and intercept values will vary slightly depending upon the experimental conditions, such as the particular spectrofluorometer used to obtain fluorescence measurements and slight

Table 4.2 Summary of standard curve for polyphosphate concentration vs. fluorescence. The standard curve for polyphosphate concentration versus DAPI-polyphosphate fluorescence was constructed based on data from polyphosphate standards ranging from 15-130 phosphorus units in length. The curve equation takes the form provided below, where Y is raw fluorescence in units of relative fluorescence units (rfu), X is concentration in units of μM P, and β_0 and β_1 are statistically determined intercept and slope values, respectively. The accuracy of the curve's measurement of concentration was determined based on the curve's 95% confidence limits.

$$Y=\beta_0+\beta_1 X$$

Summary of Standard Curve	
β_0	4.944
β_1	6.694
R^2	0.955
Accuracy of concentration measurement	±0.03μM P

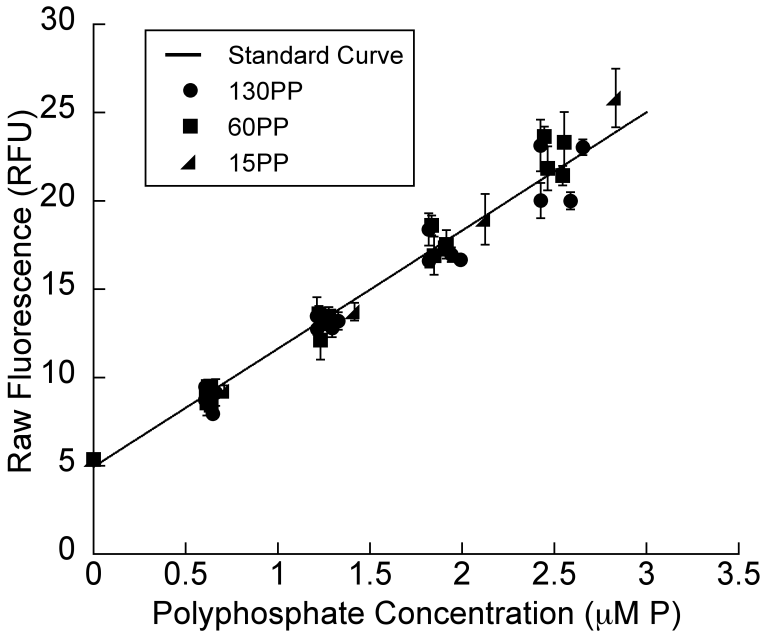

Figure 4.3 Standard curve for polyphosphate concentration v. fluorescence. The standard curve is based on data collected from standard polyphosphates between 15 and 130 phosphorus units in length that are free of the salt and age effects discussed in the main text. The standard data are provided for comparison to the standard curve. Error bars for data points represent 95% confidence limits. Fluorescence is given in relative fluorescence units (rfu). See Table 4.2 for more detail regarding the standard curve.

variations in the concentration of DAPI. Therefore, construction of new standard curves is highly recommended for any subsequent analysis in order to account for these differences.

4.4.4 Assessment of Potential Analytical Interferences from Natural Samples

Salt—The presence of salt (150mM KCl, conductivity ~10mS/cm) significantly suppressed the fluorescence yielded from the reaction of 15PP with DAPI, especially at lower polyphosphate concentrations (Figure 4.1). This salt effect was not apparent for longer polyphosphate standards between 45 and 130 phosphorus units in length (Figure 4.1). These observations suggest that in natural samples possessing a range of polyphosphate chain lengths, polyphosphates of comparable size to 15PP may also yield a suppressed fluorescence signal if analyzed in the presence of salt (i.e., conductivity above ~1mS/cm). Indeed, during sample analyses (detailed below), samples showed up to 39% lower polyphosphate contents when analyzed in a matrix of 150mM KCl-20mM HEPES as compared to analysis in a matrix of plain 20mM HEPES (conductivity ~450μS/cm). We therefore recommend the analysis of samples in a neutral-buffered freshwater matrix to ensure accurate representation of both intermediate and long chain polyphosphates.

Nucleotides—Commercial-grade adenosine 5'-triphosphate (ATP) (Sigma product #A2383) was analyzed to assess whether the current method is sensitive to nucleotide-bound polyphosphate. ATP solutions were prepared in the 20mM HEPES matrix, at various levels of P concentration ranging from 1μM P to 1mM P. The interaction of ATP with DAPI varied with the concentration of ATP. For example, at a concentration level of 1mM P, ATP fluorescence was ~600% higher than the average blank value. This relative fluorescence decreased to 100% at 100μM P and became

negligible (6-13%) at 1μM and 10μM P. Thus, measureable signal from ATP only occurred at extremely high levels of ATP that are unlikely to be encountered in biological and environmental samples [*Björkman and Karl*, 2005]. We therefore conclude that the current method discriminates between nucleotide-bound polyphosphate and inorganic storage forms of polyphosphate that typically exhibit longer chain lengths. If, in the uncommon case, high levels of ATP are expected in a sample, independent tests of ATP are available, such as the luciferase-luciferin enzyme assay [*Björkman and Karl*, 2001].

Other polymeric ions—Interferences in the quantification of polyphosphate that arise from DAPI interaction with DNA and other nucleic acids are minimized in this method based on the increase in polyphosphate specificity that occurs by illuminating samples with 415nm light and detecting fluorescence at 550nm [*Aschar-Sobbi et al.*, 2008]. The reader is referred to the work of [*Aschar-Sobbi et al.*, 2008] for a complete discussion of this point. In addition to polyphosphate and nucleic acid, DAPI is known to bind other polymeric ions such as certain lipids [*Serafim et al.*, 2002; *Streichan et al.*, 1990; *Tijssen et al.*, 1982]. Under illumination with 360nm light, the fluorescence signal that results from the binding of DAPI to these molecules overlaps that of the DAPI-polyphosphate complex [*Serafim et al.*, 2002; *Streichan et al.*, 1990]. However, the signal from lipids is weak and fades on the order of seconds [*Serafim et al.*, 2002; *Streichan et al.*, 1990]. Any interfering lipid signal that may emerge in natural samples is therefore likely to be undetectable after the seven-minute reaction time required for this method. The use of 415nm light for excitation, combined with the detection of fluorescence at 550nm may also improve the polyphosphate specificity of the current method, not just in relation to the DAPI-DNA signal [*Aschar-Sobbi et al.*, 2008], but also in comparison to any potential DAPI-lipid signal. To our knowledge, however, this has not yet been tested.

Table 4.3 Fluorometric analysis of polyphosphate in natural samples. All DAPI-based measurements of polyphosphate are based on several replicates. Where available, previously determined NMR-based measurements of polyphosphate content are presented for comparison. Details of each sample are given in [*Diaz et al.*, 2008] or [*Kolowith et al.*, 2001].

Sample	PolyP±SD (μmolP/g) DAPI method	Total P±SD (μmolP/g)	% Poly-P (DAPI method)	% Poly-P (NMR)	Reference
Marine Plankton I	11.05±3.26	123.0±1.7	10.58%	7%	Diaz et al. (2008)
Marine Plankton II	9.56±0.64	71.8±7.2	12.66%	--	Diaz et al. (2008)
Marine Plankton III	11.28±1.83	103.6±20.0	10.22%	--	Diaz et al. (2008)
Marine Sediment Trap	12.80±1.77	59.76±0.42	23.04%	10%	Diaz et al. (2008)
Marine Bacteria Enrichment Culture	95.81±6.64	410.4±2.8	23.35%	7%	Kolowith et al. 2001

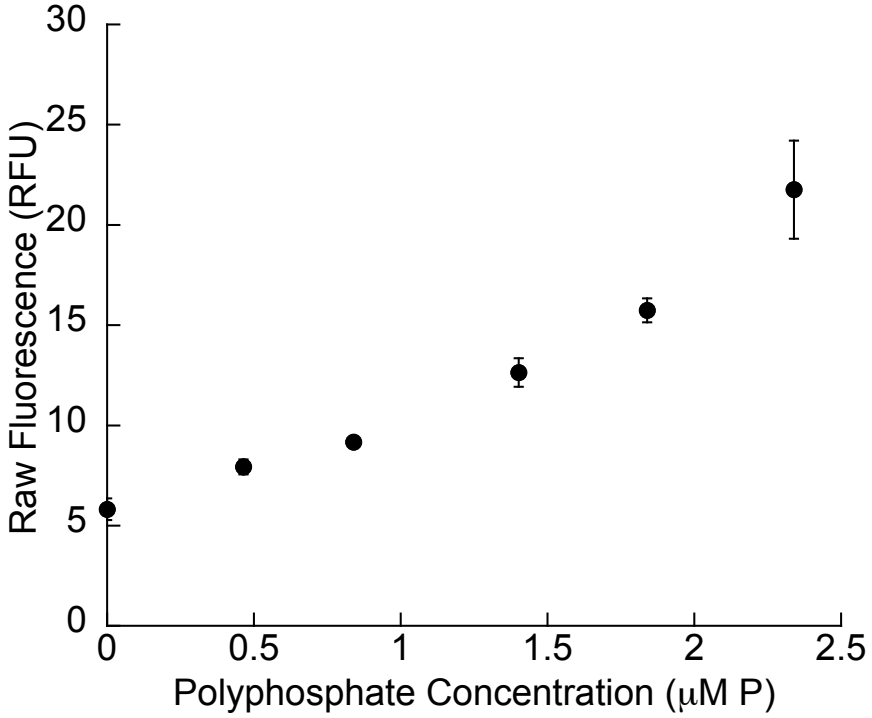

Figure 4.4 Standard addition experiment. The sample matrix of our bacterial enrichment culture sample (see Table 4.3) did not interfere with detection of standard 60PP additions. Plotted here is the fluorescence-independent calculation of polyphosphate content versus DAPI-polyphosphate fluorescence. The concentration level of 0μM polyphosphate represents the DAPI-reacted HEPES blank. The next level of concentration (~0.5uM P) represents sample solution that has not been amended with standard, i.e. the polyphosphate content inherent to the sample. The remaining points represent successively larger additions of 60PP to the sample solution. The overall pattern that emerges is equivalent to the standard curve presented in Figure 4.3. Error bars represent the standard deviation of 3-6 replicate measurements.

Sample matrix effects—We performed a standard addition experiment using the sample matrix of our bacterial enrichment culture sample (Table 4.3) and the 60PP standard to assess the potential influence of sample matrix effects on the quantification of polyphosphate. We found that the matrix of this sample did not alter the expected fluorescence from standard additions (Figure 4.4).

Charged organic species—We suspect that the presence of charged organic molecules will suppress the DAPI-polyphosphate fluorescence signal in a chain length dependent manner similar to inorganic salts, as the DAPI-polyphosphate interaction appears to be ionic. Indeed, our early experiments involving the addition of trichloroacetic acid (0.1% final concentration) inhibited the DAPI-polyphosphate reaction.

4.4.5 Sample Analyses

The conductivity of each final sample was checked prior to analysis to ensure that the sample matrix was adequately dilute with respect to salt content. Indeed, conductivities were less than 1 mS/cm for every sample, comparable to the conductivity of the plain 20mM HEPES matrix.

Fluorescence values collected from sample solutions that had been reacted with DAPI were corrected to the background fluorescence present in the sample. The background fluorescence was determined in two steps. First, a fluorescence measurement was taken on the sample in the absence of DAPI. Second, this DAPI-free fluorescence was adjusted based on the fact that the standard curve takes into account an inherent level of fluorescence from the non-reacted HEPES matrix itself. This DAPI-free HEPES blank need not be subtracted from the sample polyphosphate signal. In our experiments, for example, the non-reacted HEPES blank was typically ~1 relative fluorescence units (rfu), whereas a typical sample blank was ~5 rfu. The adjusted

sample blank would therefore attain a value of 4 rfu. This adjusted sample blank was subtracted from the signal generated by the DAPI-reacted sample, and this final corrected fluorescence was used to calculate polyphosphate content based on the standard curve. We found that consistent polyphosphate measurements were attainable for each sample over a period of at least eight days of frozen storage.

Polyphosphate ranged from 9.56-95.81μmolP/g, with the lowest content found in the phytoplankton samples (~11% total P) and the highest content found in the sediment trap and bacterial enrichment culture samples (~23%) (Table 4.3). NMR-based estimates of polyphosphate content were available for three of the natural samples examined (Table 4.3). These NMR estimates were calculated in a highly conservative manner and should be considered only as a minimum estimate of the polyphosphate content of each sample [*Diaz et al.*, 2008; *Kolowith et al.*, 2001; *Young and Ingall*, 2010]. Given the conservative nature of the NMR estimates, the DAPI-based measurements of polyphosphate were, as expected, higher than the NMR values in all cases but in general correspond well, providing an independent check of the fluorometric method.

4.5 Acknowledgements

The authors wish to thank Dr. Toshikazu Shiba and Dr. Yumi Kawazoe of Regenetiss Co., Tokyo, Japan, for generously providing their polyphosphate salts as standard materials for this research. We also thank Dr. Evgeny Pavlov of the University of Calgary for his assistance in our search for polyphosphate standards. In addition, we offer very special thanks to Dr. Julian Diaz III of Georgia State University for his instrumental assistance with our statistical analyses. This work was funded by the

National Science Foundation under grants 0849494 and 0526178, and by the US-Israel Binational Science Foundation under grant 2008216.

CHAPTER 5

THE ROLE OF POLYPHOSPHATE IN THE REDOX-SENSITIVE CYCLING OF PHOSPHORUS IN EFFINGHAM INLET, VANCOUVER ISLAND, BRITISH COLUMBIA

5.1 Abstract

A combination of field evidence and reactive transport modeling suggest that redox-sensitive polyphosphate (poly-P) cycling is a quantitatively significant process in the water column of Effingham Inlet, British Columbia. Effingham Inlet is a site possessing permanently anoxic bottom waters, with a water column redox transition zone typically occurring at least forty meters above the sediment water interface. During cruises conducted in April and July 2007, this redox transition zone was associated with sharp positive gradients in the concentrations of a variety of parameters, including soluble reactive phosphorus (SRP), particulate organic carbon (POC), nitrogen (PON), phosphorus (POP), and bacterial abundance. These patterns could not be explained by simple particle accumulation, however, as POC:POP and POC:PON ratios, in addition to cell-normalized POP concentrations, revealed that phosphorus accumulates independently of these other parameters. Approximately 30% of the particulate phosphorus at the redox transition was determined to be poly-P, based on sequential extraction. However, inorganic poly-P only accounted for ~1% of the total phosphorus at the redox transition, indicating that the dominant form of poly-P at the redox transition is likely to be organic tri-nucleotides. The quantitative contribution of poly-P cycling to the maintenance of the SRP peak present at the redox transition was constrained by a simple kinetic model of the iron system. Model results indicated that only 65% of the SRP concentration at the redox transition could be accounted for by SRP interaction with the iron system. This finding supports the hypothesis that other mechanisms capable of

accumulating dissolved phosphorus at redox transition zones exist, including redox-sensitive poly-P cycling, and furthermore provides an upper limit to the quantitative contribution of redox-sensitive poly-P cycling in the water column of Effingham Inlet.

5.2 Introduction

Phosphorus (P) is a vital nutrient for life, present as an essential component in DNA, phospholipids, and ATP. In the marine environment, P is considered the ultimate limiting nutrient over geologic timescales because slow tectonic processes control its input to the ocean, and the inputs of other nutrients are rapid by comparison (e.g. biological fixation of atmospheric N_2) [*Broecker*, 1982; *Redfield*, 1958; *Van Cappellen and Ingall*, 1996]. Mounting evidence over the last several decades has shown that P is present at limiting concentrations in vast regions of the modern ocean, leading to a growing need for a better understanding of the short-term P cycle as well [*Benitez-Nelson*, 2000; *Paytan and McLaughlin*, 2007].

A widespread process in the global P cycle is the enhanced remobilization of P from oxic-anoxic transition zones, which has been observed in lacustrine and marine waters and sediments worldwide, in both modern and ancient settings [*Golterman*, 2001; *Hupfer and Gachter*, 1995; *Ingall and Jahnke*, 1994; 1997; *Ingall et al.*, 1993; *Slomp et al.*, 2002]. This important process contributes to the redox stabilization of the atmosphere and earth surface over geologic time [*Van Cappellen and Ingall*, 1996]. Over the period of years to centuries, however, this process exacerbates ecological problems associated with anthropogenic eutrophication, e.g. the Baltic Sea [*Jilbert et al.*, 2011; *Savchuk et al.*, 2008; *Vahtera et al.*, 2007], resulting in excess water column P concentrations, changing nitrogen (N) fixation patterns, and devastating impacts on the native macrofauna and fisheries industries [*Jilbert et al.*, 2011; *Vahtera et al.*, 2007].

Because eutrophication likely leads to P-limited systems [*Codispoti et al.*, 2001; *Rabalais et al.*, 2002], combined with the fact that oxygen minimum zones in the ocean are expanding due to human activity [*Naqvi et al.*, 2000; *Rabalais et al.*, 2001; *Stramma et al.*, 2008], the ecological and biogeochemical impacts of enhanced anoxic P regeneration have an increasingly broad reach and therefore strong potential to alter global ecosystem function and the global nutrient cycles of P, N, and associated elements.

Despite the significant impacts of enhanced anoxic P regeneration on the global environment over both geologic and modern timescales, its mechanisms remain poorly constrained. The classic explanation involves the reductive dissolution of iron (Fe) oxyhydroxide mineral particles by bacteria. Under oxic conditions, Fe oxyhydroxides are stable and act as an efficient surface for P adsorption. On the other hand, under anoxic conditions Fe oxyhydroxides are unstable, and therefore P is more freely transported into adjacent waters. Although this Fe mechanism is a common and certainly well studied process (e.g., [*Froelich et al.*, 1979; *McManus et al.*, 1997; *Mortimer*, 1941; 1942; *Sundby et al.*, 1992]), its quantitative contribution to the enhanced hypoxic/anoxic regeneration of P remains poorly constrained. For example, Fe-linked P cycling has been shown to be insufficient to account for redox-sensitive P regeneration in some sedimentary environments [*Golterman*, 2001; *Ingall et al.*, 2005; *Jilbert et al.*, 2011] and water column redox transition zones [*Jilbert et al.*, 2011; *Turnewitsch and Pohl*, 2010].

An additional potential mechanism for redox-sensitive P cycling in aquatic environments is inorganic polyphosphate (poly-P) cycling by bacteria. Inorganic poly-P is a linear polymer of at least three orthophosphate molecules linked by high energy phosphoanhydride bonds, the same type of bonds present in ATP [*Brown and Kornberg*, 2004; *Kornberg*, 1995]. Inorganic poly-P is almost strictly a biogenic molecule in natural

systems and typically ranges in size from three to several hundreds of P atoms [*Kornberg*, 1995]. Poly-P is a common biomolecule found in every type of cell, and its biological purpose is multifunctional, including storage of P and energy [*Kornberg et al.*, 1999; *Rao et al.*, 2009].

Inorganic poly-P is a redox-sensitive molecule in many groups of bacteria, such as the poly-P accumulating organisms (PAOs) that are utilized in the process of enhanced biological P removal (EBPR) during wastewater treatment [*Comeau et al.*, 1986; *Nielsen et al.*, 2010; *Schuler and Jenkins*, 2003; *Seviour et al.*, 2003]. In EBPR, PAOs are enriched in anoxic reactors, presumably due to their ability to utilize inorganic poly-P as a source and substitute for ATP in the absence of oxygen as a terminal electron acceptor. Upon exposure to oxygen, the PAO-dominated community removes dissolved P in order to reform intracellular poly-P reserves, producing a system deplete in dissolved P and rich in particulate P, which can be filtered and removed [*Comeau et al.*, 1986; *Nielsen et al.*, 2010; *Schuler and Jenkins*, 2003; *Seviour et al.*, 2003].

An analogous process to EBPR may be contributing to the redox-sensitive cycling of P in aquatic systems [*Hupfer and Gachter*, 1995; *Hupfer et al.*, 2004; *Ingall and Jahnke*, 1997; *Sannigrahi and Ingall*, 2005]. Poly-P metabolism occurs along a redox potential range that overlaps microbially mediated iron reduction [*Davelaar*, 1993]. Thus, P distribution and fluxes in sediments attributed to the coupled cycling of iron and phosphate may include some component of polyphosphate metabolism. Poly-P has recently been discovered to account for a substantial portion of the total P in marine systems [*Diaz et al.*, 2008]. But the potential redox-sensitive cycling of this chemical species has historically eluded direct detection [*Davelaar*, 1993; *Gachter et al.*, 1988; *Golterman*, 2001; *Hupfer and Gachter*, 1995; *Hupfer et al.*, 2004; *Hupfer et al.*, 2008; *Sannigrahi and Ingall*, 2005; *Schulz and Schulz*, 2005].

Here, we present a set field observations and reactive transport modeling to clarify the role of poly-P in the redox-sensitive remineralization of P. Our findings lend evidence in support of the hypothesis that redox-sensitive poly-P cycling by microbes is a quantitatively significant process in marine systems.

5.3 Methods

5.3.1. Study site

Field observations were collected during April and July 2007 from Effingham Inlet, a fjord located on the west coast of Vancouver Island, British Columbia (Figure 3.1). Effingham Inlet is a very narrow basin with a dynamic bottom water topography, including a shallow (40m) sill present at the entrance to the upper basin, which restricts circulation in this area, leading to persistent bottom water anoxia. The location of the water column redox transition zone varies across seasons but is typically present between sixty and eighty meters depth, while the total depth of the basin is about 120m.

5.3.2. Sample collection and analysis

Seawater samples and *in situ* data were collected aboard the *R/V Barnes* using a CTD rosette sampler. Dissolved oxygen content and physical properties of the seawater such as temperature and salinity were measured continuously during each cast, and these data were processed using the SEASOFT software (Seabird Electronics, Inc., Washington, USA). Samples for dissolved Fe (II) and soluble reactive P (SRP) were syringe-filtered (0.45μm GF/F) and analyzed onboard according to standard colorimetric protocols [*Hansen and Koroleff*, 1999c; *Koroleff and Kremling*, 1999]. Samples for bacterial counts were fixed in 2% formaldehyde and filtered onto polycarbonate membrane filters (0.2μm). Cells were counted on an Olympus epifluorescence microscope after staining with 4',6'-Diamidino-2-phenylindole.

Particles were also collected from seawater onto 1μm GF/F filters using an *in situ* pump sampler. Particulate organic nitrogen (PON) and carbon (POC) were determined by quantifying total nitrogen and carbon on vapor acidified and non-acidified samples with a CHN elemental analyzer (Costech Instruments, Inc.) according to the method of [*Hedges and Stern*, 1984]. Particulate P was quantified by the procedure of Aspila et al. [*Aspila et al.*, 1976], while particulate P speciation was assessed using the P sequential extraction procedure developed by [*Miyata and Hattori*, 1986] and that developed by [*Ruttenberg*, 1992]. Direct quantification of inorganic poly-P was accomplished using a modified protocol of [*Diaz and Ingall*, 2010]. Extractable iron analysis was performed following 24 hour extraction of the *in situ* pump filter material into a basic solution of 5% bicarbonate, 5% citrate, and 2% ascorbic acid, subsequent acidification to pH=1 and analysis on a flame atomic adsorption spectrometer.

5.3.3. Reactive transport modeling—Oxygen and Fe system

Complete water column profiles (5-110m) of oxygen (O_2), dissolved Fe (II), and particulate Fe(III) were modeled by integrating one-dimensional steady state reactive transport equations for the transformation of each species. The following chemical reactions were considered in the model:

$$O_2 + CH_2O \rightarrow CO_2 + H_2O \quad (1)$$

$$2Fe^{2+} + 2H_2O + \frac{1}{2}O_2 \rightarrow Fe_2O_3 + 4H^+ \quad (2)$$

$$Fe_2O_3 + 4H^+ + \frac{1}{2}CH_2O \rightarrow 2Fe^{2+} + \frac{5}{2}H_2O + \frac{1}{2}CO_2 \quad (3)$$

where particulate Fe(III) is assumed to be Fe_2O_3 (hematite), dissolved Fe(II) is assumed to be free Fe^{2+}, and POC is assumed to be CH_2O. Reaction (1) represents aerobic

respiration of organic matter, reaction (2) is the oxidative precipitation of Fe^{2+} to Fe_2O_3 by molecular oxygen, and reaction (3) is the reductive dissolution of Fe_2O_3 to Fe^{2+} by particulate CH_2O, which is assumed to be oxidized completely to CO_2.

The rate law for aerobic respiration of POC (R_{AR}) was assumed to follow Michaelis-Menten kinetics. The rate equation was therefore defined as:

$$R_{AR} = \frac{R_{MaxO_2}[CH_2O][O_2]}{[O_2] + K_{MO_2}} \qquad (4)$$

where [O_2] and [CH_2O] represent the molar concentrations of POC and O_2, respectively. It was assumed that POC never limited any of the reaction rates, thus its concentration was set equal to the measured surface concentration of 7.3×10^{-5} M. The rate constants R_{MaxO_2} and K_{MO_2} were set equal to 10^{-10} min^{-1} and 3.1×10^{-8} mol L^{-1}, which are typical values for these constants [*Rabouille and Gaillard*, 1991].

The rate law for Fe(II) oxidation by oxygen (R_{Feox}) is well established [*Davison and Seed*, 1983; *Millero*, 1985; *Millero et al.*, 1987; *Sung and Morgan*, 1980] and takes the form:

$$R_{Feox}=k_{Feox}[Fe^{2+}][OH^-]^2[O_2] \qquad (5)$$

where [Fe^{2+}], and [OH^-] represent the molar concentrations of dissolved Fe (II), and the hydroxide anion, respectively, and k_{Feox} is equal to 6.154×10^{16} $min^{-1}mol^{-3}$ L^3 [*Millero*, 1985; *Millero et al.*, 1987]. The concentration of OH^- in the system was assumed to be a constant 10^{-6} M.

The rate expression for Fe (III) reduction (R_{Fered}) was defined as:

$$R_{Fered} = \frac{R_{MaxFe}[Fe_2O_3][CH_2O]}{1 + k_{in}} \qquad (6)$$

where [Fe_2O_3] represents the molar concentration of particulate Fe (III). The second order rate constant R_{MaxFe} was fit to the data using a standard least squares optimization protocol. The oxygen inhibition constant k_{in} (unitless) was defined according to the equation:

$$k_{in} = k_{0in} \exp\left(\frac{-O_{2_{sfc}}}{kO_2}\right) \quad (7)$$

where k_{0in} is the initial inhibition constant, $O_{2_{sfc}}$ is the molar concentration of oxygen at the surface (5m), k is the decay constant, and O_2 is the molar concentration of oxygen at each depth. Both k_{0in} and k were fit to the experimental data in a least squares fashion.

Taking into account reactions (1), (2), and (3), the governing equations for O_2, Fe^{2+}, and Fe_2O_3 were defined as:

Eqn (8):

$$\frac{d[O_2]}{dt} = \frac{d^2D[O_2]}{dx^2} - w\frac{d[O_2]}{dx} - \frac{R_{MaxO_2}[CH_2O][O_2]}{[O_2]+K_{MO_2}} - \frac{1}{2}k_{Feox}[Fe^{2+}][OH^-]^2[O_2]$$

Eqn (9):

$$\frac{d[Fe^{2+}]}{dt} = \frac{d^2D[Fe^{2+}]}{dx^2} - w\frac{d[Fe^{2+}]}{dx} - 2k_{Feox}[Fe^{2+}][OH^-]^2[O_2] + 2\frac{R_{MaxFe}[Fe_2O_3][CH_2O]}{1+k_{in}}$$

Eqn (10):

$$\frac{d[Fe_2O_3]}{dt} = \frac{d^2D[Fe_2O_3]}{dx^2} - s\frac{d[Fe_2O_3]}{dx} + k_{Feox}[Fe^{2+}][OH^-]^2[O_2] - \frac{R_{MaxFe}[Fe_2O_3][CH_2O]}{1+k_{in}}$$

where t=time in minutes, x=depth in meters, D is the depth-dependent dispersion coefficient in units of m^2min^{-1}, and w and s are the advection constants for the dissolved and particulate phases, respectively, in units of m min^{-1}. The dispersion coefficient was determined based on the profiles of temperature and salinity at the study site (Figure

5.1). Advection was assumed to be negligible in the system, thus each advection constant was set equal to zero.

Equations (8), (9), and (10) form a system of coupled differential equations which was solved iteratively in the Matlab® and Simulink® software package, student version (R2010a) using the numerical method of central finite difference approximation. The program codes are provided in Appendix C.

The boundary conditions for each species consisted of Neumann boundary conditions and Dirichlet conditions (Table 5.1). All concentrations used represent the measured values.

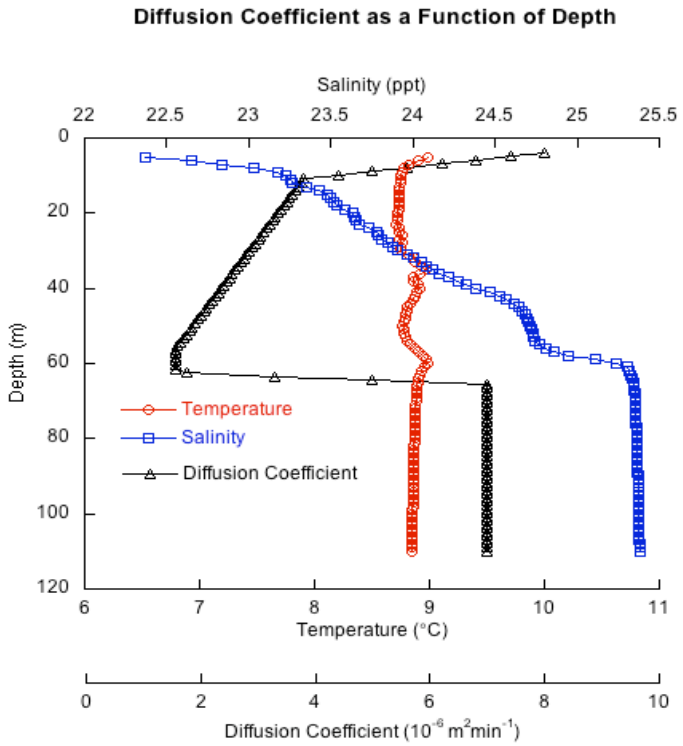

Figure 5.1 Diffusion coefficient as a function of depth

Table 5.1 Boundary conditions used in the reactive transport models of oxygen, iron, and phosphorus

Species	Depth (m)	Type	Value
Oxygen	5	Dirichlet	100.87 μM
	110	Neumann	0 μmol m^{-2} min^{-1}
Particulate Fe (III)	5	Dirichlet	0 μM
	110	Dirichlet	0.99 μM
Dissolved Fe (II)	5	Neumann	0 μmol m^{-2} min^{-1}
	110	Dirichlet	0 μM
SRP	5	Neumann	0 μmol m^{-2} min^{-1}
	100	Dirichlet	5.39 μM

5.3.4. Reactive transport modeling—SRP

Like the Fe system, SRP was modeled using one-dimensional steady state reactive transport. In order to isolate the effect of Fe cycling on SRP, the entire water column profile of SRP was modeled based solely on the interaction of SRP with the Fe system. Other processes such as SRP uptake in surface waters or SRP production through organic matter remineralization at depth were not included in the model. Notably, the SRP cycling linked to the Fe system did not influence the Fe system itself. This modeling approach is similar to that of Taillefert and Gaillard [*Taillefert and Gaillard*, 2002], who modeled dissolved lead (II) concentrations based on the species' interaction of with the Fe system.

The first reaction considered in the SRP reactive transport model is the adsorption of SRP onto the surface of particulate Fe (III) by the following reaction:

$$\alpha SRP + Fe_2O_3 \rightarrow Fe_2O_3 + \alpha \equiv SRP \quad (11)$$

where $\equiv SRP$ represents the SRP species adsorbed to the iron surface, and α is a stoichiometric coefficient relating the number of moles of SRP adsorbed to one mole of Fe_2O_3. The rate of the above reaction was assumed to be limited by the rate of Fe (III) oxyhydroxide precipitation. Thus, the rate of SRP adsorption to particulate Fe (III) (R_{ads}) can be defined as:

$$R_{ads} = k_{ads}[SRP] \quad (12)$$

where the rate constant k_{ads} is defined as:

$$k_{ads} = k_{Feox}[OH^-][O_2] \quad (13)$$

This approach follows that of [*Crosby et al.*, 1984], who modeled the adsorption of phosphate onto newly formed Fe (III) precipitates in seawater.

The second reaction considered was the reductive dissolution of particulate Fe (III) by POC, seen earlier in reaction (2), accompanied by a simultaneous release of desorbed SRP. This leads to the reaction:

$$Fe_2O_3 + \alpha \equiv SRP + \frac{1}{2}CH_2O + 4H^+ \rightarrow 2Fe^{2+} + \frac{5}{2}H_2O + \frac{1}{2}CO_2 + \alpha SRP \quad (14)$$

This reaction follows the rate law in equation (6), leading to the following governing equation for the reactive transport of SRP:

$$\frac{d[SRP]}{dt} = \frac{d^2D[SRP]}{dx^2} - w\frac{d[SRP]}{dx} - \alpha k_{ads}[SRP] + \alpha \frac{R_{MaxFe}[Fe_2O_3][CH_2O]}{1 + k_{in}} \quad (13)$$

As with the Fe system, the SRP model was solved in Matlab using the numerical method of central finite difference approximation. The stoichiometric coefficient α was determined as the atomic ratio of extractable iron to ferric oxyhydroxide bound SRP (SEDEX) measured in particles at the redox transition (see Results and Discussion

section). The boundary conditions for SRP consisted of one Dirichlet and one Neumann boundary condition; experimental data were utilized (Table 5.1).

5.4 Results and Discussion

5.4.1. Field results

Field results revealed a water column redox transition zone at approximately 60-63m depth (2.6% oxygen saturation level) (Figure 5.2). The water column profiles of particulate P and SRP exhibited peaks in concentration corresponding to this redox transition, with total particulate phosphorus (TPP) increasing by approximately 1μM within ±2m and SRP increasing by ~0.6-1μM within 1-3m (Figure 5.3). These increases in P content are well above the range of typical experimental errors associated with the measurements of TPP and SRP. For instance, duplicate measurements of particulate P agreed to within <5%, and the measured value of NIST Standard Reference Material

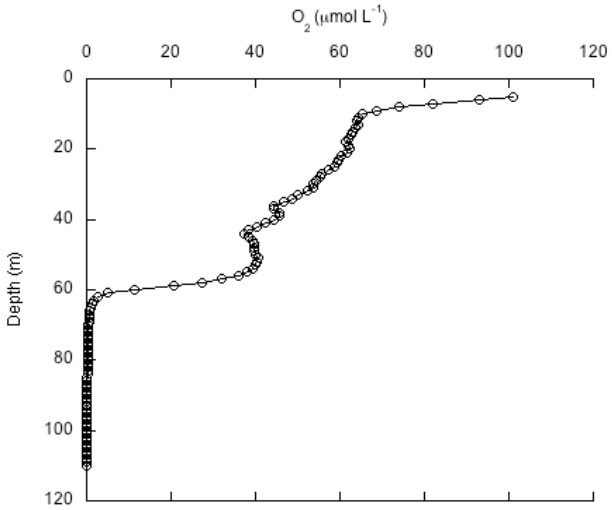

Figure 5.2 Oxygen profile. The redox transition occurs at 60-63m depth (~2.6% saturation)

1573a (tomato leaves) was within ±5% of the certified value. Measurements of SRP typically exhibited errors of <3%.

Our data indicate that these patterns in P distribution cannot be accounted for by simple particle accumulation. For example, atomic ratios of POC to particulate organic P (POP) and to TPP exhibit a sharp decrease equal to a factor of ~1.5-3 at the redox transition (Figure 5.4). In contrast, ratios of POC to particulate organic nitrogen (PON) are relatively constant with depth, indicating that phosphorus is preferentially accumulated in particulate matter relative to nitrogen at the redox transition (Figure 5.4). Notably, the error associated with the measurement of C and N is typically ±1%. One potential mechanism for redox-sensitive P cycling that has been invoked relies on the hypothesis that bacteria mineralize a larger fraction of organic matter under anaerobic conditions in order to satisfy their energetic demands [*Golterman*, 2001]. However, the marked decrease in particulate C to P ratios that occurs at the redox transition, in

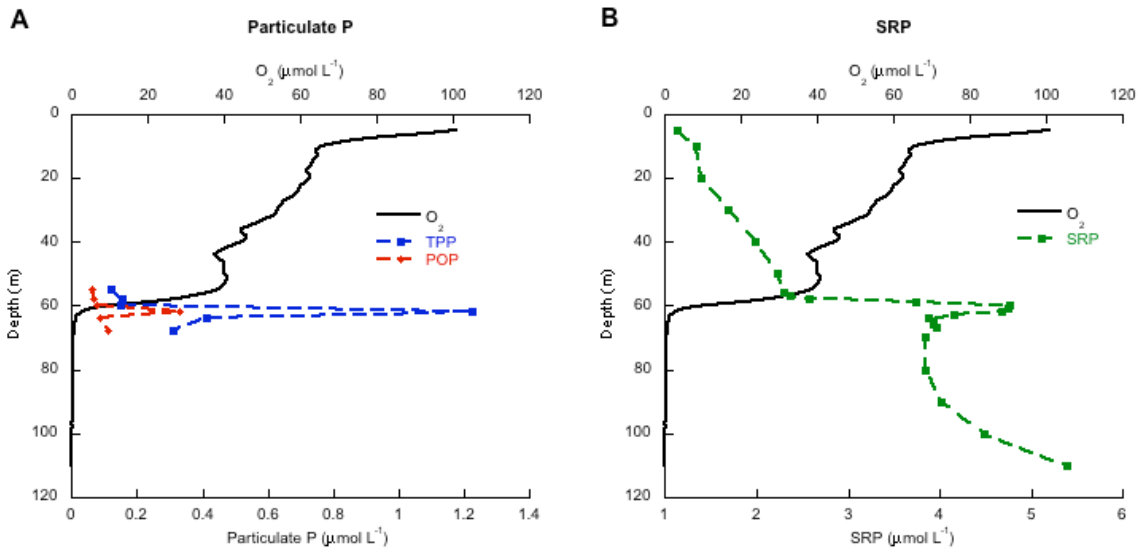

Figure 5.3 Profiles of particulate and dissolved phosphorus

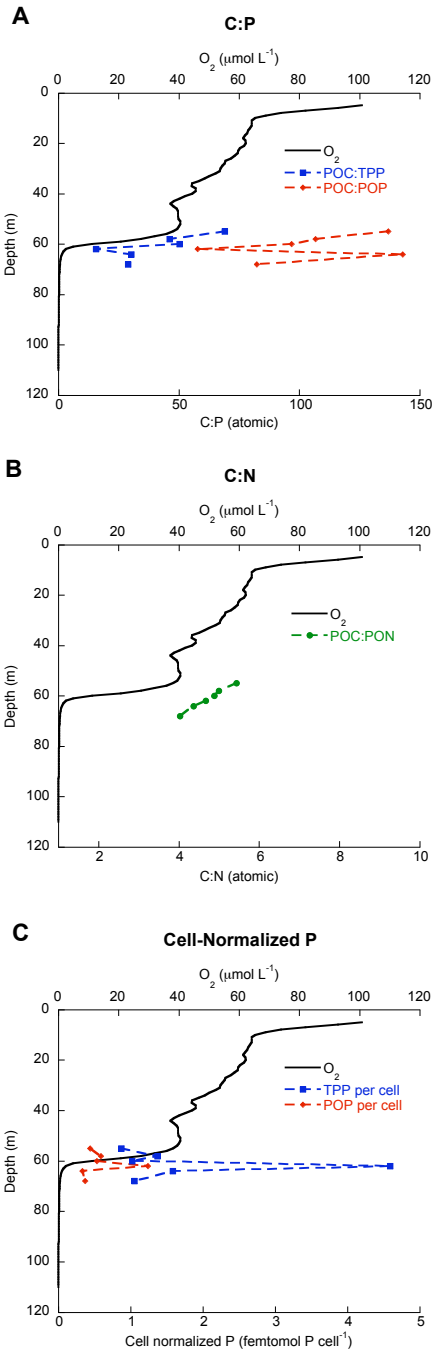

Figure 5.4 C:P ratios, N:P ratios, and cell-normalized P concentrations at the redox transition in Effingham Inlet

addition to the decoupling from N, favors an explanation involving redox-sensitive P speciation, in which an abundance of a redox-sensitive phase such as poly-P may contribute to the enhanced regeneration of SRP. Our observations are also consistent with data collected from other low-oxygen ancient and modern environments which also show a decoupling between P and organic matter [*Golterman*, 2001; *Hupfer and Gachter*, 1995; *Ingall and Jahnke*, 1994; 1997; *Ingall et al.*, 1993; *Jilbert et al.*, 2011; *Slomp et al.*, 2002].

In addition to the C:P ratios, the pattern of particulate P normalized to bacterial cell abundance also shows a dynamic pattern, with the concentration of TPP expressed per cell increasing by approximately 2.5 femtomol cell^{-1} (corresponding to a factor of 3-5) within ±2m of the redox transition (Figure 5.4). This finding furthermore demonstrates that P is more dynamic than other biologically-relevant parameters at the redox transition and suggests that the *in situ* bacterial community may store excess P under anoxic conditions relative to their constitutive demand under redox-stable conditions. Notably, this pattern is also consistent with the conceptual models of PAO's in EBPR systems.

Our results provide further insight in to the speciation of P at the redox transition. For example, the total concentration of Fe-bound P was 84.8nM, only 7% of total P. Despite this relatively low P concentration, the atomic ratio of particulate Fe (III) to Fe-bound P was 1.766 at the redox transition, which is relatively low compared to the typical Fe:P ratio in modern, fully oxygenated sediments (~40) [*Planavsky et al.*, 2010]. Sequential extraction analyses revealed that the concentration of total poly-P at the redox transition was 393.85nM, which accounts for approximately 32% of TPP at that depth. Although this concentration of poly-P is much higher than that observed in phytoplankton material from Effingham Inlet surface waters [*Diaz and Ingall*, 2010], it is not inconsistent with other previous observations of poly-P content in organisms.

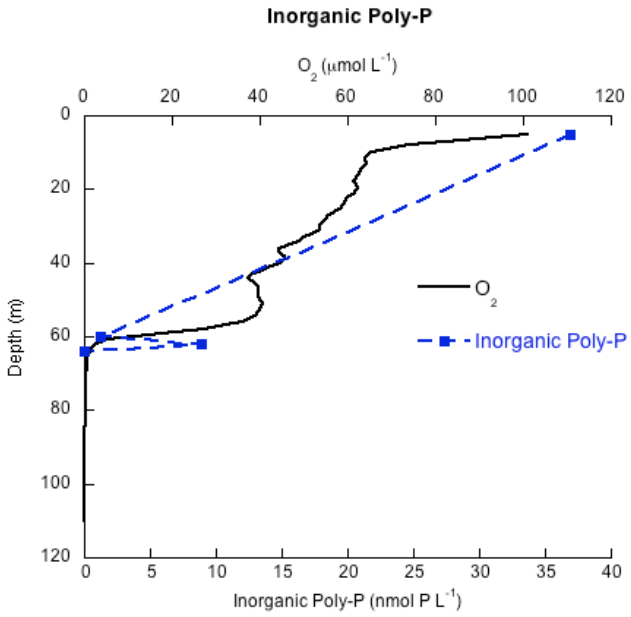

Figure 5.5 Inorganic polyphosphate profile

For example, Orchard et al. (*2010*) found that total polyphosphate accounted for up to 25% of total phosphorus in natural populations of *Trichodesmium* spp. in the Sargasso Sea. Similarly, laboratory isolates of *Skeletonema* spp. and *Thalassiosira* spp. can accumulate poly-P to levels as high as 30% and 19-43% of total phosphorus, respectively [*Perry*, 1976; *Solorzano and Strickland*, 1968]. The finding in Effingham Inlet of enhanced poly-P content (relative to surface phytoplankton material) suggests that redox-sensitive P speciation may involve a compositional shift towards higher total poly-P content.

The majority of total poly-P detected at the redox transition is likely to be in the form of organic tri-nucleotides, as direct measurements of inorganic polyphosphate were low across the redox transition. For example, at 2m above the redox transition, inorganic poly-P was present at 1.23 nM (Figure 5.5). Inorganic poly-P increased to 8.88nM at the redox transition and decreased below the detection limit at 2m below the redox transition (Figure 5.5). While this pattern of inorganic poly-P concentration is

consistent with the conceptual models of PAO's, inorganic poly-P only represents 0.7% of total P at the redox transition, suggesting it is not an important component of the P cycle. However, because this system may not satisfy steady state, the inability to detect substantial inorganic poly-P remains inconclusive. Nevertheless, the detection of abundant organic poly-P, albeit indirect, is consistent with our hypotheses, as inorganic poly-P is used as a substrate for the formation of nucleotides such as ATP in the EBPR process.

5.4.2. Model results

Model simulations succeeded in reproducing the profiles of O_2, dissolved Fe (II), and particulate Fe (III) (Figure 5.6). The fitted constants R_{MaxFe}, k_{0in}, and k attained values of 0.0495 min L mol^{-1}, 1×10^{12}, and 1.1995, respectively.

Model calculations also reproduced a peak in SRP at the redox transition (Figure 5.6), although the peak model concentration (3.13μM) was only 65% of the peak SRP concentration (4.77μM). Thus, model simulations show that Fe cycling can only account for 65% of dissolved P at the redox transition zone.

Based on this result, other mechanisms besides Fe cycling, such as poly-P cycling, must also contribute to the accumulation of SRP at the redox transition at our study site.

Note that considerable discrepancies between the SRP model and the SRP data exist (Figure 5.6), especially at the surface where modeled SRP concentrations drop to 0μM (Figure 5.6). These discrepancies and appear because of the simplicity of the SRP model. It is not the goal of this paper to necessarily reproduce the measured SRP data. Rather, the point here is to use the model as a tool to isolate the role of Fe cycling on the SRP profile. Thus, such a lack of correlation between the model and the data is expected.

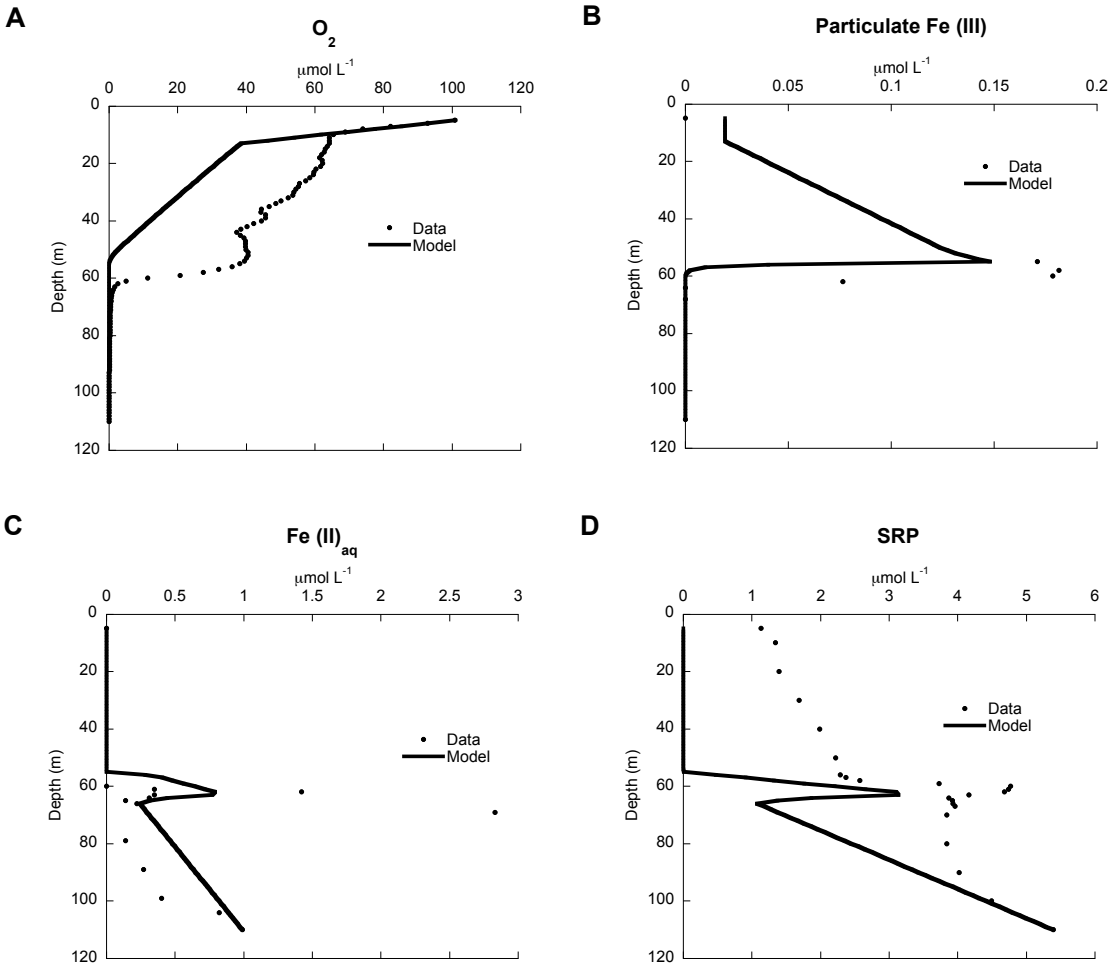

Figure 5.6 Model results

Our results are consistent with previous observations from Effingham Inlet. Ingall and colleagues (*2005*) estimated through mass balance that iron cycling was likely responsible for no more than 7% of the benthic P release from sediments in Effingham Inlet. Our current conclusions agree with this assessment at least qualitatively in that Fe cannot account for the entirety of P released under anoxic conditions [*Ingall et al.*, 2005]. Our results also support those of Sannigrahi and Ingall (*2005*), who posited a role for

poly-P in redox-sensitive cycling in Effingham based on its presnce in oxic surface sediments and absence in anoxic surface sediments of Effingham inlet.

5.6 Acknowledgements

This material is based upon work supported by the National Science Foundation under Grant No. 0526178. Thanks go to the crew of the R/V Barnes, Rick Keil and John Nuwer for assistance with field sampling, Susan Herron and Gabrielle Lyons for help during field sampling and sample analysis, and Renée Styles for assistance with sample analysis. Thanks also to George Patterson and John Platenius of the Clayoquot Field Station in Tofino, British Columbia, for providing lab space and a welcoming base for our field studies and to Meg Grantham for assistance in the use of the flame atomic adsorption spectrometer.

CHAPTER 6

CONCLUSIONS AND RECOMMENDATIONS

6.1 Redox-Sensitive Cycling of Polyphosphate

Our field data indicate that polyphosphate (poly-P), both in its organic and inorganic forms, may play a quantitatively significant role in the redox-sensitive cycling of P in the water column of Effingham Inlet. As the Fe cycle can account for 65% of the dissolved P remobilized at the redox transition, poly-P cycling may account for up to a substantial 35%. The role of poly-P in the redox-sensitive cycling of P implies a direct biological mechanism for the enhanced release of P seen in anoxic environments, a phenomenon that has been predominantly explained by abiotic or indirect biological mechanisms for over half a century. The potential role of poly-P in the redox-sensitive remobilization of P indicates that natural communities of PAO's may contribute to a negative feedback mechanism for atmospheric oxygen perturbations, as previously demonstrated in the general case [*Van Cappellen and Ingall*, 1996]. In addition, through mechanisms of redox-sensitive poly-P cycling, organisms may form a positive feedback to eutrophication and the expansion of the world's oxygen minimum zones.

Indirect observations collected from natural environments [*Hupfer and Gachter*, 1995; *Hupfer et al.*, 2008; *Sannigrahi and Ingall*, 2005; *Schulz and Schulz*, 2005] consistently point to poly-P as a quantitatively significant redox-sensitive molecule that likely contributes to the enhanced anoxic regeneration of P observed in aquatic systems worldwide. Certainly, it appears from our data and previous observations that P regeneration mechanisms are decoupled from those of C and N under anoxic conditions [*Golterman*, 2001; *Hupfer and Gachter*, 1995; *Ingall and Jahnke*, 1994; 1997; *Ingall et al.*, 1993; *Jilbert et al.*, 2011; *Slomp et al.*, 2002]. The lack of direct evidence for the role

of poly-P in this process, despite decades of research, inspires reflection as to what other potential species may be involved. One such species that has been proposed is the plant-derived molecule phytate, which bacteria may also degrade in a redox-sensitive manner [*Golterman et al.*, 1998]. In systems receiving substantial terrigenous influence such as Effingham Inlet, the role of phytate in redox-sensitive P regeneration may possibly be observable. However, this would not be the case in open oceanic systems that exhibit the same phenomenon of enhanced anoxic P regeneration.

Future studies should focus on the non-steady state kinetic modeling of the inorganic poly-P/nucleotide system to attempt to quantify the potential impact on redox-sensitive P release. Controlled incubations are yet another approach to pursue in future studies. Future work would also benefit from implementing molecular techniques, such as metagenomic approaches that would enable detection of potential PAO communities in natural redox transition environments. In addition, with the eventual engineering of viable probes, the *in situ* quantification of bacterial poly-P kinase expression would also illuminate the potential role of poly-P in the enhanced anoxic regeneration of P.

6.2 Future Research Directions

Future work in environmental polyphosphate research is likely to focus on the following:

1) kinetics and potential enzymatic control of apatite precipitation on polyphosphate surfaces

2) continued examination of the role played by polyphosphate in redox sensitive P cycling

3) potential bioavailability of exogenous polyphosphate to natural populations of aquatic microbes

4) environmental factors influencing polyP utilization and synthesis by microbes in aquatic systems

All of these research areas are certain to employ analytical methods that have already proven fruitful in the field of environmental poly-P research, including NMR, X-ray fluorescence technologies [*Diaz et al.*, 2009], and the fluorometric quantification of inorganic poly-P [*Diaz and Ingall*, 2010]. However, these methods must be complemented by other technologies. For example, environmental studies of polyphosphate would benefit immensely from the application of molecular approaches to track patterns of polyphosphate synthesis and utilization in the environment. In order to implement these metagenomic and metatranscriptomic protocols, however, *a priori* knowledge with regard to the enzyme and protein systems involved must be established. Fortunately, much of this work has already been done with regard to bacterial systems. On the other hand, eukaryotic mechanisms of polyphosphate metabolism are less well known.

While our understanding of the molecular basis underlying polyphosphate metabolism in microbes has advanced greatly over recent years, some questions remain, including:

1) How is phosphorus sensed and taken up by microbes in the ocean, including sedimentary environments, and is the process any different from the conventional picture of phosphate sensing and uptake by *E. coli*?

2) In what ways are polyphosphate and polyphosphate metabolizing enzymes involved in microbial phosphate sensing and uptake systems?

3) The enzymatic formation of polyphosphate from ATP by polyphosphate kinases is well-documented. By what additional mechanisms does polyphosphate form within cells? These may include utilization of proton-motive force for the direct enzymatic formation of polyphosphate from inorganic phosphate, or perhaps thermodynamic as opposed to direct enzymatic control of polyphosphate formation (e.g., iron oxide precipitation in magnetotactic bacteria)?

4) What significance does polyphosphate chain length hold for microorganisms, and how is chain length biologically regulated?

5) What explains the heterogeneous distribution of inorganic polyphosphate observed in *Chlamydomonas* sp. [*Diaz et al.*, 2009], and does this explanation involve acidocalcisomes?

6) Polyphosphate has a high chemical affinity for Ca^{2+} ions; are calcium-binding proteins involved in biological polyphosphate metabolism?

7) What role does polyphosphate play in the regulation of the ATP to ADP ratio in cells?

6.3 Molecular Basis of Polyphosphate Utilization and Synthesis

A number of polyphosphate metabolizing enzymes have been determined. For example, hydrolytic poly-P enzymes include exopolyphosphatases (e.g., PPX1 and PPX2 of *Escherichia coli* and scPPX1 of *Saccharomyces cerevisiae*), endopolyPase (e.g., PNN1 discovered in yeast), and poly-P/AMP phosphotransferase (PAP; originally discovered in *Acinetobacter*). Several poly-P synthesizing enzymes have been identified: polyphosphate kinase 1 (PPK1), originally discovered in *E. coli*; and PPK2, originally discovered in *Pseudomonas aeruginosa*. The only eukaryotic enzyme known to catalyze the synthesis of polyphosphate is known as VTC4, a polyphosphate polymerase [*Hothorn et al.*, 2009].

6.3.1 Polyphosphate Synthesis

PPK1 reversibly catalyzes the formation of polyphosphate by using ATP as a phosphorus source and is widely conserved in bacteria and archaea [*Rao et al.*, 2009]. For example, over 100 bacterial species possess sequences homologous to *ppk1*, including cyanobacteria and many heterotrophic bacteria common in marine environments (e.g. *Roseobacter* spp.) [*Rao et al.*, 2009]. PPK2 is usually found in organisms also possessing PPK1 [*Rao et al.*, 2009]. In contrast to PPK1, however, PPK2 favors the depolymerization of poly-P for the synthesis of GTP from GDP [*Zhang et al.*, 2002]. The slime mold *Dictostelium discoideum* is one of few eukaryotes in which

the bacterial PPK1 has been conserved; *D. discoideum* also possesses a homolog to PPK2 (DdPPK2) [*Rao et al.*, 2009]. Homologs of DdPPK2 are present in pathogenic protozoa and the eukaryotic alga *Chlamydomonas* [*Rao et al.*, 2009]. Polyphosphate metabolism is less well characterized in eukaryotes than bacteria. Recently, however, the *vtc4* gene of *S. cerevisiae* has been shown to encode a polyphosphate polymerase that appears to utilize ATP as a phosphorus source [*Hothorn et al.*, 2009]. Vtc4 also appears to integrate polyphosphate polymerization with translocation of poly-P across the vacuolar membrane [*Hothorn et al.*, 2009]. Discovery of the polyphosphate polymerase activity of Vtc4 provides new opportunities for the examination of polyphosphate synthesis in the many eukaryotes for which no other polyphosphate synthesizing enzyme is known, such as the common marine diatom *Thalassiosira pseudonana* [*Hothorn et al.*, 2009].

All known PPK enzymes require ATP (occasionally GTP as a substitute) as the phosphorus source for the synthesis of polyphosphate [*Rao et al.*, 2009]. However, the lack of PPK enzymes and homologous gene sequences to encode them in some organisms that are known to accumulate polyphosphate, especially eukaryotes, suggest that poly-P may be synthesized directly from inorganic phosphate by the utilization of proton motive force (PMF) [*Rao et al.*, 2009]. This hypothesis, however, requires further investigation.

6.3.2 Polyphosphate Utilization

Polyphosphate degrading enzymes include endopolyphosphatases (e.g., PPN1), which hydrolyze non-terminal bonds within the polyphosphate chain to make shorter polyphosphate molecules, and exopolyphosphatases (PPX enzymes), which hydrolyze terminal bonds to shorten polyphosphate molecules and produce inorganic phosphate.

Originally discovered in yeast, PPN1 (encoded by the yeast gene *PHM5*) is also present in animal cells [*Rao et al.*, 2009]. The human endopolyphosphatase encoded by *PPN1* has been linked to melanoma [*Arakaki et al.*, 2006]. Yeast null mutants for PPN1 possess higher long chain polyphosphate content than the wild type and exhibit depressed growth on minimal media [*Sethuraman et al.*, 2001].

Eukaryotic exopolyphosphatases include scPPX1 (from *S. cerevisiae*) and PPX from fungi and protozoa. Bacterial exopolyphosphatases include two enzymes originally discovered in *E. coli*: PPX1 and PPX2, which are also present in archaea and conserved in other bacteria [*Rao et al.*, 2009]. Notably, both PPX1 and PPX2 depolymerize polyphosphate chains as long as 750 phosphate units in length, while PPX1 requires Mg^{2+} as a cofactor, and PPX2 requires Ca^{2+} [*Kristensen et al.*, 2004].

The enzyme polyphosphate:AMP phosphotransferase (PAP) utilizes polyphosphate as a phosphorus and energy source for the production of ATP [*Rao et al.*, 2009]. PAP catalyzes the first step in the production of ATP from AMP by transferring the terminal phosphate unit from polyphosphate to AMP, producing ADP [*Rao et al.*, 2009]. Next, ATP is generated either by the reverse activity of PPK1, which catalyzes the transfer of the terminal phosphate unit from polyphosphate to ADP, or through the activity of AMP kinase, which produces ATP and AMP from the dismutation of ADP [*Rao et al.*, 2009]. PAP was originally described in *Acinetobacter*, a bacterial genus commonly found in wastewater treatment plants for the enhanced biological phosphorus removal process [*Bonting et al.*, 1991]. PAP has subsequently been found in a number of other bacteria, including *P. aeruginosa*, *Myxococcus xanthus,* and *Bacillus cereus* [*Ishige and Noguchi*, 2001; *Shi et al.*, 2004; *Zhang et al.*, 2005], and operates most efficiently with polyphosphate stubstrates between twenty and forty phosphate units in length [*Bonting et al.*, 1991].

Several common enzymes that typically utilize ATP as a phosphorus and energy source have evolved in some bacterial species to also utilize polyphosphate. These enzymes include the NAD kinase found in *M. tuberculosis*, *Micrococcus flavus*, and *Bacillus subtilis* [*Mori et al.*, 2004; *Rao et al.*, 2009]. This versatility of NAD kinase in the use of either ATP or polyphosphate is absent, however, in all other NAD kinases investigated [*Mori et al.*, 2004]. The glycolytic enzyme glucokinase utilizes polyphosphate or ATP as a substrate for the phosphorylation of glucose in *M. tuberculosis* [*Hsieh et al.*, 1996], *C. glutamicum*, *Propionibacterium shermanii* [*Kowalczyk et al.*, 1996], and *Arthrobacter* sp. [*Mukai et al.*, 2003]. A glucokinase has been discovered in *Microlunatus phosphovorus* that utilizes polyphosphate exclusively [*Tanaka et al.*, 2003].

6.4 Genetic Regulation of Polyphosphate Metabolism

According to the current understanding of phosphate assimilation by bacteria, originally examined in *E. coli*, dissolved inorganic phosphate can enter cells via two main routes: a low affinity inorganic phosphate transporter system (i.e., PitA and PitB), or a high affinity phosphate-specific transporter system (i.e., Pst proteins). The high affinity uptake system is under the control of the Pho regulon, a system of 38 operons that are transcriptionally activated in *E. coli* under low phosphorus availability. Also under the control of the Pho regulon are periplasmic bacterial alkaline phosphatase (BAP) for the regeneration of inorganic phosphate from organic P-esters, and *phn* gene products for the uptake of phosphonate.

A two-component histidine kinase response regulator pair controls expression of the Pho regulon by sensing the concentration of extracellular inorganic phosphate. At low phosphate concentrations (<4μM), the transmembrane histidine kinase PhoR

autophosphorylates and then activates the response regulator protein PhoB via phosphorylation. PhoB-P, a positive transcription regulator, diffuses through the cytosol and binds to the transcriptional initiation factor σ^{70}. The PhoB-P/σ^{70} complex then binds to the characteristic "phosphate box" promoter region of the Pho regulon, activating transcription. Under high phosphate concentrations (>4μM), the phosphate binding protein PstS binds inorganic phosphate in the periplasm. PstS-P then binds to the membrane-bound phosphate transporter PstABC. Together, PstS-P, PstABC, and PhoU form a complex that represses PhoR and phosphate uptake by the high affinity Pst uptake system. PhoR in the repressed state acts as a phosphatase that keeps PhoB in its deactivated form, repressing transcriptional activation of the Pho regulon.

The mechanisms by which inorganic polyphosphate and polyphosphate metabolizing enzymes participate in phosphate transport and assimilation in microbes are still unknown [*Rao et al.*, 2009]. Certain evidence, however, suggests that a *ppk-ppx* operon is involved in the assimilation of inorganic phosphate. For example, *E. coli ppk-ppx* deletion mutants exhibit only one half the wild type rate of inorganic phosphate uptake by the Pit system [*Rao et al.*, 2009]. In addition, mutants possessing defective Pit-A sequences possess exceedingly high intracellular poly-P content relative to wild type levels, while over expression of PPK1 doubles the rate of inorganic phosphate uptake [*Rao et al.*, 2009]. Furthermore, *ppk* mutants of *Streptomyces lividans* are deficient in inorganic phosphate uptake, but the phosphate demand can be satisfied by overexpression of the Pst gene [*Diaz et al.*, 2005].

APPENDIX A

FLUOROMETRIC DATA COLLECTED FROM STANDARD POLYPHOSPHATES

The complete set of standard data is available as a Microsoft Excel file, which has been submitted electronically with this thesis.

APPENDIX B

STATISTICAL OUTPUTS IN THE EVALUATION OF THE FLUOROMETRIC POLYPHOSPHATE ASSAY

Statistical Output (1): Multivariate Linear Regression Analysis of Standard Data

(Standard data were analyzed using the PASW 18.0 software package)

```
REGRESSION
  /MISSING LISTWISE
  /STATISTICS COEFF OUTS R ANOVA
  /CRITERIA=PIN(.01) POUT(.10)
  /NOORIGIN
  /DEPENDENT Yrawfl
  /METHOD=STEPWISE X1conc X2p130 X3p60 X4p15 X5rxntime X6age X7matrix X8agep13
0 X9agep60 X10agep15 X11saltyp130 X12saltyp60 X13saltyp15 X14freshp130 X15fres
hp60 X16freshp15.
```

Regression

Notes

Output Created		28-Dec-2009 16:26:55
Comments		
Input	Data	C:\Documents and Settings\jdiaz6\My Documents\ExtendedDatabase IncludingFreshDataDec09.sav
	Active Dataset	DataSet1
	Filter	<none>
	Weight	<none>
	Split File	<none>
	N of Rows in Working Data File	459
Missing Value Handling	Definition of Missing	User-defined missing values are treated as missing.
	Cases Used	Statistics are based on cases with no missing values for any variable used.
Syntax		REGRESSION /MISSING LISTWISE /STATISTICS COEFF OUTS R ANOVA /CRITERIA=PIN(.01) POUT(.10) /NOORIGIN /DEPENDENT Yrawfl /METHOD=STEPWISE X1conc X2p130 X3p60 X4p15 X5rxntime X6age X7matrix X8agep130 X9agep60 X10agep15 X11saltyp130 X12saltyp60 X13saltyp15 X14freshp130 X15freshp60 X16freshp15.
Resources	Processor Time	00:00:00.016
	Elapsed Time	00:00:00.015
	Memory Required	9892 bytes
	Additional Memory Required for Residual Plots	0 bytes

Statistical Output (1): Multivariate Linear Regression Analysis of Standard Data (continued)

```
[DataSet1] C:\Documents and Settings\jdiaz6\My Documents\ExtendedDatabaseInclu
dingFreshDataDec09.sav
```

Variables Entered/Removed[a]

Model	Variables Entered	Variables Removed	Method
1	X1conc	.	Stepwise (Criteria: Probability-of-F-to-enter <= .010, Probability-of-F-to-remove >= .100).
2	X13saltyp15	.	Stepwise (Criteria: Probability-of-F-to-enter <= .010, Probability-of-F-to-remove >= .100).
3	X6age	.	Stepwise (Criteria: Probability-of-F-to-enter <= .010, Probability-of-F-to-remove >= .100).

a. Dependent Variable: Yrawfl

Model Summary

Model	R	R Square	Adjusted R Square	Std. Error of the Estimate
1	.931[a]	.867	.867	2.29117
2	.960[b]	.922	.922	1.75260
3	.962[c]	.926	.925	1.71413

a. Predictors: (Constant), X1conc

b. Predictors: (Constant), X1conc, X13saltyp15

c. Predictors: (Constant), X1conc, X13saltyp15, X6age

Statistical Output (1): Multivariate Linear Regression Analysis of Standard Data (continued)

ANOVA[d]

Model		Sum of Squares	df	Mean Square	F	Sig.
1	Regression	15614.265	1	15614.265	2974.444	.000[a]
	Residual	2399.010	457	5.249		
	Total	18013.274	458			
2	Regression	16612.629	2	8306.315	2704.239	.000[b]
	Residual	1400.645	456	3.072		
	Total	18013.274	458			
3	Regression	16676.376	3	5558.792	1891.879	.000[c]
	Residual	1336.899	455	2.938		
	Total	18013.274	458			

a. Predictors: (Constant), X1conc

b. Predictors: (Constant), X1conc, X13saltyp15

c. Predictors: (Constant), X1conc, X13saltyp15, X6age

d. Dependent Variable: Yrawfl

Coefficients[a]

Model		Unstandardized Coefficients		Standardized Coefficients		
		B	Std. Error	Beta	t	Sig.
1	(Constant)	4.510	.185		24.435	.000
	X1conc	6.355	.117	.931	54.538	.000
2	(Constant)	5.442	.150		36.195	.000
	X1conc	6.297	.089	.923	70.614	.000
	X13saltyp15	-3.396	.188	-.236	-18.029	.000
3	(Constant)	5.806	.167		34.866	.000
	X1conc	6.298	.087	.923	72.207	.000
	X13saltyp15	-2.884	.214	-.200	-13.447	.000
	X6age	-.102	.022	-.069	-4.658	.000

a. Dependent Variable: Yrawfl

Excluded Variables[d]

Model		Beta In	t	Sig.	Partial Correlation	Collinearity Statistics: Tolerance
1	X2p130	.063[a]	3.720	.000	.172	1.000
	X3p60	.098[a]	5.957	.000	.269	.999
	X4p15	-.148[a]	-9.496	.000	-.406	1.000
	X5rxntime	-.147[a]	-9.410	.000	-.403	.999
	X6age	-.172[a]	-11.383	.000	-.470	1.000
	X7matrix	.094[a]	5.687	.000	.257	.998
	X8agep130	.024[a]	1.395	.164	.065	1.000
	X9agep60	.074[a]	4.430	.000	.203	1.000
	X10agep15	-.202[a]	-14.162	.000	-.553	1.000
	X11saltyp130	.051[a]	3.029	.003	.140	1.000
	X12saltyp60	.091[a]	5.475	.000	.248	1.000
	X13saltyp15	-.236[a]	-18.029	.000	-.645	.999
	X14freshp130	.028[a]	1.625	.105	.076	1.000
	X15freshp60	.027[a]	1.568	.117	.073	1.000
	X16freshp15	.079[a]	4.735	.000	.216	.996
2	X2p130	-.029[b]	-2.053	.041	-.096	.862
	X3p60	.011[b]	.779	.437	.036	.858
	X4p15	.027[b]	1.496	.135	.070	.524
	X5rxntime	-.027[b]	-1.722	.086	-.080	.702
	X6age	-.069[b]	-4.658	.000	-.213	.738
	X7matrix	-.001[b]	-.105	.917	-.005	.835
	X8agep130	-.035[b]	-2.593	.010	-.121	.942
	X9agep60	.002[b]	.148	.883	.007	.906
	X10agep15	-.062[b]	-3.249	.001	-.151	.458
	X11saltyp130	-.017[b]	-1.236	.217	-.058	.920
	X12saltyp60	.018[b]	1.285	.200	.060	.899
	X14freshp130	-.018[b]	-1.356	.176	-.063	.963
	X15freshp60	-.010[b]	-.747	.455	-.035	.976
	X16freshp15	.020[b]	1.496	.135	.070	.931

a. Predictors in the Model: (Constant), X1conc

b. Predictors in the Model: (Constant), X1conc, X13saltyp15

d. Dependent Variable: Yrawfl

Statistical Output (1): Multivariate Linear Regression Analysis of Standard Data (continued)

Excluded Variables[d]

Model		Beta In	t	Sig.	Partial Correlation	Collinearity Statistics: Tolerance
3	X2p130	-.025[c]	-1.784	.075	-.083	.858
	X3p60	.005[c]	.377	.706	.018	.851
	X4p15	.029[c]	1.655	.099	.077	.524
	X5rxntime	.001[c]	.090	.929	.004	.592
	X7matrix	-.011[c]	-.781	.435	-.037	.818
	X8agep130	-.006[c]	-.378	.706	-.018	.711
	X9agep60	.008[c]	.596	.551	.028	.897
	X10agep15	-.001[c]	-.044	.965	-.002	.234
	X11saltyp130	-.004[c]	-.282	.778	-.013	.878
	X12saltyp60	.015[c]	1.095	.274	.051	.897
	X14freshp130	-.030[c]	-2.250	.025	-.105	.933
	X15freshp60	-.015[c]	-1.138	.256	-.053	.970
	X16freshp15	.022[c]	1.655	.099	.077	.931

c. Predictors in the Model: (Constant), X1conc, X13saltyp15, X6age

d. Dependent Variable: Yrawfl

Statistical Output (2): Single Variable Linear Regression Analysis of Standard Data

(Standard data were analyzed using the PASW 18.0 software package)

```
REGRESSION
  /MISSING LISTWISE
  /STATISTICS COEFF OUTS R ANOVA
  /CRITERIA=PIN(.05) POUT(.10)
  /NOORIGIN
  /DEPENDENT Yrawfl
  /METHOD=STEPWISE X1conc.
```

Regression

Notes

Output Created		28-Dec-2009 17:00:49
Comments		
Input	Data	C:\Documents and Settings\jdiaz6\My Documents\AfterFreshData\NumericModelDatabaseIncludingFreshDataDec09.sav
	Active Dataset	DataSet0
	Filter	<none>
	Weight	<none>
	Split File	<none>
	N of Rows in Working Data File	328
Missing Value Handling	Definition of Missing	User-defined missing values are treated as missing.
	Cases Used	Statistics are based on cases with no missing values for any variable used.
Syntax		REGRESSION /MISSING LISTWISE /STATISTICS COEFF OUTS R ANOVA /CRITERIA=PIN(.05) POUT(.10) /NOORIGIN /DEPENDENT Yrawfl /METHOD=STEPWISE X1conc.
Resources	Processor Time	00:00:00.000
	Elapsed Time	00:00:00.000
	Memory Required	1812 bytes
	Additional Memory Required for Residual Plots	0 bytes

```
[DataSet0] C:\Documents and Settings\jdiaz6\My Documents\AfterFreshData\Numeri
cModelDatabaseIncludingFreshDataDec09.sav
```

Statistical Output (2): Single Variate Linear Regression Analysis of Standard Data (continued)

Variables Entered/Removed[a]

Model	Variables Entered	Variables Removed	Method
1	X1conc	.	Stepwise (Criteria: Probability-of-F-to-enter <= .050, Probability-of-F-to-remove >= .100).

a. Dependent Variable: Yrawfl

Model Summary

Model	R	R Square	Adjusted R Square	Std. Error of the Estimate
1	.977[a]	.955	.955	1.35412

a. Predictors: (Constant), X1conc

ANOVA[b]

Model		Sum of Squares	df	Mean Square	F	Sig.
1	Regression	12641.751	1	12641.751	6894.365	.000[a]
	Residual	597.765	326	1.834		
	Total	13239.516	327			

a. Predictors: (Constant), X1conc

b. Dependent Variable: Yrawfl

Coefficients[a]

Model		Unstandardized Coefficients		Standardized Coefficients	t	Sig.
		B	Std. Error	Beta		
1	(Constant)	4.944	.129		38.189	.000
	X1conc	6.694	.081	.977	83.032	.000

a. Dependent Variable: Yrawfl

APPENDIX C

MATLAB CODES FOR THE REACTIVE TRANSPORT MODEL IN CHAPTER 5

First Code: Filename “EIFesystem_all_variableD_OptimSub.m”

```
%THIS PROGRAM CALCULATES THE VARIATION OF Fe(II) and Fe(III) WITH DEPTH IN
%EFFINGHAM INLET WATER COLUMN IN PRESENCE OF OXYGEN AND ORGANIC CARBON. THE
%ALGORITHM USES THE CENTRAL FINITE DIFFERENCE METHOD TO CALCULATE THE
%CONCENTRATION OF OXYGEN VS DEPTH, C IS CONSIDERED CONSTANT. WITH THIS PROFILE
%IT CALCULATES THE (Fep) PROFILE THEN BOTH OF THESE PROFILES ARE ITERATED AND
%(Feaq) IS ADDED. ALL EQUATIONS ARE COUPLED AND NON-LINEAR. THE DIFFUSION
%COEFFICIENT IS VARIED WITH DEPTH ACCORDING TO THE TEMPERATURE AND SALINITY
%DATA.
%
%%%%%%%%%%%%%%%%%%%%%%%%%%%%%%%%%%%%%%%%%%%%%%%%%%%%%%%%%%%%%%%%%%%%%%%%%%%%
%
%
function optimroutine=EIFesystem_all_variableD_OptimSub(q)
global x dx m n C O2 Feaq Fep O2data Feaqdata depthFeaq Fepdata depthFep RmaxO2
KMO2 RmaxFe kin kFeox OH D Dprime Ddoubleprime w
%
% Depth vector
%
dx=1;                    % depth space - m
z=110;                   % maximum depth - m
y=5;                     % minimum depth - m
x=y:dx:z; x=x';          % depth vector - m
%
% Input data and generate linear interpolations
%
% Fe(II) aq data, concentration units are mol/L; depth units are meters:
Feaqdata=[0 0 0.35000 1.4200 0.35000 0.31000 0.14000 0.22000 2.83 0.14 0.27 0.4
0.82 0.99]*1E-6;
depthFeaq=[5 60 61 62 63 64 65 66 69 79 89 99 104 110];
% FeOOH data, concentration units are mol/L; depth units are meters:
Fepdata=[0 0.17104 0.18146 0.17855 0.076594 0 0 0]*1E-6;
depthFep=[5 55 58 60 62 64 68 110];
% O2 data, concentration units are mol/L; depth units are meters:
O2data=[0.00010087 9.2916e-05 8.2125e-05 7.3906e-05 6.8844e-05 6.5353e-05
6.4209e-05 6.4166e-05 6.4291e-05 6.3603e-05 6.3084e-05 6.2788e-05 6.1912e-05
6.1378e-05 6.2172e-05 6.2294e-05 6.1581e-05 6.0347e-05 5.9678e-05 5.9500e-05
5.8538e-05 5.7256e-05 5.5534e-05 5.5222e-05 5.4506e-05 5.3837e-05 5.3609e-05
5.2234e-05 5.0125e-05 4.8588e-05 4.6716e-05 4.4422e-05 4.4241e-05 4.5672e-05
4.5625e-05 4.4375e-05 4.2209e-05 4.0231e-05 3.8447e-05 3.7281e-05 3.8187e-05
3.9288e-05 3.9791e-05 3.9725e-05 3.9725e-05 3.9966e-05 4.0537e-05 4.0506e-05
4.0109e-05 3.9487e-05 3.8175e-05 3.5853e-05 3.1937e-05 2.7472e-05 2.0788e-05
1.1203e-05 4.9094e-06 2.5750e-06 1.6469e-06 1.1937e-06 9.1875e-07 7.8750e-07
6.4687e-07 5.7188e-07 5.3750e-07 4.6875e-07 4.0000e-07 3.6250e-07 3.3125e-07
3.0625e-07 2.8438e-07 2.7187e-07 2.6875e-07 2.5000e-07 2.5625e-07 2.4687e-07
2.3437e-07 2.4062e-07 2.2813e-07 2.0937e-07 1.7813e-07 1.4375e-07 1.3438e-07
1.1562e-07 1.0625e-07 1.0000e-07 1.0000e-07 9.3750e-08 8.4375e-08 7.1875e-08
6.5625e-08 6.2500e-08 5.9375e-08 6.2500e-08 5.0000e-08 4.6875e-08 3.7500e-08
2.5000e-08 2.1875e-08 2.1875e-08 2.1875e-08 2.1875e-08 1.5625e-08 1.2500e-08
6.2500e-09 0.0000];
O2data=O2data';
%
Fepdatai=interp1(depthFep, Fepdata, x);
Feaqdatai=interp1(depthFeaq, Feaqdata, x);
```

```
%
% Input of parameters: Boundary Conditions
%
Feaqsfc=0;        % concentration of Feaq at x=5 - mol/L
Feaqbw=9.9e-7; % concentration of Feaq at x=m - mol/L
fFep=0;          % flux of Fep at x=5 - mol/m^2/min
Fepbw=0;       % concentration of Fep at x=m - mol/L
fO2=0;           % flux of O2 at x=m - mol/m^2/min
O2sfc=1.0087e-4;   % concentration of O2 at x=5 - mol/L
OH=10^-6;          % hydroxide ion concentration at pH=8
C=73.0889e-6; % concentration of organic C (from data at x=5) - mol/L
%
% Input of parameters: Transport Coefficients
%
xa=x(1:8,1);
xb=x(9:53,1);
xc=x(54:58,1);
xd=x(59:61,1);
xe=x(62:106,1);
ye=7*10^-6*ones(size(xe),1);
ya=-6e-7*xa+0.8e-5+6e-7*xa(1,1);
yb=-5e-8*xb+(ya(length(ya),1)+5e-8*xa(length(xa),1));
yc=yb(length(yb),1)*ones(length(xc),1);
yd=[1.75e-6; 3.3e-6; 5e-6];
D=[ya' yb' yc' yd' ye']';               % Definition of D as a function of
depth - [m^2 min^-1]
Dprime=[(ones(size(ya))*-6e-7)' (ones(size(yb))*-5e-8)' 0*yc' 0*yd' 0*ye']';
Ddoubleprime=[0*ya' 0*yb' 0*yc' 0*yd' 0*ye']';
w=0;            % Advection constant for aqueous phase - m/min
s=0;            % Advection constant for particulate phase - m/min
%
% Input of parameters: Reaction Rate Constants
%
kFeox=6.154e16; % rate constant for Fe2+ oxidation by O2 - L^3/mol^3/min^-1
RmaxFe=q(1);    % OM oxidation rate constant by Fe - L/mol/min
RmaxO2=10^-10;  % OM oxidation rate constant by oxygen - 1/min
KMO2=3.1*10^-8;     % Monod constant for oxygen consumption - mol/L
k0in=q(2);  % Initial inhibition constant
k=q(3);     % decay constant for the inhibition constant
a=0.1;      % coefficient for the oxygen decreases of the first run
%
% Original concentration profile of O2, Fep, and Feaq:
%
O2g=exp(-x/10)*O2sfc; O2=O2g;
Feaqg=exp(x/z)*Feaqbw; Feaq=Feaqg;
Fepg=exp(-x/z)*1E-7; Fep=Fepg;
%
% Calculation of the coefficients - Transport Only, D varies with Depth
%
AO=D/dx^2+(2*Dprime-w)./(2*dx);
BO=-2*D./dx^2+Ddoubleprime;
EO=D/dx^2+(-2*Dprime+w)./(2*dx);
AFeaq=D/dx^2+(2*Dprime-w)./(2*dx);
BFeaq=-2*D/dx^2+Ddoubleprime;
EFeaq=D/dx^2+(-2*Dprime+w)./(2*dx);
AFep=D/dx^2+(2*Dprime-s)./(2*dx);
BFep=-2*D/dx^2+Ddoubleprime;
EFep=D/dx^2+(-2*Dprime+s)./(2*dx);
%
% Build the matrix of oxygen
%
MO=BO-(RmaxO2*C*a)./(O2+KMO2);
m=length(x);        % columns corresponding to the number of equations
n=length(x);        % rows corresponding to the n-1 number of equations
T=spdiags([AO MO EO],[-1,0,1],m,n);
```

```
TT=full(T((2:n-1),:));
OO=[1 zeros(1,n-1);TT;zeros(1,n-2) -1 1];
rhsO=((RmaxO2*C*(1-a).*O2)./(KMO2+O2));
RHSO=[O2sfc;rhsO((2:n-1),1);fO2];
O2=OO\RHSO;

Tol =1;
%
% Iteration on oxygen
%
while Tol > 1e-8,
%
% Calculate the inhibition constant with depth
%
    kin=k0in*exp(-O2sfc./(O2*k));
%
% Calculation of the Fep profile with O2 and Feaq
%
    Fep1=Fep;
    MFep=BFep-(RmaxFe*C)./(1+kin);
    T=spdiags([AFep MFep EFep],[-1,0,1],m,n);
    TT=full(T((2:n-1),:));
    FepFep=[-1 1 zeros(1,n-2);TT;zeros(1,n-1) 1];
    rhsFep=-(kFeox*OH^2.*Feaq.*O2);
    RHSFep=[fFep;rhsFep((2:n-1),1);Fepbw];
    Fep=FepFep\RHSFep;
    IFep= (Fep-Fep1);
%
% Calculation of the Feaq profile with Fep, and O2
%
    Feaq1=Feaq;
    MFeaq=BFeaq-(2*kFeox*OH^2.*O2);
    T=spdiags([AFeaq MFeaq EFeaq],[-1,0,1],m,n);
    TT=full(T((2:n-1),:));
    FeaqFeaq=[1 zeros(1,n-1);TT;zeros(1,n-1) 1];
    rhsFeaq=-2*((RmaxFe.*Fep*C)./(1+kin));
    RHSFeaq=[Feaqsfc;rhsFeaq((2:n-1),1);Feaqbw];
    Feaq=FeaqFeaq\RHSFeaq;
    IFeaq=(Feaq-Feaq1);
%
% Build the new matrix of oxygen
%
    O21=O2;
    MO=BO-1/2*kFeox*OH^2.*Feaq-(RmaxO2*C*a)./(O2+KMO2);
    T=spdiags([AO MO EO],[-1,0,1],m,n);
    TT=full(T((2:n-1),:));
    OO=[1 zeros(1,n-1);TT;zeros(1,n-2) -1 1];
    rhsO=((RmaxO2*C*(1-a).*O2)./(KMO2+O2));
    RHSO=[O2sfc;rhsO((2:n-1),1);fO2];
    O2=OO\RHSO;
    IO2=(O2-O21);
%
    Tol=[norm(IFep) norm(IFeaq) norm(IO2)];
    Tol=norm(Tol)
%
end
% Compute the Difference between the model and experimental data in units
% of uM:
optimroutine=(Fep-Fepdatai+Feaq-Feaqdatai)*1e7;
```

Second Code: Filename “EIFesystem_all_variableD_OptimMain.m”

```
% This program is the main routine for the optimization of parameters in
% the reactive transport model of O2, Fep, and Feaq (subroutine
% EIFesystem_all_variableD_OptimSub.m) and SRP (EISRP_variableD_OptimSub.m)
%
%%%%%%%%%%%%%%%%%%%%%%%%%%%%%%%%%%%%%%%%%%%%%%%%%%%%%%%%%%%%%%%%%%%%%%%%%%%
%
clear
global x O2 Feaq Fep O2data Feaqdata depthFeaq Fepdata depthFep D
%
% Enter initial guesses and bounds for parameters in Fe system:
%
q0(1)=5e-2;     % Initial guess for RmaxFe
q0(2)=1e12;      % Initial guess for k0in
q0(3)=1.2;          % Initial guess for k
%
lbq(1)=0;
lbq(2)=0;
lbq(3)=0;
%
ubq(1)=1;
ubq(2)=1e50;
ubq(3)=100;
%
q=lsqnonlin(@EIFesystem_all_variableD_OptimSub,q0,lbq,ubq);
%
% Plot Model results vs. data:
%
figure(1)
subplot(2,2,2)
plot(O2,-x,O2data,-x)
ylabel('Depth - [m]')
xlabel('M')
title('Oxygen')

subplot(2,2,3)
plot(Fep,-x,Fepdata,-depthFep,'o')
ylabel('Depth - [m]')
xlabel('M')
title('Fep')

subplot(2,2,4)
plot(Feaq,-x,Feaqdata,-depthFeaq,'o')
ylabel('Depth - [m]')
xlabel('M')
title('Feaq')
```

Third Code: Filename “EISRP_variableD.m”

```
%THIS PROGRAM CALCULATES THE VARIATION OF SRP IN THE %EFFINGHAM INLET WATER
%COLUMN BASED ON THE Fe(II) and Fe(III) PROFILES.
%
%%%%%%%%%%%%%%%%%%%%%%%%%%%%%%%%%%%%%%%%%%%%%%%%%%%%%%%%%%%%%%%%%%%%%%%%%%%%%%%%
%%%%%%%%%%%%%%%%%%%%%%%
%
%function optimroutine=EISRP_variableD_OptimSub(u)
global x dx m n C Fep RmaxFe kin D Dprime Ddoubleprime w SRP SRPdata depthSRP
OH O2
%
% Input data and generate linear interpolations
%
% SRP data, concentration units are mol/L; depth units are meters:
SRPdata=[1.13 1.34 1.4 1.69 1.99 2.22 2.2900 2.3700 2.5700 3.7300 4.7700 4.7400
4.6800 4.1600 3.8700 3.9200 3.9300 3.96 3.84 3.84 4.02 4.49 5.39]*1E-6;
depthSRP=[5 10 20 30 40 50 56 57 58 59 60 61 62 63 64 65 66 67 70 80 90 100
113];
%
SRPdatai=interp1(depthSRP, SRPdata, x);
%
% Input of parameters: Boundary Conditions
%
fSRP=0;          % flux of SRP at x=5 - mol/m^2/min
SRPbw=5.39e-6;     % concentration of SRP at x=m - mol/L
%
% Input of parameters: Reaction Rate Constants, etc.
%
kFeox=6.154e16; % rate constant for Fe2+ oxidation by O2 - L^3/mol^3/min^-1
alpha=1/1.766;     % Stoichiometric coefficient of SRP to one mol Fep
kads=kFeox*OH^2.*O2;
%
% Calculation of the coefficients - Transport Only, D varies with Depth
%
ASRP=D/dx^2+(2*Dprime-w)./(2*dx);
BSRP=-2*D./dx^2+Ddoubleprime;
ESRP=D/dx^2+(-2*Dprime+w)./(2*dx);
%
% Build the matrix of SRP
%
    MSRP=BSRP-alpha*kads;
    T=spdiags([ASRP MSRP ESRP],[-1,0,1],m,n);
    TT=full(T((2:n-1),:));
    SRPSRP=[-1 1 zeros(1,n-2);TT;zeros(1,n-1) 1];
    rhsSRP=-alpha*((RmaxFe.*Fep*C)./(1+kin));
    RHSSRP=[fSRP;rhsSRP((2:n-1),1);SRPbw];
    SRP=SRPSRP\RHSSRP;
%
figure(2)
plot(SRP,-x,SRPdata,-depthSRP,'o')
```

REFERENCES

Ahlgren, J., et al. (2005), Sediment depth attenuation of biogenic phosphorus compounds measured by P-31 NMR, *Environmental Science & Technology*, *39*(3), 867-872.

Algeo, T. J., and E. Ingall (2007), Sedimentary C-org : P ratios, paleocean ventilation, and Phanerozoic atmospheric pO(2), *Palaeogeography Palaeoclimatology Palaeoecology*, *256*(3-4), 130-155.

Arakaki, A. K., et al. (2006), High precision multi-genome scale reannotation of enzyme function by EFICAz, *BMC Genomics*, *7*.

Armstrong, F. A., and S. Tibbitts (1968), Photochemical combustion of organic matter in seawater, for nitrogen, phosphorus and carbon determination, *J. Marine Biol. Assoc.*, *48*, 143-152.

Armstrong, R. A., et al. (2001), A new, mechanistic model for organic carbon fluxes in the ocean based on the quantitative association of POC with ballast minerals, *Deep-Sea Research Part Ii-Topical Studies in Oceanography*, *49*(1-3), 219-236.

Aschar-Sobbi, R., et al. (2008), High sensitivity, quantitative measurements of polyphosphate using a new DAPI-Based approach, *Journal of Fluorescence*, *18*(5), 859-866.

Aspila, K. I., et al. (1976), Semiautomated method for determination of inorganic, organic, and total phosphate in sediments, *Analyst*, *101*(1200), 187-197.

Ault-Riche, D., et al. (1998), Novel assay reveals multiple pathways regulating stress-induced accumulations of inorganic polyphosphate in *Escherichia coli*, *Journal of Bacteriology*, *180*(7), 1841-1847.

Barcellona, M. L., et al. (1990), Time-resolved fluorescence of DAPI in solution and bound to polydeoxynucleotides, *Biochemical and Biophysical Research Communications*, *170*(1), 270-280.

Benitez-Nelson, C. R. (2000), The biogeochemical cycling of phosphorus in marine systems, *Earth-Science Reviews*, *51*(1-4), 109-135.

Benitez-Nelson, C. R., et al. (2004), Phosphonates and particulate organic phosphorus cycling in an anoxic marine basin, *Limnology and Oceanography*, *49*(5), 1593-1604.

Bertsch, P. M., and D. B. Hunter (2001), Applications of synchrotron-based X-ray microprobes, *Chemical Reviews*, *101*(6), 1809-1842.

Bidle, K. D., and F. Azam (1999), Accelerated dissolution of diatom silica by marine bacterial assemblages, *Nature*, *397*(6719), 508-512.

Björkman, K., and D. M. Karl (1994), Bioavailability of inorganic and organic phosphorus compounds to natural assemblages of microorganisms in Hawaiian coastal waters, *Marine Ecology-Progress Series*, *111*(3), 265-273.

Björkman, K. M., and D. M. Karl (2001), A novel method for the measurement of dissolved adenosine and guanosine triphosphate in aquatic habitats: applications to marine microbial ecology, *Journal of Microbiological Methods*, *47*(2), 159-167.

Björkman, K. M., and D. M. Karl (2005), Presence of dissolved nucleotides in the North Pacific Subtropical Gyre and their role in cycling of dissolved organic phosphorus, *Aquat. Microb. Ecol.*, *39*(2), 193-203.

Boese, J., et al. (1997), Carbon edge XANES spectroscopy of amino acids and peptides, *Journal of Electron Spectroscopy and Related Phenomena*, *85*(1-2), 9-15.

Bonting, C. F. C., et al. (1991), Properties of polyphosphate:AMP phosphotransferase of *Acinetobacter* strain-210a, *Journal of Bacteriology*, *173*(20), 6484-6488.

Boswell, C. D., et al. (2001), Phosphate uptake and release by *Acinetobacter johnsonii* in continuous culture and coupling of phosphate release to heavy metal accumulation, *Journal of Industrial Microbiology & Biotechnology*, *26*(6), 333-340.

Brandes, J. A., et al. (2004), Examining marine particulate organic matter at sub-micron scales using scanning transmission X-ray microscopy and carbon X-ray absorption near edge structure spectroscopy, *Marine Chemistry*, *92*(1-4), 107-121.

Brandes, J. A., et al. (2007), Characterization of minerals and organic phosphorus species in marine sediments using soft X-ray fluorescence spectromicroscopy, *Marine Chemistry*, *103*(3-4), 250-265.

Broecker, W. S. (1982), Ocean chemistry during glacial time, *Geochimica et Cosmochimica Acta*, *46*(10), 1689-1705.

Brown, M. R. W., and A. Kornberg (2004), Inorganic polyphosphate in the origin and survival of species, *Proceedings of the National Academy of Sciences of the United States of America*, *101*(46), 16085-16087.

Buesseler, K. O., et al. (2007), Revisiting carbon flux through the ocean's twilight zone, *Science*, *316*(5824), 567-570.

Cazaux, J. (1985), The influence of radiation-damage (microscopic causes) on the sensitivity of auger electron spectroscopy and x-ray photoelectron spectroscopy, *Applied Surface Science*, *20*(4), 457-471.

Chu, S. P. (1942), The influence of the mineral composition of the medium on the growth of planktonic algae Part 1. Methods and culture media, *Journal of Ecology*, *30*, 284-325.

Clark, J. E., et al. (1986), Isolation of intact chains of polyphosphate from *Propionibacterium shermanii* grown on glucose or lactate, *Journal of Bacteriology*, *168*(3), 1212-1219.

Clark, L. L., et al. (1998), Marine phosphorus is selectively remineralized, *Nature*, *393*(6684), 426-426.

Clark, L. L., et al. (1999), Marine organic phosphorus cycling: Novel insights from nuclear magnetic resonance, *American Journal of Science*, *299*(7-9), 724-737.

Codispoti, L. A., et al. (2001), The oceanic fixed nitrogen and nitrous oxide budgets: Moving targets as we enter the anthropocene?, *Scientia Marina*, *65*, 85-105.

Comeau, Y., et al. (1986), Biochemical model for enhanced biological phosphorus removal, *Water Research*, *20*(12), 1511-1521.

Crosby, S. A., et al. (1984), Kinetics of phosphate adsorption by iron oxyhydroxides in aqueous systems, *Estuarine Coastal and Shelf Science*, *19*(2), 257-270.

Davelaar, D. (1993), Ecological significance of bacterial polyphosphate metabolism in sediments, *Hydrobiologia*, *253*(1-3), 179-192.

Davison, W., and G. Seed (1983), The kinetics of the oxidation of ferrous iron in synthetic and natural waters, *Geochimica Et Cosmochimica Acta*, *47*(1), 67-79.

de Jonge, M. D., et al. (2010a), Quantitative 3D elemental microtomography of Cyclotella meneghiniana at 400-nm resolution, *Proceedings of the National Academy of Sciences of the United States of America*, *107*(36), 15676-15680.

de Jonge, M. D., et al. (2010b), An energy and intensity monitor for X-ray absorption near-edge structure measurements, *Nuclear Instruments & Methods in Physics Research Section a-Accelerators Spectrometers Detectors and Associated Equipment*, *619*(1-3), 154-156.

Diaz, J., et al. (2008), Marine polyphosphate: A key player in geologic phosphorus sequestration, *Science*, *320*(5876), 652-655.

Diaz, J., et al. (2009), Characterization of phosphorus, calcium, iron, and other elements in organisms at sub-micron resolution using X-ray fluorescence spectromicroscopy, *Limnology and Oceanography: Methods*, *7*, 42-51.

Diaz, J. M., and E. D. Ingall (2010), Fluorometric Quantification of Natural Inorganic Polyphosphate, *Environmental Science & Technology*, *44*(12), 4665-4671.

Diaz, M., et al. (2005), The high-affinity phosphate-binding protein PstS is accumulated under high fructose concentrations and mutation of the corresponding gene affects differentiation in *Streptomyces lividans*, *Microbiology-Sgm*, *151*, 2583-2592.

Dyhrman, S. T., et al. (2007), Microbes and the Marine Phosphorus Cycle, *Oceanography*, *20*(2), 110-116.

Dyhrman, S. T., et al. (2009), A microbial source of phosphonates in oligotrophic marine systems, *Nature Geoscience*, *2*(10), 696-699.

Eixler, S., et al. (2005), Extraction and detection methods for polyphosphate storage in autotrophic planktonic organisms, *Hydrobiologia*, *533*, 135-143.

Eppley, R. W. (1962), Hydrolysis of polyphosphates by *Porphyra* and other seaweeds, *Physiol. Plantarum*, *15*, 246-251.

Froelich, P. N., et al. (1979), Early oxidation of organic-matter in pelagic sediments of the eastern equatorial atlantic - suboxic diagenesis, *Geochimica Et Cosmochimica Acta*, *43*(7), 1075-1090.

Gachter, R., et al. (1988), Contribution of bacteria to release and fixation of phosphorus in lake sediments, *Limnology and Oceanography*, *33*(6), 1542-1558.

Glaeser, R. M. (1971), Limitations to significant information in biological electron microscopy as a result of radiation damage, *Journal of Ultrastructure Research*, *36*(3-4), 466-&.

Golterman, H., et al. (1998), Presence of and phosphate release from polyphosphates or phytate phosphate in lake sediments, *Hydrobiologia*, *364*, 99-104.

Golterman, H. L. (2001), Phosphate release from anoxic sediments or 'What did Mortimer really write?', *Hydrobiologia*, *450*(1-3), 99-106.

Grynpas, M. D., et al. (2002), Porous calcium polyphosphate scaffolds for bone substitute applications in vivo studies, *Biomaterials*, *23*(9), 2063-2070.

Hansen, H. P., and F. Koroleff (1999a), Determination of polyphosphates, in *Methods of Seawater Analysis*, edited by K. Grasshoff, et al., p. 202, Wiley, New York.

Hansen, H. P., and F. Koroleff (1999b), Determination of silica, in *Methods of Seawater Analysis*, edited by K. Grasshoff, et al., p. 159, Wiley-VCH, Weinhem.

Hansen, H. P., and F. Koroleff (1999c), Determination of dissolved inorganic phosphate, in *Methods of Seawater Analysis*, edited by K. Grasshoff, et al., pp. 170-174, Wiley-VCH.

Hedges, J. I., and J. H. Stern (1984), Carbon and nitrogen determinations of carbonate-containing solids, *Limnology and Oceanography*, *29*(3), 657-663.

Hedges, J. I., et al. (2002), The biochemical and elemental compositions of marine plankton: A NMR perspective, *Marine Chemistry*, *78*(1), 47-63.

Hitchcock, A. P., and I. Ishii (1987), Carbon k-shell excitation spectra of linear and branched alkanes, *Journal of Electron Spectroscopy and Related Phenomena*, *42*(1), 11-26.

Hothorn, M., et al. (2009), Catalytic Core of a Membrane-Associated Eukaryotic Polyphosphate Polymerase, *Science*, *324*(5926), 513-516.

Hsieh, P. C., et al. (1996), Kinetic mechanisms of polyphosphate glucokinase from *Mycobacterium tuberculosis*, *Biochemistry*, *35*(30), 9772-9781.

Hupfer, M., and R. Gachter (1995), Polyphosphate in lake-sediments - P-31 NMR-spectroscopy as a tool for its identification, *Limnology and Oceanography*, *40*(3), 610-617.

Hupfer, M., et al. (2004), Origin and diagenesis of polyphosphate in lake sediments: A P-31-NMR study, *Limnology and Oceanography*, *49*(1), 1-10.

Hupfer, M., et al. (2008), Methods for detection and quantification of polyphosphate and polyphosphate accumulating microorganisms in aquatic sediments, *International Review of Hydrobiology*, *93*(1), 1-30.

Ingall, E., and R. Jahnke (1994), Evidence for enhanced phosphorus regeneration from marine-sediments overlain by oxygen depleted waters, *Geochimica Et Cosmochimica Acta*, *58*(11), 2571-2575.

Ingall, E., and R. Jahnke (1997), Influence of water-column anoxia on the elemental fractionation of carbon and phosphorus during sediment diagenesis, *Marine Geology*, *139*(1-4), 219-229.

Ingall, E., et al. (2005), Sediment carbon, nitrogen and phosphorus cycling in an anoxic fjord, Effingham Inlet, British Columbia, *American Journal of Science*, *305*(3), 240-258.

Ingall, E. D., et al. (1993), Influence of water column anoxia on the burial and preservation of carbon and phosphorus in marine shales, *Geochimica Et Cosmochimica Acta*, *57*(2), 303-316.

Ingall, E. D., et al. (2011), Phosphorus K-edge XANES spectroscopy of mineral standards, *Journal of Synchrotron Radiation*, *18*(2).

Ishige, K., and T. Noguchi (2001), Polyphosphate : AMP phosphotransferase and Polyphosphate : ADP phosphotransferase activities of *Pseudomonas aeruginosa*, *Biochemical and Biophysical Research Communications*, *281*(3), 821-826.

Jackson, G. A., and P. M. Williams (1985), Importance of dissolved organic nitrogen and phosphorus to biological nutrient cycling, *Deep-Sea Research Part a-Oceanographic Research Papers*, *32*(2), 223-235.

Jacobsen, C. (2000), X-ray microscopy using FELs: possibilities and challenges, in *Biomedical Applications of Free-Electron Lasers*, edited by G. S. Edwards and J. C. Sutherland, pp. 16-25, SPIE, San Jose.

Jilbert, T., et al. (2011), Beyond the Fe-P-redox connection: preferential regeneration of phosphorus from organic matter as a key control on Baltic Sea nutrient cycles, *Biogeosciences Discussions*, *doi: 10.5194/bgd-8-655-2011*.

Karl, D. M., et al. (1997), The role of nitrogen fixation in biochemical cycling in the subtropical North Pacific Ocean, *Nature*, *388*, 533-538.

Karl, D. M., and K. Yanagi (1997), Partial characterization of the dissolved organic phosphorus pool in the oligotrophic North Pacific Ocean, *Limnology and Oceanography*, *42*(6), 1398-1405.

Karl, D. M., and K. M. Björkman (2002), Dynamics of DOP, in *Biogeochemistry of Marine Dissolved Organic Matter*, edited by D. A. Hansell and C. A. Carlson, pp. 249-366, Academic Press, New York.

Katz, M. E., et al. (2004), Evolutionary trajectories and biogeochemical impacts of marine eukaryotic phytoplankton, *Annual Review of Ecology Evolution and Systematics*, *35*, 523-556.

Keck, K., and H. Stich (1957), The widespread occurrence of polyphosphate in lower plants, *Ann. Botany*, *21*, 611-619.

Kenney, W. F., et al. (2001), Changes in polyphosphate sedimentation: a response to excessive phosphorus enrichment in a hypereutrophic lake, *Canadian Journal of Fisheries and Aquatic Sciences*, *58*(5), 879-887.

Kirz, J., et al. (1995), Soft-x-ray microscopes and their biological applications, *Quarterly Reviews of Biophysics*, *28*(1), 33-130.

Kolowith, L. C., et al. (2001), Composition and cycling of marine organic phosphorus, *Limnology and Oceanography*, *46*(2), 309-320.

Kornberg, A. (1995), Inorganic polyphosphate - toward making a forgotten polymer unforgettable, *Journal of Bacteriology*, *177*(3), 491-496.

Kornberg, A., et al. (1999), Inorganic polyphosphate: A molecule of many functions, *Annual Review of Biochemistry*, *68*, 89-125.

Koroleff, F., and K. Kremling (1999), Analysis by spectrophotometry: Iron, in *Methods of Seawater Analysis*, edited by K. Grasshoff, et al., p. 340, Wiley, New York.

Kowalczyk, T. H., et al. (1996), Initial rate and equilibrium isotope exchange studies on the ATP-dependent activity of polyphosphate glucokinase from *Propionibacterium shermanii*, *Biochemistry*, *35*(21), 6777-6785.

Kristensen, O., et al. (2004), Structural characterization of the stringent response related exopolyphosphatase/guanosine pentaphosphate phosphohydrolase protein family, *Biochemistry*, *43*(28), 8894-8900.

Krom, M. D., et al. (1991), Phosphorus limitation of primary productivity in the eastern Mediterranean Sea, *Limnology and Oceanography*, *36*(3), 424-432.

Kuhl, A. (1962), Inorganic phosphorus uptake and metabolism, in *Physiology and biochemistry of algae*, edited by R. A. Lewin, Academic Press, New York.

Kulaev, I., and T. Kulakovskaya (2000), Polyphosphate and phosphate pump, *Annual Review of Microbiology*, *54*, 709-734.

Lam, P. J., et al. (2006), Wintertime phytoplankton bloom in the subarctic Pacific supported by continental margin iron, *Global Biogeochemical Cycles*, *20*(1).

Lawerence, B. A., et al. (1998), Two internal pools of soluble polyphosphate in the cyanobacterium *Synechocystis* sp. strain PCC 6308: An in vivo P-31 NMR spectroscopic study, *Archives of Microbiology*, *169*(3), 195-200.

Leapman, R. D., and R. L. Ornberg (1988), Quantitative electron-energy loss spectroscopy in biology, *Ultramicroscopy*, *24*(2-3), 251-268.

Lehmann, J., et al. (2009), Synchrotron-based near-edge X-ray Spectroscopy of NOM in soils and sediments, in *Biophysico-Chemical Processes Involving Natural Nonliving Organic Matter in Environmental Systems*, edited by P. M. Huang and N. Senesi, p. 729, Wiley & Sons.

Lieberman, L. (1888), Uber das Nuclein der Hefe und Kunstliche Darstellung eines Nucleus Eiweiss und Metaphosphatsaure, *Berichte der Deutschen Chemischen Gesellschaft*, *21*, 598-607.

London, R. A., et al. (1992), Role of X-ray induced damage in biological microimaging, in *Soft X-ray Microscopy*, edited by C. J. Jacobsen and J. E. Trebes, pp. 333-340, SPIE, Bellingham, Washington.

Louanchi, F., et al. (2001), Dissolved inorganic carbon, alkalinity, nutrient and oxygen seasonal and interannual variations at the Antarctic Ocean JGOFS-KERFIX site, *Deep-Sea Research Part I-Oceanographic Research Papers*, *48*(7), 1581-1603.

MacRae, M. J. D., et al. (1994), Seasonal phosphorus deficiency in the Mississippi River plume: unusual large areal extent during the record flood of 1993, *Eos Trans. Am. Geophys. Union*, *75*(3), 30.

Mateo, P., et al. (2006), Physiological differences between two species of cyanobacteria in relation to phosphorus limitation, *Journal of Phycology*, *42*(1), 61-66.

McManus, J., et al. (1997), Phosphorus regeneration in continental margin sediments, *Geochimica Et Cosmochimica Acta*, *61*(14), 2891-2907.

McNulty, I., et al. (2003), The 2-ID-B intermediate-energy scanning X-ray microscope at the APS, *Journal De Physique Iv*, *104*, 11-15.

Meyer, A. (1904), Orientierende Untersuchungen ueber Verbreitung, Morphologie, und Chemie des Volutins, *Bot. Zeitung*, *62*(1), 113-152.

Millero, F. J. (1985), The effect of ionic interations on the oxidation of metals in natural waters, *Geochimica Et Cosmochimica Acta*, *49*(2), 547-553.

Millero, F. J., et al. (1987), The oxidation kinetics of Fe (II) in seawater, *Geochimica Et Cosmochimica Acta*, *51*(4), 793-801.

Miyata, K., and A. Hattori (1986), A Simple Fractionation Method for Determination of Phosphorus Components in Phytoplankton: Application to Natural Populations of Phytoplankton in Summer Surface Waters of Tokyo Bay, *Journal of the Oceanographical Society of Japan*, *42*, 255-265.

Miyata, K., et al. (1986), Variation of cellular phosphorus composition of Skeletonema costatum and Heterosigma akashiwo grown in chemostats, *Marine Biology*, *93*(2), 291-297.

Mori, S., et al. (2004), Crystallographic studies of *Mycobacterium tuberculosis* polyphosphate/ATP-NAD kinase complexed with NAD, *Journal of Bioscience and Bioengineering*, *98*(5), 391-393.

Mortimer, C. H. (1941), The exchange of dissolved substances between mud and water in lakes, *Journal of Ecology*, *29*, 280-329.

Mortimer, C. H. (1942), The exchange of dissolved substances between mud and water in lakes, *Journal of Ecology*, *30*, 147-201.

Mortlock, R. A., and P. N. Froelich (1989), A simple method for the rapid determination of biogenic opal in pelagic marine sediments, *Deep-Sea Research Part a-Oceanographic Research Papers*, *36*(9), 1415-1426.

Mukai, T., et al. (2003), Characterization and molecular cloning of a novel enzyme, inorganic polyphosphate/ATP-glucomannokinase, of *Arthrobacter* sp strain KM, *Applied and Environmental Microbiology*, *69*(7), 3849-3857.

Myneni, S. C. B. (2002), Soft X-ray spectroscopy and spectromicroscopy studies of organic molecules in the environment, in *Rev. Mineral. Geochem. Applications of Synchrotron Radiation in Low-Temperature Geochemistry and Environmental Sciences*, edited by P. Fenter, et al., pp. 485-579.

Nagata, T., et al. (2006), Engineering expression of bacterial polyphosphate kinase in tobacco for mercury remediation, *Applied Microbiology and Biotechnology*, *72*(4), 777-782.

Naqvi, S. W. A., et al. (2000), Increased marine production of N2O due to intensifying anoxia on the Indian continental shelf, *Nature*, *408*(6810), 346-349.

Nesmeyanova, M. A. (2000), Polyphosphates and enzymes of polyphosphate metabolism in *Eschericia coli*, *Biochemistry-Moscow*, *65*(3), 309-314.

Nielsen, P. H., et al. (2010), A conceptual ecosystem model of microbial communities in enhanced biological phosphorus removal plants, *Water Research*, *44*(17), 5070-5088.

Nikata, T., et al. (2001), Photometric estimation of intracellular polyphosphate content by staining with basic dye, *Analytical Sciences*, *17 Supplement*, il675-il678.

Oh, K. S., et al. (2005), Preparation and in vivo studies of beta-TCP based bone cement containing polyphosphate.

Orchard, E. D., et al. (2010), Polyphosphate in Trichodesmium from the low-phosphorus Sargasso Sea, *Limnology and Oceanography*, *55*(5), 2161-2169.

Paytan, A., et al. (2003), Selective phosphorus regeneration of sinking marine particles: evidence from P-31-NMR, *Marine Chemistry*, *82*(1-2), 55-70.

Paytan, A., and K. McLaughlin (2007), The oceanic phosphorus cycle, *Chemical Reviews*, *107*(2), 563-576.

Peak, D., et al. (2002), Solid-state speciation of natural and alum-amended poultry litter using XANES spectroscopy, *Environmental Science & Technology*, *36*(20), 4253-4261.

Perry, M. J. (1976), Phosphate utilization by an oceanic diatom in phosphorus-limited chemostat culture and in oligotrophic waters of Central North-Pacific, *Limnology and Oceanography*, *21*(1), 88-107.

Planavsky, N. J., et al. (2010), The evolution of the marine phosphate reservoir, *Nature*, *467*(7319), 1088-1090.

Rabalais, N. N., et al. (2001), Hypoxia in the Gulf of Mexico, *Journal of Environmental Quality*, *30*(2), 320-329.

Rabalais, N. N., et al. (2002), Nutrient-enhanced productivity in the northern Gulf of Mexico: past, present and future, *Hydrobiologia*, *475*(1), 39-63.

Rabouille, C., and J. F. Gaillard (1991), Towards the EDGE - early diagenetic global explanation - a model depicting the early diagenesis of organic-matter, O2, NO3, Mn, and PO4, *Geochimica Et Cosmochimica Acta*, *55*(9), 2511-2525.

Rao, N. N., et al. (1998), Inorganic polyphosphate in *Escherichia coli*: the phosphate regulon and the stringent response, *Journal of Bacteriology*, *180*(8), 2186-2193.

Rao, N. N., et al. (2009), Inorganic Polyphosphate: Essential for Growth and Survival, *Annual Review of Biochemistry*, *78*, 605-647.

Redfield, A. C. (1958), The biological control of chemical factors in the environment, *American Scientist*, *46*(3), 205-221.

Renninger, N., et al. (2004), Uranyl precipitation by *Pseudomonas aeruginosa* via controlled polyphosphate metabolism, *Applied and Environmental Microbiology*, *70*(12), 7404-7412.

Romans, K. M., et al. (1994), Buoyancy regulation in the colonial diazotrophic cyanobacterium Trichodesmium tenue - ultrastructure and storage of carbohydrate, polyphosphate, and nitrogen, *Journal of Phycology*, *30*(6), 935-942.

Ruiz, F. A., et al. (2001), The polyphosphate bodies of *Chlamydomonas reinhardtii* possess a proton-pumping pyrophosphatase and axe similar to acidocalcisomes, *Journal of Biological Chemistry*, *276*(49), 46196-46203.

Ruttenberg, K. C. (1992), Development of a sequential extraction method for different forms of phosphorus in marine sediments, *Limnology and Oceanography*, *37*(7), 1460-1482.

Ruttenberg, K. C., and R. A. Berner (1993), Authigenic apatite formation and burial in sediments from non-upwelling, continental-margin environments, *Geochimica Et Cosmochimica Acta*, *57*(5), 991-1007.

Sannigrahi, P., and E. Ingall (2005), Polyphosphates as a source of enhanced P fluxes in marine sediments overlain by anoxic waters: Evidence from P-31 NMR, *Geochemical Transactions*, *6*(3), 52-59.

Sannigrahi, P., et al. (2005), Cycling of dissolved and particulate organic matter at station Aloha: Insights from C-13 NMR spectroscopy coupled with elemental, isotopic and molecular analyses, *Deep-Sea Research Part I-Oceanographic Research Papers*, *52*(8), 1429-1444.

Sannigrahi, P., et al. (2006), Nature and dynamics of phosphorus-containing components of marine dissolved and particulate organic matter, *Geochimica Et Cosmochimica Acta*, *70*(23), 5868-5882.

Savchuk, O. P., et al. (2008), The Baltic Sea a century ago - a reconstruction from model simulations, verified by observations, *Journal of Marine Systems*, *74*(1-2), 485-494.

Schuler, A. J., and D. Jenkins (2003), Enhanced biological phosphorus removal from wastewater by biomass with different phosphorus contents, part II: Anaerobic adenosine triphosphate utilization and acetate uptake rates, *Water Environment Research*, *75*(6), 499-511.

Schulz, H. N., and H. D. Schulz (2005), Large sulfur bacteria and the formation of phosphorite, *Science*, *307*(5708), 416-418.

Serafim, L. S., et al. (2002), Methods for detection and visualization of intracellular polymers stored by polyphosphate-accumulating microorganisms, *Journal of Microbiological Methods*, *51*(1), 1-18.

Sethuraman, A., et al. (2001), The endopolyphosphatase gene: Essential in *Saccharomyces cerevisiae*, *Proceedings of the National Academy of Sciences of the United States of America*, *98*(15), 8542-8547.

Seviour, R. J., et al. (2003), The microbiology of biological phosphorus removal in activated sludge systems, *Fems Microbiology Reviews*, *27*(1), 99-127.

Shi, X. B., et al. (2004), Inorganic polyphosphate in *Bacillus cereus*: Motility, biofilm formation, and sporulation, *Proceedings of the National Academy of Sciences of the United States of America*, *101*(49), 17061-17065.

Shiba, T., et al. (2003), Modulation of mitogenic activity of fibroblast growth factors by inorganic polyphosphate, *Journal of Biological Chemistry*, *278*(29), 26788-26792.

Slomp, C. P., et al. (2002), Enhanced regeneration of phosphorus during formation of the most recent eastern Mediterranean sapropel (S1), *Geochimica Et Cosmochimica Acta*, *66*(7), 1171-1184.

Slomp, C. P., et al. (2004), Controls on phosphorus regeneration and burial during formation of eastern Mediterranean sapropels, *Marine Geology*, *203*(1-2), 141-159.

Solorzano, L., and J. D. H. Strickland (1968), Polyphosphate in seawater, *Limnology and Oceanography*, *13*(3), 515-518.

Solorzano, L., and J. H. Sharp (1980), Determination of total dissolved phosphorus and particulate phosphorus in natural waters, *Limnology and Oceanography*, *25*(4), 754-757.

Stramma, L., et al. (2008), Expanding oxygen-minimum zones in the tropical oceans, *Science*, *320*(5876), 655-658.

Streichan, M., et al. (1990), Polyphosphate-accumulating bacteria from sewage plants with different processes for biological phosphorus removal, *Fems Microbiology Ecology*, *73*(2), 113-124.

Sundby, B., et al. (1992), The phosphorus cycling in coastal marine sediments, *Limnology and Oceanography*, *37*(6), 1129-1145.

Sung, W., and J. J. Morgan (1980), Kinetics and product of ferrous iron oxygenation in aqueous systems, *Environmental Science & Technology*, *14*(5), 561-568.

Sutula, M., et al. (2004), Effect of seasonal sediment storage in the lower Mississippi River on the flux of reactive particulate phosphorus to the Gulf of Mexico, *Limnology and Oceanography*, *49*(6), 2223-2235.

Taillefert, M., and J.-F. Gaillard (2002), Reactive transport modeling of trace elements in the water column of a stratified lake: Iron cycling and metal scavenging, *Journal of Hydrology*, *256*, 16-34.

Talmon, Y. (1987), Electron beam radiation damage to organic and biological cryospecimens, in *Cryotechniques in Biological Electron Microscopy*, edited by R. A. Steinbrecht and K. Zierold, pp. 64-84, Springer, Berlin.

Tamburini, F., et al. (2003), Investigating the history of East Asian monsoon and climate during the last glacial-interglacial period (0-140 000 years): mineralogy and geochemistry of ODP Sites 1143 and 1144, South China Sea, *Marine Geology*, *201*(1-3), 147-168.

Tanaka, S., et al. (2003), Strictly polyphosphate-dependent glucokinase in a polyphosphate-accumulating bacterium, *Microlunatus phosphovorus*, *Journal of Bacteriology*, *185*(18), 5654-5656.

Tijssen, J. P. F., et al. (1982), Localization of polyphosphates in *Saccharomyces fragilis*, as revealed by 4',6-Diamidino-2-Phenylindole fluorescence, *Biochimica Et Biophysica Acta*, *721*(4), 394-398.

Turnewitsch, R., and C. Pohl (2010), An estimate of the efficiency of the iron- and manganese-driven dissolved inorganic phosphorus trap at an oxic/euxinic water column redoxcline, *Global Biogeochemical Cycles*, *24*.

Twining, B. S., et al. (2003), Quantifying trace elements in individual aquatic protist cells with a synchrotron X-ray fluorescence microprobe, *Analytical Chemistry*, *75*(15), 3806-3816.

Twining, B. S., et al. (2004a), Element stoichiometries of individual plankton cells collected during the Southern Ocean Iron Experiment (SOFeX), *Limnology and Oceanography*, *49*(6), 2115-2128.

Twining, B. S., et al. (2004b), Cellular iron contents of plankton during the Southern Ocean Iron Experiment (SOFeX), *Deep-Sea Research Part I-Oceanographic Research Papers*, *51*(12), 1827-1850.

Tyrell, T. (1999), The relative influence of nitrogen to phosphorus on oceanic primary production, *Nature*, *400*, 525-531.

Vahtera, E., et al. (2007), Internal ecosystem feedbacks enhance nitrogen-fixing cyanobacteria blooms and complicate management in the Baltic Sea, *Ambio*, *36*(2-3), 186-194.

Van Cappellen, P., and R. A. Berner (1991), Fluorapatite crystal-growth from modified seawater solutions, *Geochimica Et Cosmochimica Acta*, *55*(5), 1219-1234.

Van Cappellen, P., and E. D. Ingall (1994), Benthic phosphorus regeneration, net primary production, and ocean anoxia - a model of the coupled marine biogeochemical cycles of carbon and phosphorus, *Paleoceanography*, *9*(5), 677-692.

Van Cappellen, P., and E. D. Ingall (1996), Redox stabilization of the atmosphere and oceans by phosphorus-limited marine productivity, *Science*, *271*(5248), 493-496.

Vangroenestijn, J. W., et al. (1987), ATP production from polyphosphate in *Acinetobacter* strain-210A, *Archives of Microbiology*, *148*(1), 14-19.

Vetter, T. A., et al. (2007), Combining reverse osmosis and electrodialysis for more complete recovery of dissolved organic matter from seawater, *Separation and Purification Technology*, *56*(3), 383-387.

Vogt, S. (2003), MAPS: A set of software tools for analysis and visualization of 3D X-ray fluorescence data sets, *Journal De Physique Iv*, *104*, 635-638.

Wiame, J.-M. (1947), Yeast metaphosphate, *Federation Proceedings*, *6*, 302.

Yamagata, Y., et al. (1991), Volcanic production of polyphosphates and its relevance to prebiotic evolution, *Nature*, *352*(6335), 516-519.

Yamaoka, M., et al. (2008), Effect of inorganic polyphosphate in periodontitis in the elderly, *Gerodontology*, *25*(1), 10-17.

Young, C. L., and E. D. Ingall (2010), Marine dissolved organic phosphorus composition: insights from samples recovered using combined electrodialysis/reverse osmosis, *Aquatic Geochemistry*.

Zhang, H. Y., et al. (2002), A polyphosphate kinase (PPK2) widely conserved in bacteria, *Proceedings of the National Academy of Sciences of the United States of America*, *99*(26), 16678-16683.

Zhang, H. Y., et al. (2005), Inorganic polyphosphate in the social life of *Myxococcus xanthus*: Motility, development, and predation, *Proceedings of the National Academy of Sciences of the United States of America*, *102*(38), 13416-13420.